PERFORMANCE EVALUATION AND CFD SIMULATION OF MULTIPHASE TWIN-SCREW PUMPS

A Dissertation

by

ABHAY RAVINDRA PATIL

Submitted to the Office of Graduate Studies of
Texas A&M University
in partial fulfillment of the requirements for the degree of

DOCTOR OF PHILOSOPHY

Chair of Committee,	Gerald L. Morrison
Committee Members,	Je-Chin Han
	Yassin A. Hassan
	Robert E. Randall
Head of Department,	Andreas A. Polycarpou

August 2013

Major Subject: Mechanical Engineering

ABSTRACT

Twin-screw pumps are economical alternatives to the conventional multiphase system and are increasingly used in the oil and gas industry due to their versatility in transferring the multiphase mixture with varying Gas Void Fraction (GVF). Present work focuses on the experimental and numerical analysis of twin-screw pumps for different operating conditions. Experimental evaluation aims to understand steady state and transient behavior of twin-screw pumps. Detailed steady state evaluation helped form better understanding of twin-screw pumps under different operating conditions. A comparative study of twin-screw pumps and compressors contradicted the common belief that compressor efficiency is better than the efficiency of twin-screw pumps. Transient analysis at high GVF helped incorporate necessary changes in the design of sealflush recirculation loop to improve the efficiency of the pump. The effect of viscosity of the sealflush fluid at high GVF on pump performance was studied. Volumetric efficiency was found to be decreased with increase in viscosity.

Flow visualization was aimed to characterize phase distribution along cavities and clearances at low to high GVF. Dynamic pressure variation was studied along the axis of the screw which helped correlate the GVF, velocity and pressure distribution.

Complicated fluid flow behavior due to enclosed fluid pockets and interconnecting clearances makes it difficult to numerically simulate the pump. Hence design optimization and performance prediction incorporates only analytical approach and experimental evaluation. Current work represents an attempt to numerically simulate

a multiphase twin-screw pump as a whole. Single phase 3D CFD simulation was performed for different pressure rise. The pressure and velocity profile agreed well with previous studies. Results are validated using an analytical approach as well as experimental data. A two-phase CFD simulation was performed for 50% GVF. An Eulerian approach was employed to evaluate multiphase flow behavior. Pressure, velocity, temperature and GVF distributions were successfully predicted using CFD simulation. Bubble size was found to be most dominant parameter, significantly affecting phase separation and leakage flow rate. Better phase separation was realized with increased bubble size, which resulted in decrease in leakage flow rate. CFD results agreed well with experimental data for the bubble size higher than 0.08 mm.

DEDICATION

To my Family and Shah Sir

ACKNOWLEDGEMENTS

I would like to thank Dr. Morrison for giving me this opportunity, and his teaching, faith and patience towards me. It was not only his knowledge about the research but his ability to work one on one with students and to help them whenever needed. It was very helpful especially during the initial stages of research. I learned a lot from him not only about the research but also about life. I feel extremely lucky to have him as my advisor. Thank you very much sir.

I would like to thank my committee members, Dr. Je Han, Dr. Hassan, and Dr. Randall for their guidance and support and valuable suggestion during the course of research.

I also would like to thank all my labmates and friends who not only helped me with research but also made my time at the Turbolab enjoyable. Thanks to Shankar, Rhyan, Beki, Daniel, Sahand and Ted for helping in building the test rig and running the experiments. Suggestions from Emanuel relating to the CFD simulation were very helpful. Thanks to Joey, Scott, Ameen, Nicolas, Daniel, Sujan, and Mohammet for being there whenever needed. I really appreciate the help I received from Ray Mathews. Thanks to Dr. Scott and Jun Xu from Shell for the funding and supporting this project. Thanks to Colfax Corporation and Leistritz Corporation for providing the twin-screw pumps.

I am thankful to Sachin Pawar, Bhanesh, Alok and Rohit for their support and help during all this time.

None of this would have been possible without constant love, support and patience of my parents, my brother and my lovely wife. I would like to express my heart-felt gratitude to my family.

NOMENCLATURE

m	Mass
p	Pressure
GVF	Gas Volume Fraction
CFD	Computational Fluid Dynamics
TSP	Twin-Screw Pump
CC	Circumferential Clearance
FC	Flank Clearance
RC	Root Clearance
n	Number of threads
n_t	Number of thread on one side of the screw
x	Mass fraction
μ	Viscosity
$\dot{m}_g$	Mass of gas
$\dot{m}_l$	Mass of liquid
ρ_l	Density of liquid
ρ_g	Density of gas
V	Volume
s	Suction
D	Discharge, Displacement volume
D_r	Root diameter

D_e	External diameter
Z	Compressibility factor
Δt	Time step
q	Flow rate GPM
F_r	Radial force
D_t	Tip diameter of screw rotor
ξ	Ratio of root diameter to tip diameter of the screw
P	Pitch
N	Speed
Q_{th}	Theoretical volumetric flow rate
Q_a	Actual volumetric flow rate
$Q_{leakage}$	Leakage volumetric flow rate
Q_l	Liquid flow rate
Q_g	Gas flow rate
M	Torque
ω	Angular velocity
P_{drive}	Drive power
P_{fluid}	Power used in conveying fluid
$P_{friction}$	Power lost in friction
P_{actual}	Actual power spent
P_l	Power lost in leakage flow
P_{rec}	Power spent on liquid recirculation

$P_{visc,turb}$	Power lost due to viscous and turbulent effect
$P_{Mechanical\ losses}$	Power lost in mechanical losses
P_l	Actual work done in moving the liquid
n	Polytropic index
k	Adiabatic index
V_{acfm}	Gas flow rate in actual cubic feet per minute
$P_{g,poly}$	Work done for polytropic compression
$P_{g,iso}$	Work done for isothermal compression
η_v	Volumetric efficiency
η_{eff}	Pump Effectiveness
η_{mech}	Mechanical Efficiency
PID	Proportional integral derivative
GUI	Graphical User Interface
ν	Kinetic viscosity
ρ	Density
ε	Turbulent dissipation rate
k	Turbulent kinetic energy
μ_t	Turbulent viscosity
y^*	Dimensionless velocity near wall
y_p	Distance from point p to the wall
$\hat{\rho}_q$	Effective density of the phase q

E	Empirical constant (=9.793)
F	Force vector
g_i	Gravity vector
$\bar{q}$	Heat flux
U_c	Mean velocity magnitude
S	Modulus of the mean rate of strain tensor
P_r	Molecular Prandtl number for energy
ρ_{yq}	Phase reference density of the phase q
α_q	Phasic volume fraction
P_{rt}	Prandtl number for energy
h	Specific enthalpy
c_p	Specific heat of the fluid
$\bar{\tau}$	Stress-strain tensor
T	Temperature of the fluid
k_p	Turbulent kinetic energy at the near-wall node p
V_q	Volume fraction of phase q
κ	Von Karman constant (=0.4187)

CONTENTS

Page

LIST OF FIGURES

FIGURE Page

LIST OF TABLES

1 INTRODUCTION

Multiphase pumping technology is increasingly being used in the oil and gas industry as an alternative to conventional multi-phase production system. Multiphase pumps are used to boost a multiphase mixture composed of mainly gas and liquid and sometimes sand particles in suspension with the fluid. Emergence of this technology started three decades ago as a retrofit to existing systems. However, the surge of new developments and successful field trials in the multiphase technology have made it a well-established alternative.

In mid 1970s, the French Institute of Petroleum (IFP) started research on topside application of oil-field multiphase pumping. In 1983, a joint venture was formed between Shell, Mobil, BP, and Stothert & Pitt in order to develop an effective multiphase pump using meshing and counter rotating twin screws. In the same year, a multiphase model of a topside twin screw pump was successfully deployed on an onshore test rig in the UK, followed by offshore commissioning of a twin screw pump both in Malaysia for Shell and in North Sea for BP (Dolan et al. 1988).

After successful deployment of topside multiphase pumps, efforts have been started to deploy the pumps in deep water wellheads. The first deep water multiphase helicon-axial pump was installed successfully by Shell in 1995 and the first subsea multiphase twin screw pump was installed by CNR in 2005 in the North Sea (Hua et al. 2012). As a result of the successful performance of multiphase pumps in different field

conditions, the market became increasingly competitive, requiring highly reliable and capable pumping solutions.

Oil wells typically produce a mixture of gas, oil, water and occasionally sand particles, natural gas hydrates, and waxes (Dal Porto and Larson 1997), the composition of which changes throughout the life of the well. Variation in composition as pressure and temperature of the mixture varies from bottom hole to wellhead is experienced. The multiphase mixture is transferred trough a single line and required pressure is boosted through multiphase pumping technology.

Due to the nature of multiphase mixtures, it becomes difficult to predict the condition of the flow at any future point in time, resulting in no as such "normal" operating conditions for multiphase pumps. This makes it extremely important to understand the interaction between the transient condition in the wellhead and the multiphase pump. This makes the selection of pump very important for the particular wellhead condition and the multiphase pump must be designed to accommodate the uncertainty of actual reservoir output with wide operating range and economic feasibility (Martin 2003).

1.1 Conventional multiphase production system and multiphase pumps

A reservoir typically produces a multiphase mixture of oil, gas, water, and sand. The system transferring this mixture to a central facility is called Multiphase production system. Initially, the multiphase mixture is transferred short distances using reservoir energy. But when reservoir pressure head is not enough, the only option to transfer the

mixture is to separate the flow using a separator and use a liquid pump and a compressor to transfer the liquid and gas through separate lines. A schematic of a conventional multiphase production system is shown in Figure 1.1.

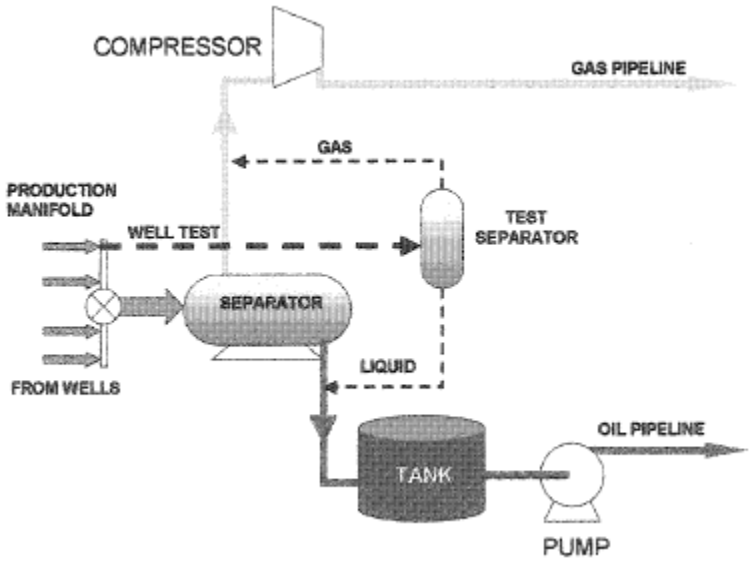

Figure 1.1: Conventional multiphase production system (Martin 2003)

A multiphase pump as shown in Figure 1.2 eliminates the necessity of separation of different phases. The wellhead pressure is boosted and the mixture is transported to a central facility through single line. Well production can be changed using a multiport valve and a multiphase flow meter can be used to test the condition of flow for each well. A single multiphase pump replaces a compressor, separator and liquid pump. Elimination of equipment in conventional system can save about 30% for the same production (Xu 2008). Moreover, a significant footprint and infrastructure required to

support the equipment can be reduced using multiphase pumps. With multiphase pumps, a reservoir considered being less productive due to low pressure head and remoteness can be harnessed effectively. With global oil production reaching its peak, those untouched reservoirs cannot be left unused.

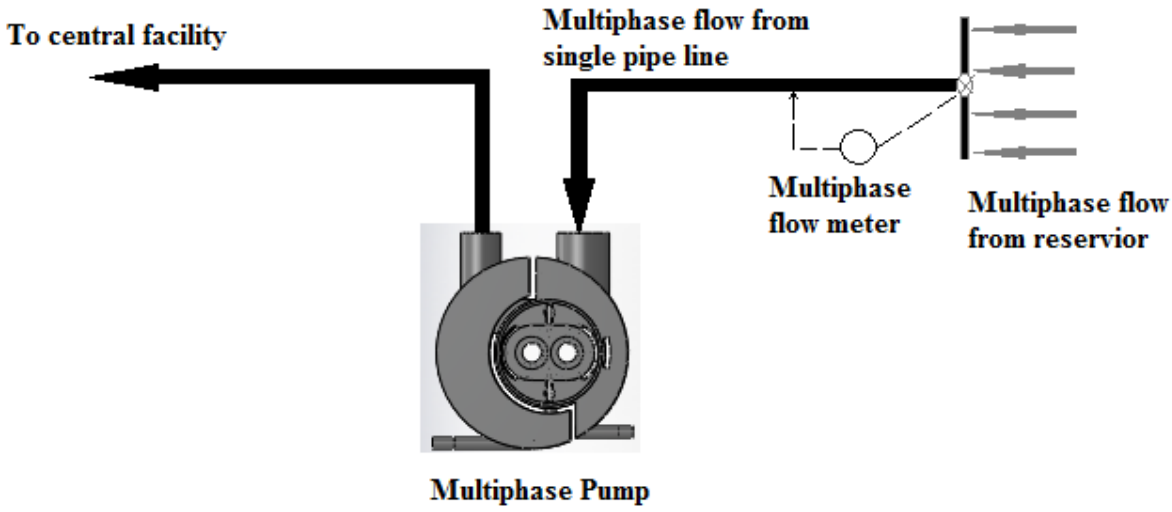

Figure 1.2: Multiphase pump production system

Oil reservoirs are mostly characterized by gaseous components with low wellhead pressures. Multiphase mixture with high gas content, typically more than 95%, is considered as wet gas. With gas prices consistently rising, one of the challenges for multiphase pumps is wet gas production and transport. The industry is seeking economical ways to improve the recovery of gas reservoir by deploying multiphase pumps for wet gas compression. Multiphase pumps experience a severe loss of efficiency at GVF of 100% due to internal leakage back to the pump inlet. On the other

hand, compressors can be damaged with an increase in the liquid content. To address this issue, efforts have been made to improve the efficiency of multiphase pumps in the range of 97% to 100% GVF along with compressors to be more tolerant of fraction of liquid ranging from 1% to 4% (Scott et al. 2006).

Even though multiphase pumps are designed to handle a multiphase mixture, an engineer has to rely on the single phase curve provided by the manufacturer to predict and correlate the performance in actual field condition. Recently, effort have been made to develop twin screw pump models to evaluate the mixture leakage flow, temperature increase and pressure profile across the screw rotor. Most of the tools already developed either assume isothermal compression and liquid only leakage flow or adiabatic compression with homogeneous mixture leakage flow in the gap. In actual conditions, the flow path in the screw pump is very complicated with mutual interaction of two phases between the different clearances and fluid pockets.

Analytical models can predict the performance based on numerous assumptions. But in order to develop a good pump, the design engineer must know the fluid dynamics phenomenon in the circumferential as well as flank and root clearances. Existing analytical tools assumes either liquid sealing or homogeneous mixture in the clearances. But none of the tools provide any information about gas infiltration inside the gap, the effect of localized pressure drop and the velocity of each phase. A large void still exists between the detailed model which would provide complete quantitative information about the pump performance and the existing tools.

2 LITERATURE REVIEW

2.1 Twin Screw Pump Modeling and experimental testing

The literature review discusses previous work including experimental testing as well as analytical and numerical evaluation of multiphase twin-screw pumps. Screw pumps are categorized as positive displacement pumps. Its invention is credited to Greek polymath Archimedes back in 3rd century BC. Previously, screw-pumps have been used for water conveyance purpose in agriculture. Recently, they have been used in various fields. The potential of twin screw pumps in the oil and gas industry was not realized until before mid-80 and early 90's. The main reason behind the surge of multiphase pumps was the need to simultaneously pump the gas and liquid in order to reduce capital, footprint, and operational expenses for onshore and offshore oil production sites, especially deep water production. Disposal of natural gas through flaring and venting was another concern for the oil and gas industry. Minimization of this wastage became essential in order to realize maximum possible production of hydrocarbons.

Dolan et al. 1988, discussed the disadvantages of using conventional multiphase production system, reasons for developing the pumping system capable of transporting gas/liquid mixtures and the design, construction, and testing of the multiphase twin-screw pump based on the requirement. The pump demonstrated the ability to transport the mixture with varying gas volume fraction (GVF). Multiphase pump performance up to GVF of 95% was studied by Karge 1988. Performance was observed at different GVF

and operating speeds. Power required and volume flow rate is analyzed as a function of pressure differential.

Neumann 1991 highlighted some of the key problems associated with twin-screw pumps. Tests were conducted on a 1000KW vertically installed subsea pump. Based on design the pump was expected to run for 6 months without any failure. The objective couldn't be achieved due to failure of the mechanical seals. A multiphase mixture with 100 % GVF could be delivered but with very high heat generation. A maximum GVF of 95% was defined as the cut off point for this pump. Additional boost liquid injection was supplied from a separator downstream the pump.

Vetter and Wincek 1993 developed the first modeling tool for the twin-screw pump. The proposed model was used to evaluate volumetric performance of multiphase twin-screw pumps. The screw pump was modeled as a series of parallel discs translating from suction to discharge with the volume between discs representing sealed chambers. The model was capable of evaluating single phase and two phase leakage flow. It also included deflection of the spindle due to differential pressure distribution and its effect on the backflow. The model assumes clearances are occupied with liquid phase only, and gas compression is isothermal as a result of high specific heat of the liquid phase. Flow balance and the chamber pressure are computed by dividing relevant chamber into differential time segment. Iteration stops when the liquid volume differs slightly from the previously computed value. Results show good agreement with experimental data for the GVF ranging from 0% to 85%. But results deviate from experimental data for GVF

higher than 90% because the model assumes liquid only leakage flow through clearances causing perfect sealing of gases thereby overestimating the volumetric flow rate.

The pressure distribution across the screw-pump was investigated. The pressure distribution increases linearly across the clearances from suction to discharge because of equal leakage flow. However, with two phase flow, the pressure distribution deviates from linear to parabolic. Figure 2.1 shows the justification.

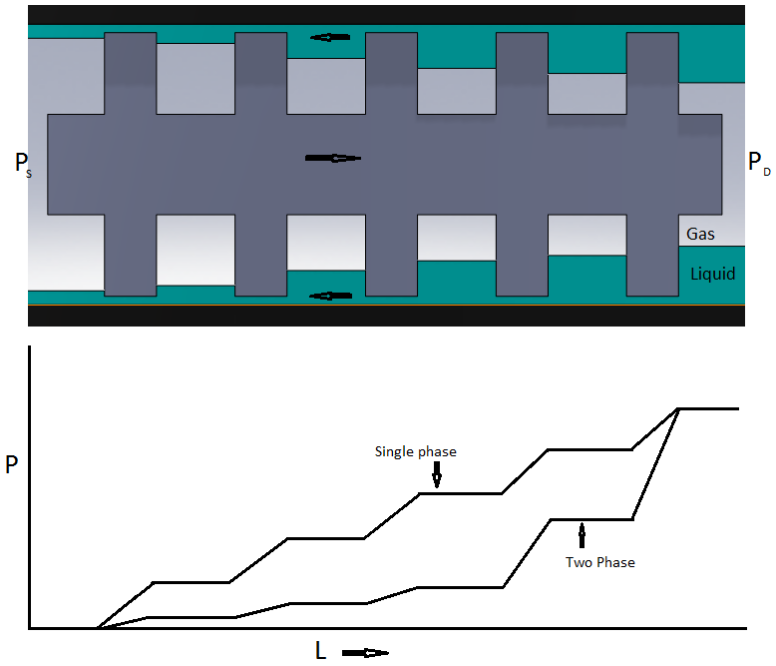

Figure 2.1: Simplified twin-screw Pump model with pressure distribution

Vetter et al. 2000 modified the twin-screw pump model developed by Wincek. This work investigated circumferential clearance (CC), root clearance (RC) and flank clearance (FC) leakage flow and is validated with experimental data from Vetter and

Wincek 1993. CC leakage flow being most effective one modeled with superimposing pressure differential component and rotational component. Elastic deformation due to pressure differential is taken into account and a suitable algorithm included to model eccentricity. The model includes parallel leakage flow along with serial leakage flow which reflects real screw pump model. However, similar to Wincek, the author assumed isothermal compression. Isothermal compression cannot be justified for the screw-pump running at high GVF and pressure differential as heat generated by gas compression cannot be absorbed by the liquid.

Egashira et al. 1998 developed model to predict back flow in the twin-screw pump. He represented the empirical equation for the pressure distribution along spindle length using experimental data.

Reservoir production often contains sand particles in suspension with multiphase mixture. Operational consequences due to the presence of solid particles has to be accounted for since wear and abrasion of the pump results in increase in suction pressure and temperature and decreased flow rate capacity, sometimes, wear of the seal can stop operation immediately. Dorenbos et al. 2001 highlighted this issue. Four different case studies in different field application are presented with almost same sand content in all applications. Presence of sand showed mixed results with some screws worn very little with no effect on pump performance while critical changes in pump performance are observed in other cases. No general benchmark rule could be set due to sand presence. With this, the author concluded that any design improvement in the pump to incorporate the effect of sand presence can be achieved through operational experiences only.

Feng et al. 2001 presented rotor profile generation, geometrical characteristics and leakage flow model within multiphase twin-screw pump. Each leakage path was modeled differently based on previous conventions. Real flow rate was defined as the backflow between first chamber and suction. Three different backflow regions are defined namely contact lines (root clearance), blowholes (flank clearances) and lobe tip clearance (circumferential clearance). Backflow through lobe tip clearance was assumed to be filled with liquid only because of dominance of centrifugal forces. It was solved using incompressible, viscous, laminar flow equation.

$$\dot{m}_l = \frac{\rho \pi d h^3 \Delta p}{12 \mu L} \tag{2.1}$$

Leakage flow through blow hole was modeled as two phase flow through an orifice. It was defined as

$$\dot{m} = \frac{c \alpha \varepsilon A(\emptyset) \sqrt{2 \rho_l \Delta p}}{(1-x)\theta + x \sqrt{\rho_l / \rho_g}} \tag{2.2}$$

$$\dot{m}_g = x \dot{m} \tag{2.3}$$

$$\dot{m}_l = (1-x) \dot{m} \tag{2.4}$$

where α is the coefficient of flow through the orifice calculated from experiment, ε is the gas expansion coefficient, and c is devised from experiments, which is used as a correction factor representing deviation from the reality. $A(\emptyset)$ is the cross section area of the blow hole. θ is a coefficient which represents slide ratio between gas and liquid. Back flow through contact line clearance was modeled as two phase adiabatic flow

between two flat plates. The model was validated using experimental data. Tests were conducted with GVF varying between 80 and 98 %, rotational speed varying between 1500 rpm to 2400 rpm and pressure differential from 0 MPa to 1.4 MPa. The pressure profile shows good agreement except at exhaust due to the pulsating nature of the flow. Volumetric efficiency agrees well with data.

Seal failure is one of the major concerns for twin-screw pump operation. Beside the low viscosity mixture, sand presence and high circumferential velocity affects the seal performance. Novice solution of smart seals is invented by Bornamann Pumps (Muller-Link 2002). The seal uses a pair of concentric throttle bushing and mechanical seal which direct the product leakage flow back to the inlet side of the pump, thus avoiding any leak to the environment. Improved design solved the critical issue of seal failure and the system successfully ran for more than 6,000 without any failure.

A new method to generate effective clearances using regression of pump performance with pure liquid was developed by Martin 2003. Different from other models it does not need the dimensions of clearances. It uses data from the pump characteristic curve provided by the manufacturer. Effective clearance is calculated by linear regression using a least square approximation. The model assumes isothermal compression. Following equations represent the mass balance in set of control volumes at certain time.

$$V_s\left[\frac{p_s Z_1}{p_1 Z_s}-1\right]+(q_1-q_0)\Delta t=0$$
$$V_1\left[\frac{P_1 Z_2}{P_2 Z_1}-1\right]+(q_2-q_1)\Delta t=0 \qquad 2.5$$

$$\vdots$$

$$V_{n-1}\left[\frac{p_{n-1}Z_D}{p_D Z_{n-1}} - 1\right] + (q_n - q_{n-1})\Delta t = 0$$

Cooper and Prang 2004 proposed a similar model but with some improvements. They made similar assumptions to design the model. The slip flow model was greatly simplified by assuming liquid sealing in circumferential clearances (CC) as well as root and flank clearances. In case of two phase flow, the entire compression of gas occurs in the last chamber and the pressure profile follows a parabolic path along the spindle. The pressure differential causes a radial load on the spindle that causes screw deflection in the liner. Radial forces are proportional to differential load. Increase in pressure differential changes the circumferential clearance causing the variable pressure profile on screw with low pressure profile on top and high pressure profile on bottom. Resultant is radial force.

$$F_r = PD_t * (1 + \xi) * \Delta p \qquad 2.6$$

This deflection causes more slip flow than if CC were constant.

The paper also discusses the effect of viscous heating caused by shearing of viscous liquid while passing through clearances. Average viscosity is found iteratively from viscosity versus temperature relationship. This kind of analysis is useful to the designer especially in case of performance of the pump for the long run.

Singh 2003 and Martin 2003 have presented evidence of decreasing the slip flow rate with increase in viscosity while Chan 2006 found contradicting results compared to former results. A model developed by Martin predicted higher volume flow rate due to

reduced slip flow volume at the suction. Based on this prediction, Singh tested the Bornemann pump with integrated recirculation chamber for various liquid viscosities at high GVF up to 100 %. Figure 2.2 shows significant increase in gas flow rate with increase in viscosity.

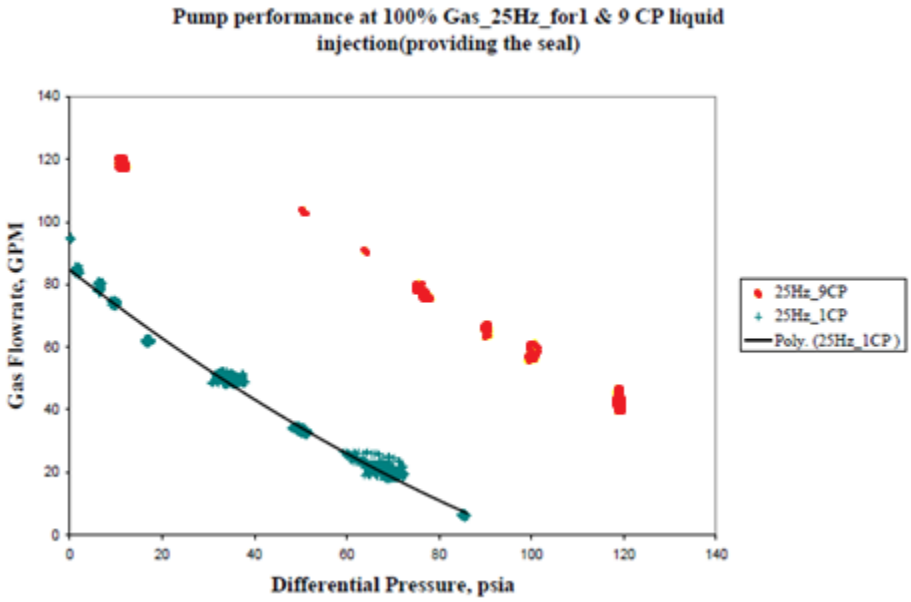

Figure 2.2: Gas flow rate versus pressure differential for different liquid viscosities (Singh 2003)

To further validate the results shown by Singh 2003, Chan 2006 tested the performance of the same pump with different viscosities and pressure differentials. For single phase flow there was significant reduction in the slip flow with increased viscosity, while the results exhibited contradicting behavior with the addition of gas.

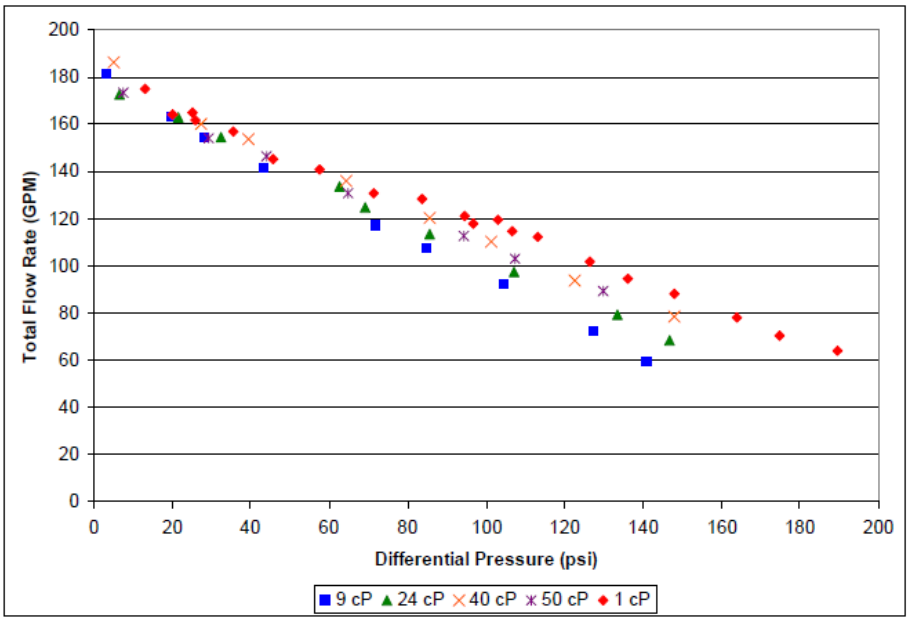

Figure 2.3: Total flow rate versus differential pressure at 95% GVF and 1350 RPM (Chan 2006)

Figure 2.3 indicates the effect of increased viscosity on pump performance. There was no increase in the flow rate at low differential pressure; however pump performance dropped with increased viscosity with increased pressure drop. Interesting thing about it is performance was poorest at 9 cp. Flow rate gradually increased and tends to match with pure water curve with increased viscosity. Due to inherent instability of testing at 100 % GVF most of the tests Chan conducted are at 0%, 70%, and 95% GVF.

Jian Xu 2008 extended the work carried by Martin 2003. The previous model simulated the liquid slip. This model is able to simulate gas and liquid slip in the clearances. Thermodynamic modeling is included to simulate pressure as well as temperature profile along the screw. Model is validated with experimental data and

shows good match with data ranging from 0% to 99% GVF. Interestingly the pressure distribution prediction does not follow traditional approach. Curves become steeper from 50 % to 90%. However with GVF varying from 90 % to 98% the pressure profile moves towards linear. The model also includes performance prediction with liquids of different viscosities. Pressure distribution is shown in Figure 2.4.

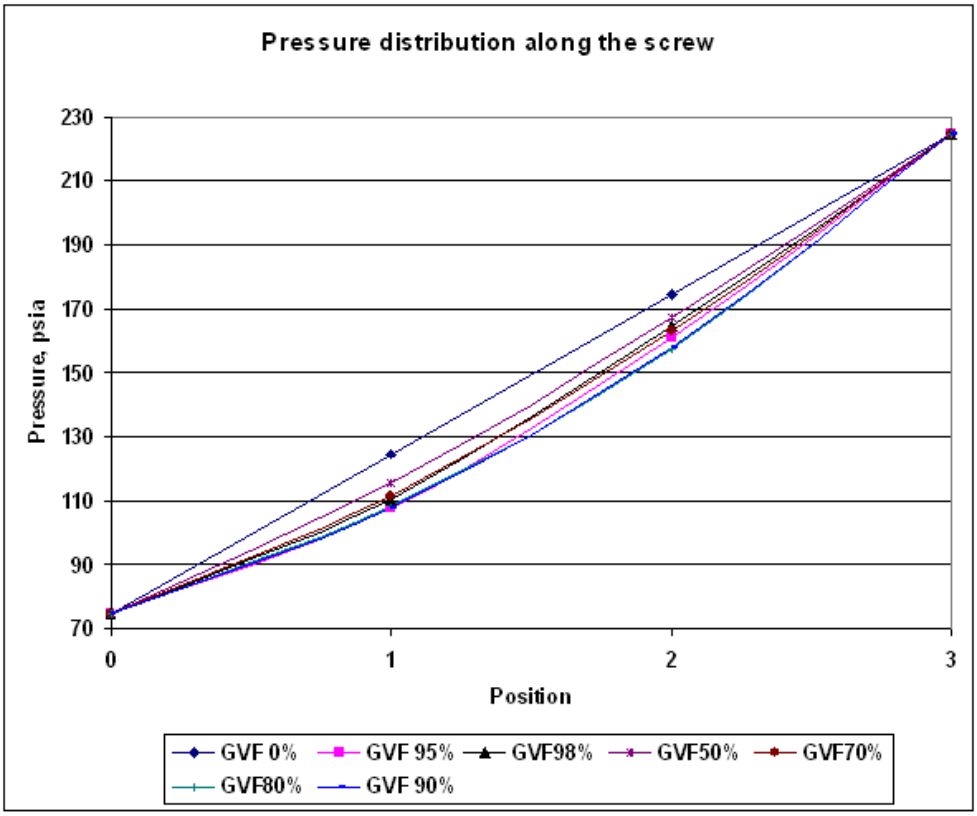

Figure 2.4: Pressure distribution along the screw (Jian Xu 2008)

Rabiger 2009 developed an analytical tool to simulate the twin screw-pump. It utilizes a fully coupled screw-pump model and heat transfer model which enables solid

liquid interaction, independent thermodynamic model and Navier-Stoke model to analyze leakage flow. The double threaded twin-screw pump was considered for this study. Inflow and outflow conditions are calculated to analyze the temperature and pressure profile along the axial direction for the "lifetime" of chamber. "Lifetime" here is referred to creation of chamber at suction till merging in to discharge. General equations of thermodynamics are used to determine inflow and outflow processes.

Heat transfer between liquid and gas phase occurs at interfacial areas between the two phases. Due to interaction, two phases are assumed to be in equilibrium. Heat flux is then set equal to heat transfer rate through the interfacial area. Leakage flow through the gaps is categorized as pressure driven multiphase compressible flow and the couette flow. The circumferential gap was modeled as a rectangular path with homogeneous flow. Decrease in temperature due to expansion is the resultant of compressibility of mixture. A homogeneous equilibrium model is used to calculate the variable gas density. Flow was represented by steady state mass, momentum and energy equations. A flow rate factor was introduced to account for eccentricity. Pressure profile predicted by this model agrees with non-isothermal model by Jian Xu 2008. Comparison between experimental and theoretical analysis showed satisfactory match.

Flow visualization tests at circumferential clearance were carried out by Rabiger 2009 at high GVF. Figure 2.5 shows fluid composition and quality inside chamber and clearance. The study shows fluid composition inside the clearance consists of two well mixed phases at high GVFs. There is little variation in the flow pattern inside the closed

chamber and clearance. The fluid composition inside the chamber is mainly affected by backflow from the clearance rather than the rotation of screw rotor.

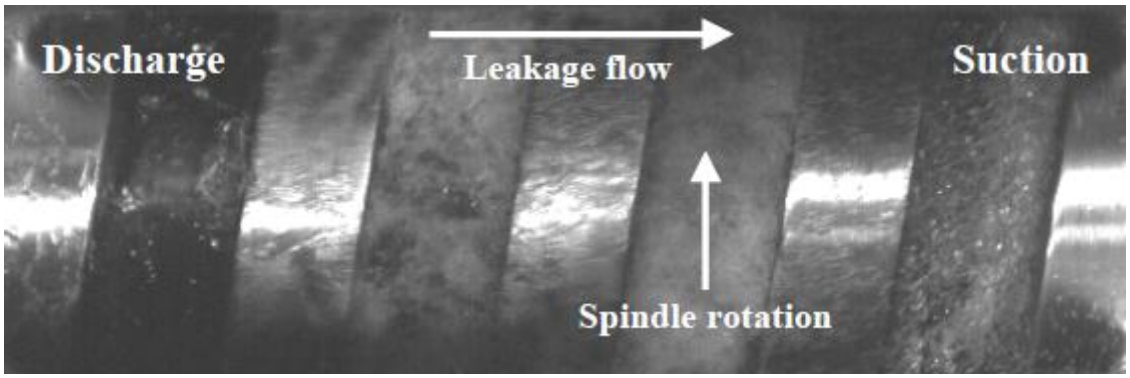

Figure 2.5: Leakage flow visualization through circumferential clearance at 2000 rpm and 90% GVF (Rabiger 2009)

2.2 Literature review on numerical modeling

There is a significant amount of literature available on multiphase twin-screw pumps pertaining to experimental testing and analytical modeling. Analytical models are mainly used to predict the performance in specific conditions only. Analytical methods are complemented with simplified assumptions which otherwise are far deviating from realistic conditions. Although significant research work has been published on the use of CFD in different fields, little has been written about CFD simulation of twin-screw pumps. The main reason behind this is the complexity of the pump design itself and the complicated fluid path inside the pump. Some CFD software offers the required facility to model moving mesh imposed with rotating boundary conditions. If modeled with

care, CFD methods can be used to predict the mean flow behavior inside the complex geometry of a twin-screw pump. Internal pressures, temperature and velocity distributions can be estimated along the machine. These data along with distribution of GVF can be used to set the benchmark about the complex flow behavior and provide the means to calculate the overall efficiency of the pump. Further it can also be used to form the relationship of GVF inside the pockets and GVF inside the clearances, and the slip velocity in the clearances.

By using CFD, characteristics of leakage flow can be highlighted, corrected and ultimately the size of the pump can be reduced. Reduced leakage flow will lead to increased overall efficiency which in turn will reduce the cost of developing the pumps by reducing the amount of time and money spent on experimental testing and further development of the pump. This section discusses the prior numerical work done on twin screw pumps/compressors.

2.2.1 CFD simulation of twin-screw pump:

The only work utilizing numerical simulations of a multiphase twin-screw pump is published by Beijnum 2007. A 3D model was created and leakage flow rate was predicted using a commercial CFD package. Leakage flows in the screw-pump were characterized using flow in an annulus with the cylinder rotating inside and the flow through stationary labyrinth seal. The Reynolds number was calculated using flow in the annulus. Comparison of the different turbulent models shows little effect on accuracy. Different types of dynamic mesh techniques such as smoothing, dynamic layering,

remeshing methods and Arbitrary Lagrangian Eulerian (ALE) formulation are discussed. However, those methods are very difficult to implement in the case of multidimensional problem. ALE formulation is recommended because of its simplicity. Figure 2.6 shows 3D meshed geometry. Flow through stationary twin screw pump was simulated with low differential pressures up to 9600 Pascal. Solution converged with the use of low under relaxation factors. Figure 2.7 shows the comparative study between numerical solution and analytical approach. At higher Reynolds number, the mean axial velocity of the numerical solution deviates from analytical approach. Leakage flow was simulated with different elongation of the screws in the axial direction. Leakage flow was observed to be increased with increase in elongation. The clearance between liner and screws (circumferential clearance) contributed the major portion of leakage flow.

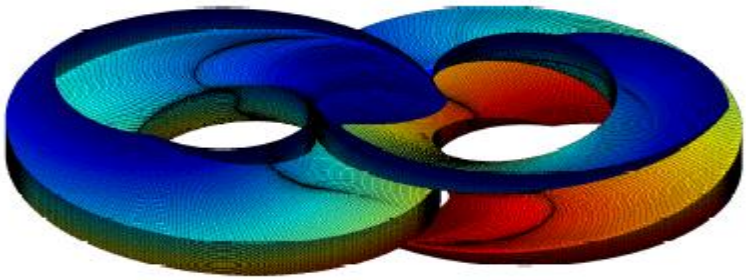

Figure 2.6: Three dimensional structured screw surface mesh for one thread of a twin screw pump (Beijnum 2007)

$\Delta p\ [Pa]$	$\dot{m}\ [kg/s]$	$\langle v_{ax} \rangle\ [m/s]$			Re	$\dot{m}_2\ /\ \dot{m}\ [\%]$
		eq. (2.4) $\delta_{io} = 0$	eq. (2.4) $\delta_{io} = 1.5$	numeric		
300	0.7	0.072	0.072	0.074	19	4.0
600	0.9	0.144	0.142	0.145	37	5.7
1200	1.4	0.29	0.28	0.277	70	7.0
2400	2.1	0.58	0.54	0.51	129	8.6
4800	3.2	1.15	1.0	0.90	227	10.8
9600	4.8	2.3	1.8	1.51	381	11.1

Figure 2.7: Water leakage flow rate for three dimensional stationary twin screw pump (Beijnum 2007)

2.2.2 CFD simulation of twin-screw compressors:

Demirdzic et al. 1994 demonstrated the applicability of unstructured moving mesh in coupled fluid flow, heat transfer and stress analysis problems. It can be used in solid body stress analysis and fluid flow analysis independently as well as in a coupled manner. The method is based on solution of an integral form of conservation equations which are satisfied if the problem is solved on moving mesh. Mass momentum and energy is balanced on numerical mesh of finite number of contiguous volumes of arbitrary topology. All dependent variables are stored in the geometric center of control volumes, and a set of nonlinear equations are solved using SIMPLE.

Kovacevic et al. 2000 modeled dynamic flow losses in a screw compressor suction chamber using CFD. A numerical grid was generated using 2D transfinite interpolation, also combined with layer meshing scheme. Standalone CAD-CFD interface was used to produce 3D grid of the suction chamber. Finite volume code COMET was used to obtain the numerical solution. The solution predicts the dependability of dynamic flow losses on fluid flow in the suction chamber.

Stosic et al. 2002 performed screw compressor design optimization procedure using analytical algorithm for profile generation coupled with hydrodynamic and thermodynamic processes within the machine. Multivariable optimization is performed against the compressor specific power. Three distinct profiles were calculated with lowest compressor specific power as an optimization criterion. Model also included the oil injection, fluid flow process and thermodynamic process.

Kovacevic et al. 2004 analyzed screw compressor performance using 3D numerical simulation. Screw compressor domain was divided into number of cross sections along the rotor axis and then each cross section is meshed using transfinite interpolation technique. Oil injected screw compressor model was designed and developed for which a numerical model is built. Flow was described using mass averaged equations of continuity, momentum and energy accompanied by turbulent model equations. Commercial tool comet was used to simulate the flow. Oil is treated here as passive fluid and energy balance equations for two phase flow were presented. Forces are calculated based on pressure in each chamber multiplied by corresponding cell area. Subsequently, torque and compressor power transmitted are calculated. Compressor efficiency was calculated as a ratio of actual volumetric flow rate to theoretical flow rate. Results agree well with experimental data.

Compression of gas induces large pressure differential and the increase in temperature in the screw compressors which leads to the leakage flow through clearances and deflection of the rotor. Effort has been continuously made to reduce the clearances. This makes it necessary to understand the interaction between the fluid flow

and rotor deflection. Kovacevic et al. 2004 addressed solid fluid interaction in the screw compressor. A 3D numerical procedure is presented to model both fluid and solid domain. Figure 2.8 shows numerical mesh. A commercial solver is used to analyze the fluid flow and solid deformation simultaneously. Results show deformation of the rotor due to large pressure differential (Figure 2.9) and enlargement in the rotors due to increase in the temperature. Deflection causes change in clearances resulting in increased back flow. Rotor enlargement causes decreased backflow path which results in increased efficiency.

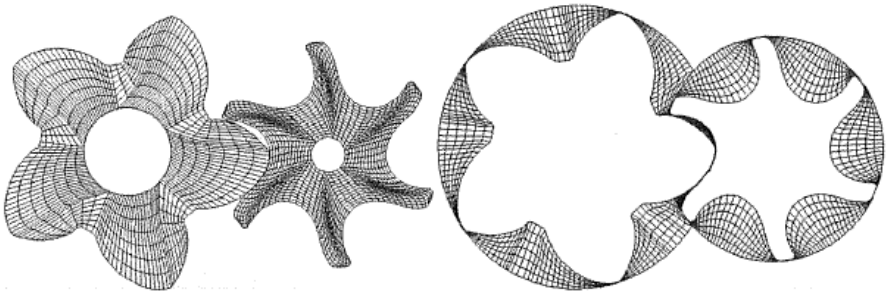

Figure 2.8: Numerical mesh for rotors and fluid domain (Kovacevic et al. 2004)

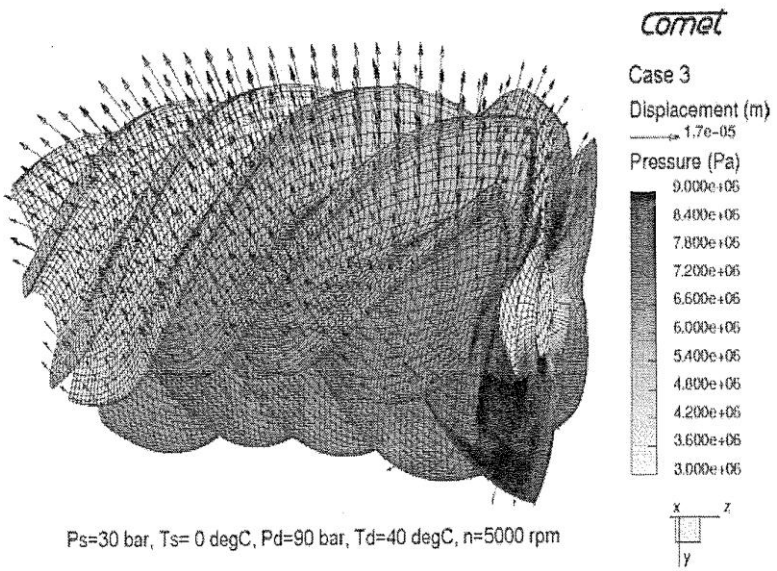

Figure 2.9: Deformation of high pressure compressor (Kovacevic et al. 2004)

Fryc and Vimmr 2006 presented 2D numerical simulations of air flow in clearance gaps between the rotor and housing of a screw compressor. The rotor is assumed to be stationary with ideal gas assumption. Three different turbulent models namely, Baldwin-Lomax, Spalart-Allmaras and k-epsilon are used and compared. All the models predict agreeable results without shockwave. The value of mass flow rate varies slightly based on selected numerical method. The authors also analyzed grid dependence of the models with k-epsilon being more grid dependent and took more time for computation. Vimmr and Fryc 2006 extended the current work by imposing the rotation to the rotor. Computations are performed in the moving reference frame using moving mesh concept. Results in Figure 2.10 show speed rotation doesn't have significant effect on the resulting velocity flow field.

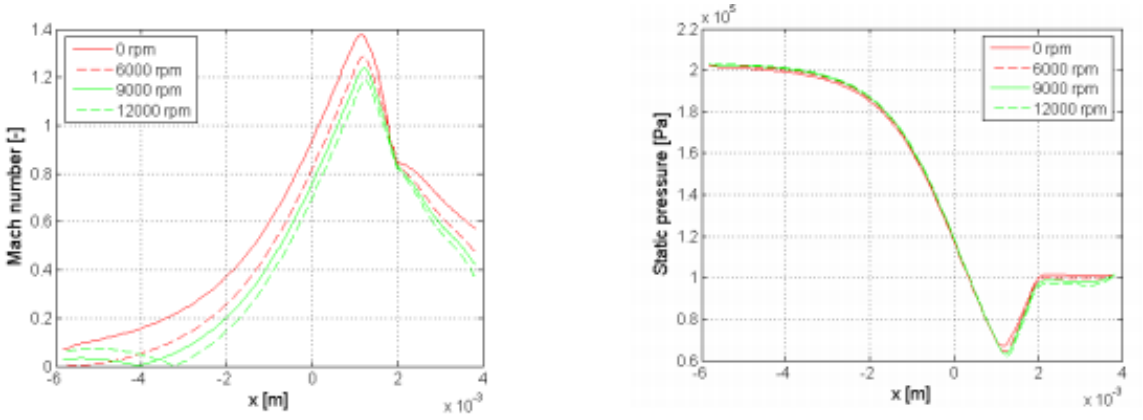

Figure 2.10: Mach number and static pressure distribution for different speeds (Vimmr and Fryc 2006)

Kovacevic et al. 2010 performed Laser Doppler velocimetry to measure mean and fluctuating velocity fields in the screw compressors. A transparent window made up of acrylic was built for optical access in the chamber. The following observations are made. Velocity variation is seen more near the leading edge of the rotor and varies by 10 % from one chamber to another. The velocity field at the discharge is complex and unstable with very steep velocity gradients near the leading edge of rotor. The axial velocity distribution in the discharge port strongly depends on rotor angular position since the rotor periodically covers and uncovers the discharge chamber from fluid pocket.

3 MISSION STATEMENT

Twin screw pumps are a relatively new technology with lots to explore. This raises the question about reliability of the pump. This research aims to understand all round aspects of twin screw pump which will help make it economically feasible, and attractive to the oil and gas industry. The first phase of this work will evaluate the performance of multiphase twin screw pump under different operating conditions. Performance will mainly be characterized based on leakage flow rate, mechanical efficiency and effectiveness; their interdependence, and the factors affecting them. The following issues are addressed

- Experimental testing under Gas Volume Fraction (GVF) ranging from 50% to 100% at different differential pressure.
- Transient response of the pump under high GVF to study thermodynamic effect of gas compression on pump performance.
- Effect of viscosity on leakage flow rate.
- Comparative study of two different pumps with different recirculation design and theoretical flow rate.
- At high GVF, a multiphase pump works like compressor. Theoretical analysis is performed based on the thermodynamic processes and experimental data to compare the performance of the multiphase pump with the isentropic compressor.

The nature of a multiphase mixture changes drastically over the time and sometimes GVF varies from 0% to 100%. Pumps mostly used to handle this range of

GVF are positive displacement pumps and helicon axial pumps. Each type is effective for a particular flow case however, special design of twin screw pump permits handling of a wide range of GVF. However minimum liquid required for sealing the clearances must be recirculated for efficient performance of pump. Most of the vendors claim that their twin screw pumps can handle 100 % GVF, but they may or may not include recirculation liquid in their claim (Hua 2012). This study will establish the method (originally suggested by Jun Xu, Shell) to evaluate the optimum recirculation flow rate of liquid required to effectively seal the leakage path.

Until now, the nature of two phase flow in the clearances has been obscure with varying GVF. Previous work by various researchers assumes complete liquid sealing for GVF up to 85% and gas infiltration through the clearance beyond GVF greater than 85% with homogeneous two phase mixture. It would be more realistic if the flow is treated as two separate phases with different velocities and temperatures. Detailed consideration of different superficial phase velocities will increase the accuracy of leakage flow and help understand the effect of GVF at inlet on subsequent clearance backflow. Detailed study of two phase leakage flow by simulating two-phase mixing, separation, heat transfer and swirling is made possible using CFD simulation. The present study undertakes three-dimensional CFD simulation of two phase flow at 50% GVF. Grid independence and suitable turbulent model will be evaluated. Internal pressures, velocity, GVF distributions and their effect on leakage flow will be estimated along the machine. The model will be simulated at different operating speeds and pressure rise conditions. Numerical results will be validated with experimental results.

The next phase of research highlights a flow visualization study and transient variation of different parameters inside a clear twin screw pump. Leakage flow visualization along different clearances is observed at different GVF and operating speeds. This gives more accurate and quantitative information about phase composition and fluid velocities inside the clearances. Flow visualization study also serves as a benchmark tool for the numerical results obtained through CFD simulations. Furthermore a flow visualization study will help understand the relationship between GVF at the inlet and GVF in the clearances. Transient analysis which consists of study of pressure field in different fluid pockets as well as clearances concludes the work.

4 THEORY OF MULTIPHASE TWIN-SCREW PUMP

4.1 Volumetric flow capacity of twin screw pump

Multiphase twin-screw pumping technology is one of the widely used solutions for multiphase production in the oil and gas industry. Conventionally it was used in the process industry for polymer processing and pumping highly viscous fluids in food and chemical industries.

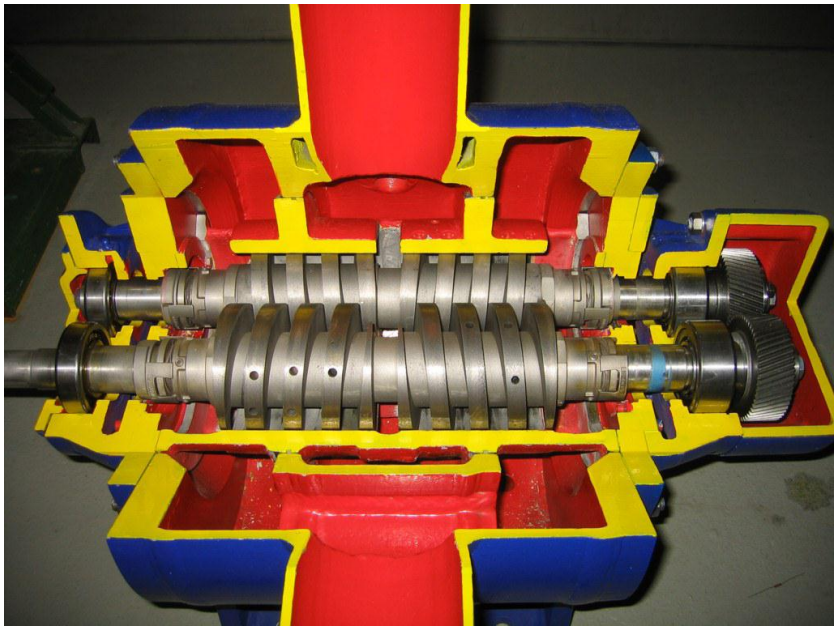

Figure 4.1: Cutaway of multiphase twin-screw pump (Chan 2006)

As the name indicates the main components of a twin-screw pump consist of two counter rotating screw rotors positively displacing the fluids. One of the rotors is directly connected to the drive motor and another rotor is driven by the means of timing gears as

shown in Figure 4.1. Two rotors are encased by a liner with very tight clearances. This type of arrangement avoids direct contact between the two rotors and the rotor liner thereby avoiding the wear of the pump even in the worst loading condition, true especially when pumping unpredictable GVF. Existing twin-screw pumps employ dual intake single exhaust flow system as shown in Figure 4.1. Configurations like this axially balanced the screws with opposite forces canceling each other from both sides. The screw rotor meshes together retaining a limited clearance while rotating freely inside the liner housing. This causes vacuum pressure enabling the fluid to flow towards the pump. Fluid is positively transported through C-shaped cavities (Figure 4.2) which move axially from inlet to the discharge. Because of low axial velocity of the fluid through cavity, twin-screw pumps are very gentle and there is low shearing of fluid being pumped.

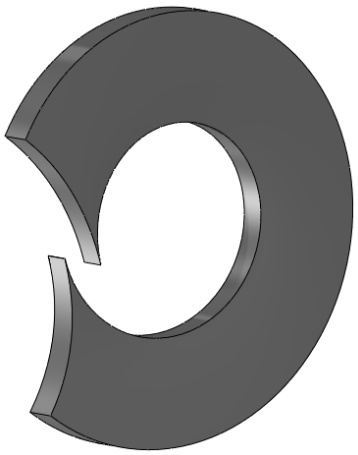

Figure 4.2: Fluid path (chamber) created by the meshing of screws

Figure 4.3 shows the single side of meshing counter rotating screws. Following geometric parameters are necessary to define the theoretical capacity of twin-screw pumps.

Pitch (P) is the distance between two end points for one complete turn of the screw. Screw length (l_s) is the length of one set of screw, Root diameter (D_r), and External diameter (D_e). Displacement volume (D) is purely geometrical term defined as the volume of fluid displaced with one rotation of screw.

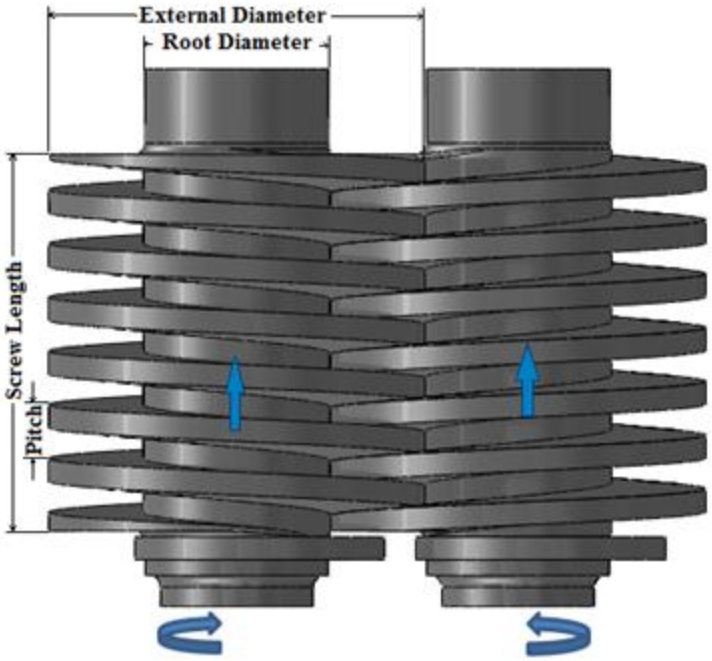

Figure 4.3: Geometric parameters of twin-screw pump

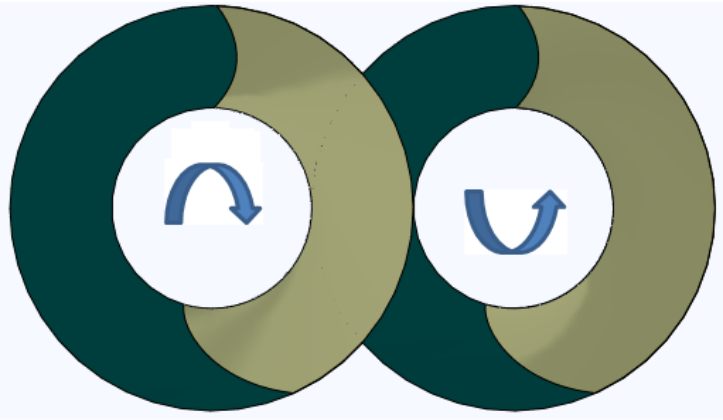

Figure 4.4: Cross section of twin-screw pump

Figure 4.4 shows the cross section. The dark area corresponds to the fluid between the screws and casing. This area remains constant along the axial direction at each pitch distance. Same cross section ensures smooth fluid delivery of the fluid. The displacement volume can be defined as

$$D = A \times \mathrm{P} \tag{4.1}$$

Theoretical flow rate (Q_{th}) is the product of theoretical volume displaced per revolution and the speed

$$Q_{th} = D \times N \tag{4.2}$$

However, with the clearances present between screws and liner there is slip from outlet to inlet driven by pressure differential. Since the clearances are important in order to avoid direct contact between the screw-screw and screw-liner, the actual flow rate is less than the theoretical flow rate. With the clearances present, there is steady rise in pressure along the axis of the rotor which prevents the excessive deflection of rotor due to imbalance in the radial forces. Small clearances reduce the leakage flow rate and

improve the volumetric efficiency. However, it may lead to higher friction losses in case of viscous fluids and possibly metal to metal contact in a case of heavy loading. The designer needs to choose a compromise between clearance sizes to obtain an optimized performance and the pump life.

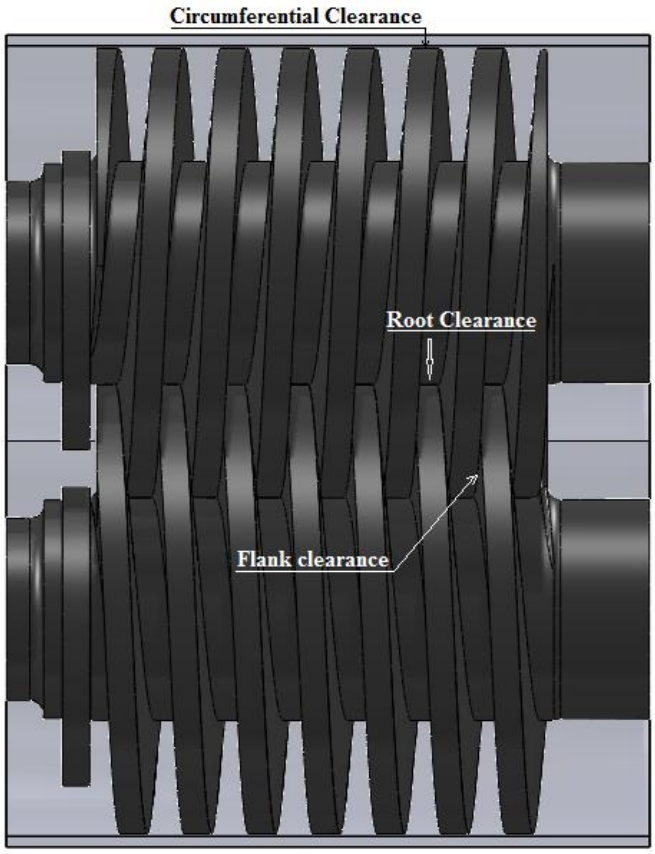

Figure 4.5: Different clearances between screw rotors and liner

Figure 4.5 shows different locations in the pump where leakage flow occurs. The location between screw rotors and liner is called as circumferential clearance and by far the most important one as around 80 % of total leakage flow is contributed by circumferential clearance in the case of double threaded screws (Vetter and Wincek 1993). Flank clearance is the gap between flanks of screw rotors which contribute about 5 % of total leakage flow as observed by Wincek. Root clearance is located between outer diameter of the screw and root diameter of another screw. It contributes around 15 % of total leakage flow. In the case of single threaded screws, the combination of circumferential clearances and flank clearances contributes more than 85 % of the leakage (Xu 2008).

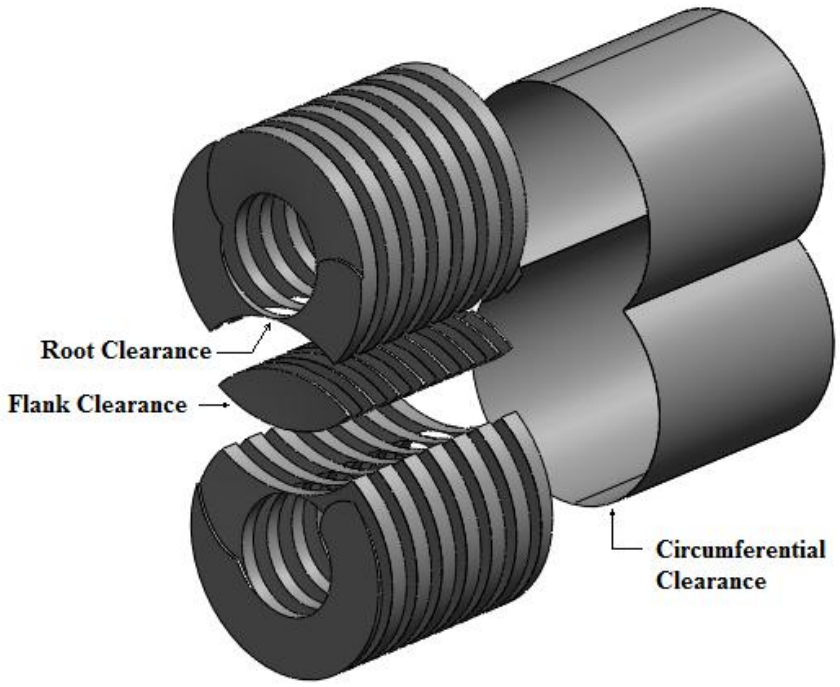

Figure 4.6: Fluid path formed due to intermeshing of screws

Figure 4.6 shows segregated structure of fluid continuum in the twin-screw pump. The actual flow rate of the pump is now the difference between theoretical flow rate and leakage flow through clearances.

$$Q_a = Q_{th} - Q_{leakage} \tag{4.3}$$

Volumetric Efficiency (η_v) is the ratio of actual flow rate to theoretical flow rate.

$$\eta_v = \frac{Q_a}{Q_{th}} \tag{4.4}$$

4.2 Mechanical efficiency and effectiveness of the multiphase twin-screw pump

Efficiencies of the pump are defined in different ways in different studies. In general, mechanical efficiency is defined as the ratio of power delivered to the fluid to transfer it from inlet to exhaust to the power input to the pump. Power input to the pump is the drive power and defined as

$$P_{drive} = M \cdot \omega \tag{4.5}$$

In the direct sense drive power is nothing but electrical power supplied to motor to run the pump. Therefore, this work utilizes electrical power supplied as P_{drive}. Drive power is further divided in to power used in conveying the fluid (P_{fluid}) and the power lost due to the friction ($P_{friction}$). P_{fluid} is further resolved in to power actually spent on pumping the multiphase mixture (P_{net}), and the power lost in leakage flow through clearances ($P_{leakage}$). $P_{friction}$ is the sum of friction incurred due to viscous and turbulence effects, and the friction due to mechanical losses in the components of the pump.

$$P_{drive} = P_{fluid} + P_{friction} \quad 4.6$$

$$P_{fluid} = P_{net} + P_{leakage} \quad 4.7$$

$$P_{friction} = P_{visc,turb} + P_{Mechanical\ losses} \quad 4.8$$

Actual power (P_{net}) has two components, liquid power (P_l) and gas power (P_g). P_l is the actual work done in moving the liquid (including sealflush fluid) from suction pressure condition to the discharge pressure condition. It is expressed by

$$P_l = Q_l \cdot \Delta p \quad 4.9$$

where Δp is pressure difference across the pump, and Q_l is volumetric flow rate of liquid. Gas flow rate is characterized by a compressible process. Basic principles of thermodynamics are used to characterize two phase flow in the twin-screw pump. Temperature, pressure and volume are the main parameters which affects compression process in the multiphase pumps. A change in any of these variables changes the performance of the pump.

An energy balance is utilized to evaluate the work requirement of multiphase twin screw pump operating from 0 % to 100 % GVF. Their design is such that change in potential energy head and kinetic energy head is negligible. Work performed is defined as the product of force by distance and to evaluate the work, path of compression process must be known. The working of the twin-screw pump with varying GVF plays a decisive role in deciding whether it is isothermal, polytropic or adiabatic.

While running the pump it was observed that temperature rise is a function of GVF with the process being close to isothermal for low GVF and becoming polytropic

with increase in gas content. Starting from any given temperature, there was a consistent rise in temperature proceeding towards ideal discharge temperature for adiabatic case. Process at high GVF can be modeled as polytropic process and represented as

$$dP = Vdp \tag{4.10}$$

P is the work performed, V is volume and p is absolute pressure.

Using $pV^n = constant$ due to the polytropic nature of the pump, work done for polytropic case can be obtained as

$$P_{poly} = \frac{n}{n-1} p_{inlet} V_{inlet} \left[\left(\frac{p_{outlet}}{p_{inlet}} \right)^{\frac{n-1}{n}} - 1 \right] \tag{4.11}$$

where the pressures are expressed in absolute values since the ideal gas law was used to derive the equation. For value of $n = \frac{C_p}{C_v}$, above formula give theoretical adiabatic HP.

For low GVF, the temperature rise through pump is very small, so the system can be treated as isothermal. Equation 4.10 becomes

$$P_{isothermal} = p_{inlet} V_{inlet} \ln \left[\frac{p_{outlet}}{p_{inlet}} \right] \tag{4.12}$$

In order to evaluate the actual performance of the pump, an ideal condition of the pump is defined. Hydraulic power of the pump is power imparted to the multiphase mixture to overcome the same pressure differential if it were a single phase liquid. Hydraulic power is the ideal power which can be used to set the benchmark in term of effectiveness of the pump which compares actual performance with the ideal performance of the pump.

$$P_{hydraulic} = (Q_l + Q_g) \cdot \Delta p \tag{4.13}$$

Volumetric efficiency (η_{vol}) represents the ability of the pump to transport multiphase mixture flow against leakage flow rate. Leakage flow rate also represent the hydraulic load balancing by linearly distributing the pressure along the axis for single phase flow, and sealing the gas in case of multiphase flow.

$$\eta_{vol} = \frac{Q_{actual}}{Q_{th}} = \frac{Q_l + Q_g}{Q_l + Q_g + Q_{leakage}} = \frac{P_{hydraulic}}{P_{fluid}} \tag{4.14}$$

Pump effectiveness ($\eta_{effectiveness}$) can be seen as the ability of the pump to impart the power to multiphase fluid as compared to the power delivered to single phase liquid. Ability of the pump to compress the gas degrades as the liquid content in the multiphase mixture goes down. This can be represented as

$$\eta_{effectiveness} = \frac{P_l + P_g}{P_{hydraulic}} = \frac{P_{net}}{P_{hydraulic}} \tag{4.15}$$

Mechanical Efficiency (η_{mech}) represents friction losses incurred due to viscous and turbulence effect in the cavities as well as different clearances, mechanical losses due to friction inside bearings, seals, and gears. It is the true measure of pump performance about what has been spent and what the outcome is.

$$\eta_{mech} = \frac{P_l + P_g}{P_{drive}} = \frac{P_{net}}{P_{drive}} \tag{4.16}$$

5 EXPERIMENTAL FACILITY

This chapter highlights the experimental test rig set up and multiphase facilities available at the Turbomachinery Laboratory at Texas A&M University. Resources available at the Turbomachinery Lab make it an ideal location to perform multiphase flow analysis in rotating machinery. Two twin-screw pumps were tested with different sizes and different flow rate capacity. Although pumps were tested in ideal conditions with mixtures of air and water as multiphase fluid, data obtained from this testing represents the benchmark performance of the pump operating under different operating conditions and agrees well with the real life performance of the pump.

The first pump to be tested was a 60 HP, 230 gpm twin-screw pump with internal sealflush recirculation designed for multiphase flow by Leistritz Corporation. The main purpose of evaluating this pump in the current study is to observe the transient behavior of the pump under very high gas volume fraction, and the effect of seal flush recirculation fluid using different viscosity fluids. The second pump to be tested was an external sealflush recirculation, 200 HP, 633 GPM, multiphase TSP by Colfax Corporation. Steady state as well as transient analysis was performed and its performance was compared with the Leistritz TSP pump. This section describes the design of the test rig for the MR-200 multiphase twin-screw pump. The Leistritz pump is discussed in a subsequent section.

Facilities at the Turbomachinery Laboratory allow easy installation and modification of the test rig. This section describes the resources available, system

infrastructure set up, data acquisition, and instrumentation used to investigate MPP technology.

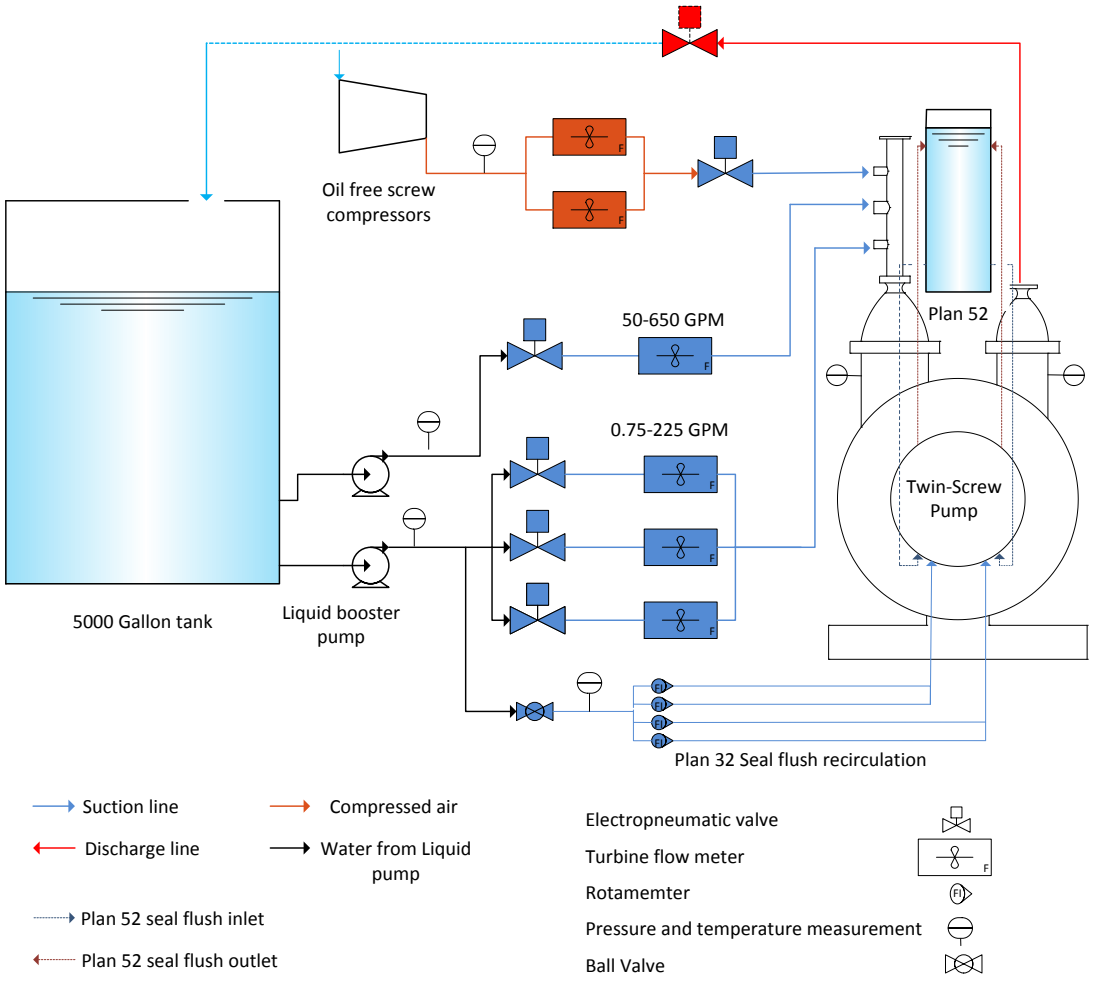

Figure 5.1: Flow loop diagram of Colfax MR-200 twin-screw pump

Figure 5.1 shows the circuit diagram of the system flow structure. The water flow loop consist of two booster pumps with capacities of 135 GPM and 550 GPM

respectively at 120 psig. The flow rate of the water is controlled using electro-pneumatic valves. The air flow loop consists of oil free screw compressors with a common reservoir. An uninterrupted supply of pressurized air ensures the smooth running of the pump and avoids any back flow during the breakdown of conveyance. Compressed air from the reservoir is controlled by the mean of an electro-pneumatic valve. The air and water flow rates are independently measured using turbine flow meters before mixing inside the intake manifold just above pump inlet. The multiphase mixture is then transported against differential pressure from inlet to exhaust and back to the water tank by the means of the multiphase twin-screw pump. Water is recirculated back to inlet and air escapes to atmosphere.

The water flow loop consists of a 5000 Gallon water tank and two booster pumps with 135 GPM and 550 gpm capacity respectively. Booster pumps supply water at 120 PSI maximum pressure. Pressure is held constant using a back pressure regulator. The flow rate of water is controlled by the means of electro-pneumatic valves which are operated by 4-20 mA input supplied by NI-9205 module. Four different flow meters are used to monitor and record the varying water flow rate with overlapping capacity which completes the requirement of multiphase twin screw pump operation at varying GVF.

The air flow loop consists of three oil free screw compressors with 150 PSI capacity. Supply air pressure available at the inlet of test chamber is usually 120-130 PSI which is sufficient to fulfill the current requirement. Two turbine meters of overlapping capacity are connected in parallel. Air flow rate is controlled by the means of an electro-pneumatic valve operated by 4-20 mA. A pressure transducer and temperature

thermocouple are installed just before the flow meters. Sensor data and control valve operation are monitored and controlled from the LabVIEW program. Water being incompressible, the water control system serves to control the flow rate of water while flow rate of the air is used to control the pump inlet pressure, consequently air control system controls the pressure of the air and holds it at constant desired value. Air and water from each channel enters into the suction manifold where it mixes at constant pressure. A pressure relief valve is installed to ensure safe operation of the pump. Pressure and temperature data are recorded at the inlet of the pump.

A Twin-screw pump displaces the fluid against a differential pressure. An electro-pneumatic valve operated by a 4-20 mA input is used to generate the required exhaust pressure to match the real life operational environment. The pressure is manually controlled by sending the required signal since the exhaust flow rate is pulsating due to the nature of operation.

Speed control of twin-screw pumps has always been a challenge in subsea applications. Variable Frequency Drives (VFD's) are mainly used in traditional systems. VFD in the field must be able to handle varying condition of load and GVF. The VFD used to control the speed of the twin-screw pumps supports 200 HP AC motor with 5 to 60 HZ frequency.

5.1 MR-200 Colfax multiphase twin-screw pump

The MR-200 pump under investigation is 200 HP, multiphase twin-screw pump by Colfax Corporation with rated capacity of 633 GPM as shown in Figure 5.2. The pump is factory tested with 750 PSI differential pressure.

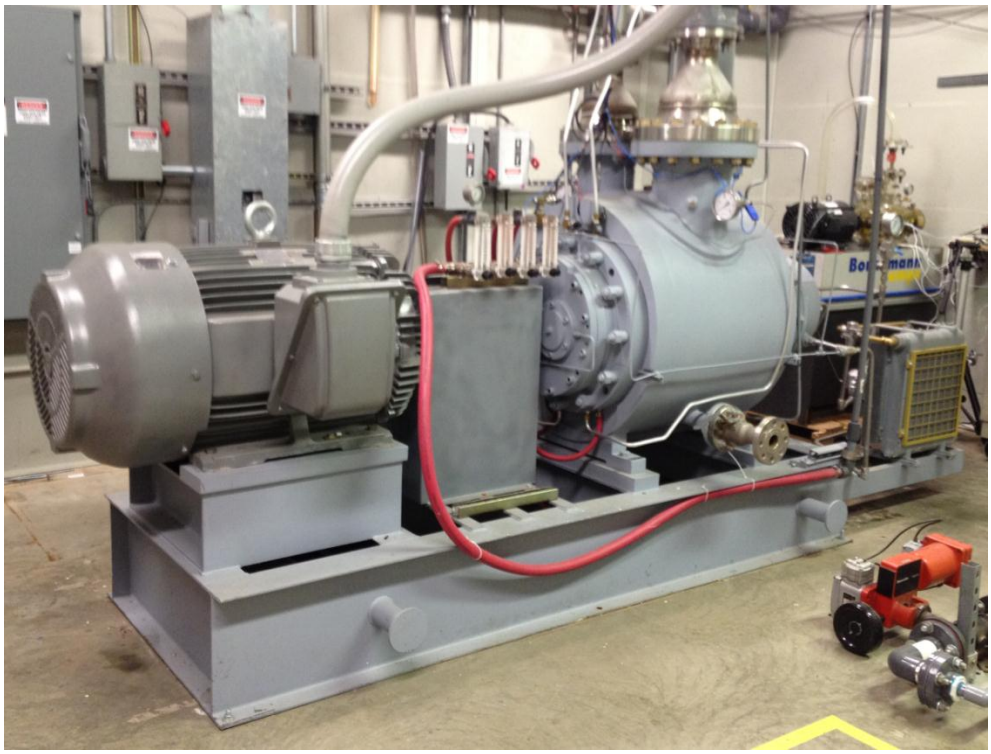

Figure 5.2: MR-200 Colfax multiphase twin-screw pump

The pump uses four; single cartridge type of mechanical seals at the end of both screws. Generally, seal selection depends on properties of the working fluid, temperature and operating conditions. Safe operations of mechanical seals require external recirculation of seal flush fluid. The pumps employ API plan 32 which requires external

source of water supply with at least 1 bar higher than suction pressure. Fluid used in plan 32 passes over seal faces entering inlet of the pump.

A second type of circulation system follows API Plan 52. It is based on principle of natural convection with water recirculation occurring due to density difference. Non-pressurized external reservoir with10 Gallon capacity is mounted on pump. Buffer fluid from reservoir is supplied between lip seal and seal faces.

5.2 Leistritz pump

Figure 5.3: Leistritz pump assembly

The Leistritz multiphase twin-screw pump as received is shown in the Figure 5.3. It is rated at 60 HP, 229 gpm capacity. Sealflush fluid is fed by liquid recirculation provided on the skid. The main difference between the Colfax twin-screw pump and the Leistritz pump was the methodology to provide liquid recirculation at high GVF for sealing the gaps as well as cooling the seals. The Leistritz pump employed a close loop recirculation with 6% sealflush liquid supplied from a 50 Gallon boot tank driven by exhaust pressure (Figure 5.4). Sealflush flow varied from 6 to 25 GPM based on pressure differential across the pump. Flow across the seal flush can be optimized using a needle valve.

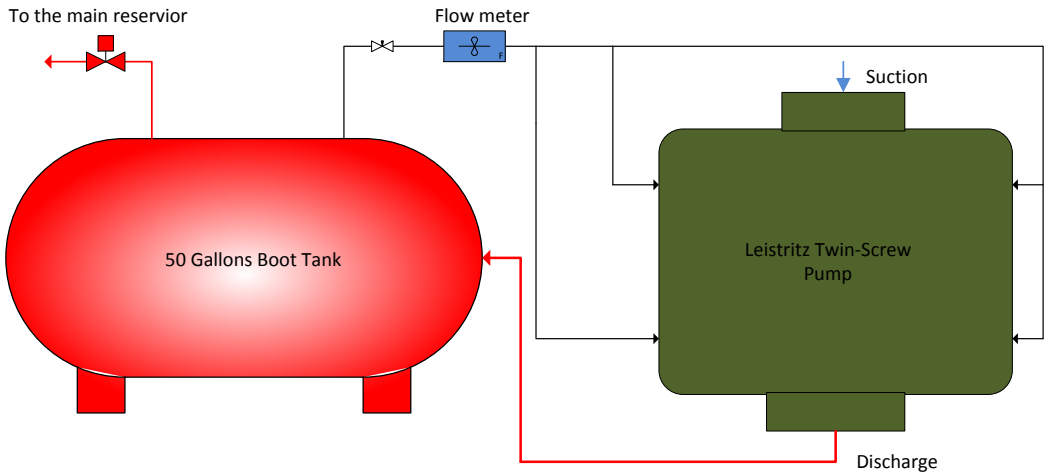

Figure 5.4: Sealflush recirculation system in Leistritz

The Colfax pump has complex geometrical design with a reservoir built around the liner of the pump with a 0.07 mm concentric slit connecting from exhaust to suction.

Analysis of the fluid flow through this slit becomes important in order to calculate the true GVF at the inlet.

5.3 Effect of temperature rise due to gas compression

A twin-screw pump operating at high gas volume fraction behaves like a compressor and thermodynamic issues arise with the compression of gas. The gas compression process changes from isothermal to isentropic depending on the value of GVF and the pumps mechanical process. In the existing systems, at high GVF, sealflush recirculation liquid is used to seal the chambers. This liquid will absorb some of the heat of compression. As seen from previous work (Neumann 1991), twin-screw pump performance deteriorates with rise in temperature due to decreased volumetric efficiency. This work studies the effect of temperature rise on wet gas compression for extended period of time and varying pressure rise.

5.4 Effect of liquid viscosity on pump performance

The Leistritz pump transient performance is evaluated at 100% GVF for an extended period of time with different viscosity of the seal flush fluid. Guar gel is used to increase the viscosity of the fluid. The guar gel is non-Newtonian pseudoplastic fluid and viscosity can be represented as a function of shear rate.

$$\mu = K(\gamma)^{n-1} \qquad 5.1$$

K is the flow consistency index while *n* is the flow behavior index. Chan 2006 used data from a viscometer to calculate the value of *n.* The gel exhibits power law behavior. Liquid becomes more non-Newtonian as gel concentration is increased. Different apparent viscosity concentrations were obtained by mixing the measured quantity of guar as suggested by Halliburton, supplier of the guar gel.

5.5 Instrumentation and Data Acquisition

To measure the pump performance and flow characteristics of the pump, different types of sensors, flow meters and control valves are used and integrated into an NI platform of data acquisition cards. LabVIEW is used for PID control of the flow rate at the inlet, manual control of pressure at the outlet, and data recording at different points of the flow loop. The graphical User Interface by LabVIEW is shown in the Figure 5.5. The left side of the GUI enables the user to monitor and record the data. The right side is the control panel and mainly allows the user to control the parameters at the inlet and outlet of the pump.

Figure 5.5: LabVIEW front panel for monitoring, recording and controlling the parameters

Experimentally measured values can be biased due to the reliability and accuracy of the measurement system. The following section enlists various types of sensors and different modules of data acquisition systems with associated accuracy.

Pressure Sensors: Solid state pressure sensors from Omega PX-481 A series were used. Input: 9-30 VDC, Output: 1 to 5 VDC. Sensors used are enlisted in Table 5.1.

Table 5.1: Pressure sensors used in experimental testing

Location	Principle	Manufacturer	Accuracy	Range
Air Inlet	Solid State	Omega	0.3 %BFSL maximum	0-200 PSI
Pump Inlet				0-200 PSI
Pump Exhaust				0-500 PSI
API plan 32 Inlet				0-200 PSI
API plan 52 Outlet				0-200 PSI

Temperature Sensors: T-type thermocouples from Omega were used to measure the temperature. They are constructed with 304 stainless steel sheath with $1/8^{th}$ and $1/16^{th}$ inch ungrounded probe diameter which provides low thermal mass for the given application. They are integrated with NI 9213 with built in CJC which converts voltage potential to temperature in the LabVIEW reading. Accuracy of thermocouple is ±0.22 F.

Flow meters: Turbine blades inside the flow meter rotate as flow passes through it. Rotation is proportional to the flow velocity. As each turbine blade passes through the magnetic field generated by the meters magnetic pick up, an AC voltage pulse is generated which is proportional to volume flow rate of air. The same principle is used in both, air and water flow meters. Table 5.2 shows details of different flow meters used in test set up.

Table 5.2: Flow meters used in experimental testing

Type	Manufacturer	Accuracy	Repeatability	Range
Air flow meters	Daniel Industries	1%	0.1%	10-100 ACFM
	Omega FTB-935			2-28 ACFM
Water flow meters	Omega FTB-933			40-650GPM
	Daniel Industries			25-250 GPM
	Omega FTB-1425			5-50 GPM
	Omega FTB-1422			0.75-7.5 GPM

Different types of NI models were used to record and control the parameters in the flow loop. The modules 9205, 9213, and 9265 were integrated on NI 9172 chassis and programmed in LabVIEW for execution. Analog to digital conversion took place at 1000 samples/second.

Module 9205 is used to acquire data from various pressure sensors, VFD drive, and the photoelectric sensor to measure the speed at $\pm$10V. Absolute accuracy of NI 9205 is 6230 μV.

Module 9213 with a built in cold junction is used to acquire thermocouple data. Accuracy of this module depends partly on thermocouple type and accuracy, the temperature being measured, and the cold-junction temperature.

Module 9265 is used to control the electro-pneumatic Masoneilan valves for flow control. 4-20 mA is used to operate the valves. High sampling rate of this module enabled successful implementation of PID control for the air flow.

6 COMPUTATIONAL FLUID DYNAMIC ANALYSIS OF TWIN-SCREW PUMP

CFD has proven its capability for the analysis of centrifugal machines. Its ability to represent the flow domain within the pump helps optimize the design and hence the output of the pump. CFD simulation of a twin-screw pump possesses significant challenge due to the complex flow path and complexity of its operation. This work represents the attempt to evaluate single and 2-phase flow analysis inside the twin-screw pump.

A solid model provided by Colfax with little modifications due to error in the assembly of screws was used to generate the flow field geometry. Circumferential and root clearances were unaffected while there was some change in flank clearances. Edited geometry is exported to Gambit 2.4.6, an ANSYS product. This mesh is then transported to Fluent 13.0, an ANSYS solver used for CFD analysis.

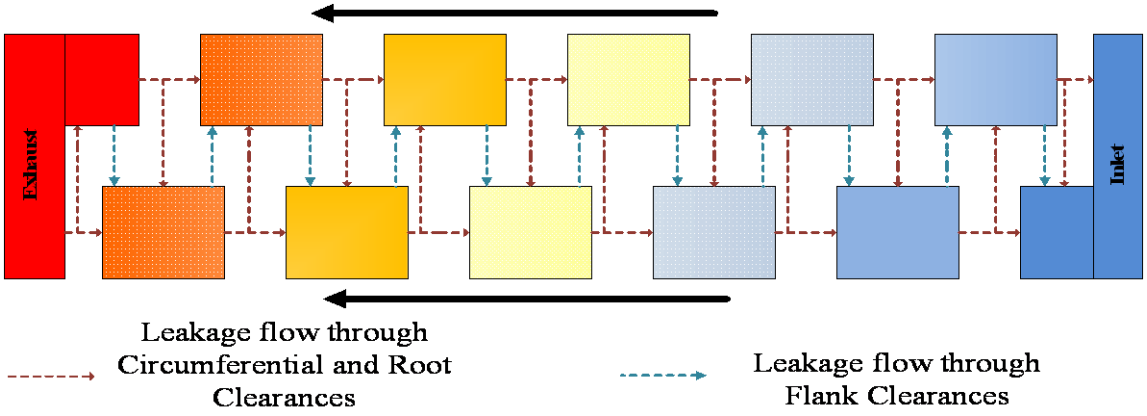

Figure 6.1: Simplified leakage flow path through different clearances for single threaded twin-screw pump

The simplified structure of the leakage flow path between different clearances from inlet to exhaust is shown in the figure 6.1. Due to the complex flow structure, a fine mesh is required at some critical places. To make the model solvable by a super micro PC, the number of elements needed to be kept to minimum while making no compromise on the quality of the grid. The flow path was divided in to three main categories, namely fluid pockets, circumferential and root clearances, and flank clearances. Circumferential and root clearance zone was meshed using hexahedral elements with 100 % structural mesh, while flank clearances are characterized by combination of structured and unstructured mesh. Fluid pockets are meshed with hexahedral elements with the unstructured cooper meshing scheme. 6.7 million nodes are generated before any adaption (Figure 6.2). Skewness is shown in Figure 6.3.

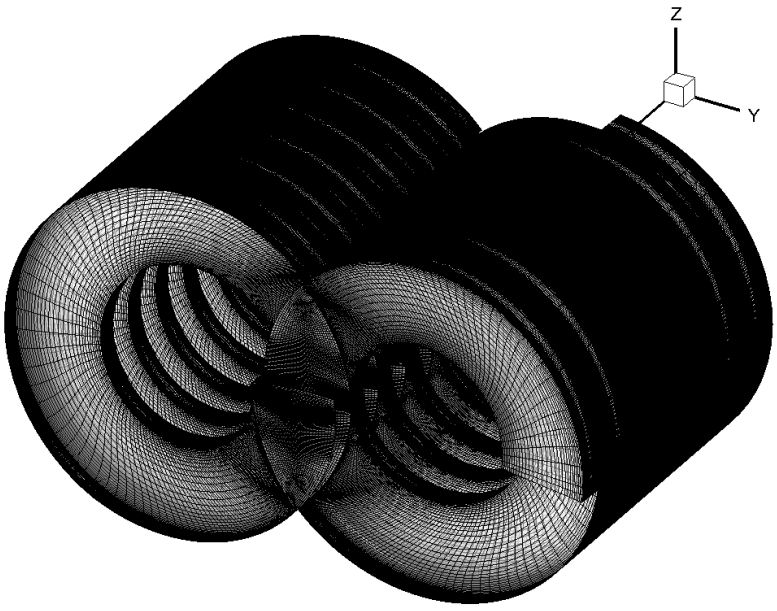

Figure 6.2: 3D Mesh model of Twin-Screw Pump Flow Path

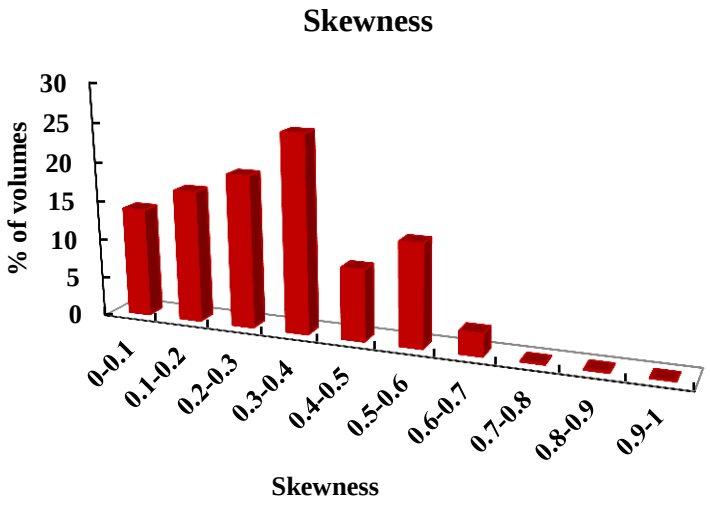

Figure 6.3: Skewness distribution

Velocities of fluid flow in the twin-screw pump are characterized by the rotation of the screw and the pressure differential. Even though the clearances are very fine, inertial forces are predominant in the clearances and flow is turbulent. Reynolds Averaging Navier Stoke (RANS) offers an economic approach for the computation of complex turbulent flows. The most common models used are k-epsilon and k-omega models. These models simplify the problem to the solution of two additional transport equations and introduce turbulent viscosity to calculate Reynolds stresses.

Turbulent flows are significantly affected by the presence of a wall. Tangential velocity is reduced by viscous damping however turbulence is rapidly augmented away from near wall region by production of turbulence kinetic energy due to large velocity gradients. Therefore accurate representation of flow in the near-wall region is necessary in order to obtain satisfactory solution.

One of the approaches is to use a set of semi empirical formulas and functions that link the solution variable at the near-wall cells and the corresponding quantities on the wall. The law-of-the-wall for velocity yields

$$U^* = \frac{1}{\kappa}\ln(Ey^*) \equiv \frac{U_p C_\mu^{1/4} K_p^{1/2}}{\tau_\omega/\rho} \qquad 6.1$$

$$y^* = \frac{\rho C_\mu^{1/4} k_p^{1/2} y_p}{\mu} \qquad 6.2$$

where U^* is the dimensionless velocity and y^* is the dimensionless distance from the wall. The values of y^* for which wall functions are suitable depends on Reynolds number of the flow. To avoid y^* dependence it is important to insure that the boundary layer is covered with enough structured cells than to ensure certain y^* value.

6.1 Modelling of twin screw pump for single phase flow

A solid model of the MR-200 twin-screw pump flow path was provided by Colfax corporation. It is a single threaded, dual intake, single exhaust pump with 633 GPM theoretical capacity at 1800 RPM. Water is used as a working fluid. If the exact value of pressure is known at the screw inlet and outlet, the modelling of Suction chamber and Exahust chamber can be avoided as the total leakage flow rate is constant and is independent of the screw rotation. This is true for single phase incompressible fluid. In the present case, the pressure is not known at the inlet and outlet of the screws. The boundary conditions at the screw inlet and outlet does not reflct the true boundary conditions of the pump. However, the purpose of this study is to understand the flow

behavior inside the screws. The pressure inlet at the suction chamber and pressure outlet at the discharge chamber are used as a boundary conditions for this case. at the The basic modelling of the pump will help undetand the distribution of pressure and velocity field inside the pump which will in turn help model suction and discharge in later stages.

Intermeshing of the screws in the liner housing creates a set of sealed pockets which moves axially from inlet to outlet with the velocity based on pitch and rotational velocity of the screws. To determine the steady state leakage flow analysis, the concept of moving reference frame is used. Equations of motion are modified to incorporate the additional term which occurs due to a moving reference frame.

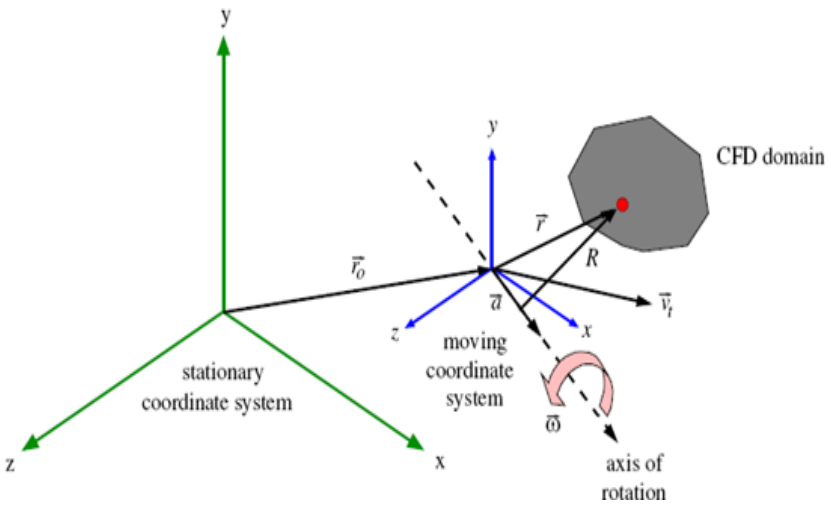

Figure 6.4: Stationary and moving reference frame

Figure 6.4 shows stationary and moving reference frame with linear velocity $\vec{v}_t$ and angular velocity $\vec{\omega}$. The relationship between relative velocity and absolute velocity is described by

$$\vec{v}_r = \vec{v} - \vec{u}_r \qquad 6.3$$

where

$$\vec{u}_r = \vec{v}_t + \vec{\omega} \times \vec{r} \qquad 6.4$$

$\vec{v}$ is absolute velocity, $\vec{v}_r$ is relative velocity and $\vec{u}_r$ is velocity of moving frame realative to inertial reference frame. Equation of motions can be formulated by either relative velocity as a dependant variable or absolute velocity as dependant variable. Results obtained from numerical simulation are compared and validated using experimental data further described in result and discussion sections.

6.2 Two phase flow simulation.

There is no literature reported to date on the two phase CFD simulation of the twin-screw pump. Current work represents the effort to make two phase simulation possible and bridge the gap between analytical tool and experimental analysis. Single phase analysis was carried out by imposing the pressure boundary conditions at the inlet and outlet of clearances. But two phase flow analysis needs different treatment of the inlet and outlet as the phase distribution is unknown.

Due to centrifugal action, liquid is pushed against the liner. However, the opposite rotation with forward movement of the screws causes incomplete separation of

the phases. Intermeshing also possess the disturbance at the boundary area. Initial analysis of 2 phase flow consists of 2D CFD simulation of rotating disc with axial velocity to help understand the phase distribution along the chambers and clearances with pure rotation. Results obtained with 2D simulation can be used as a benchmark for 3D simulation.

The Euler-Euler approach is used to model low GVF (GVF<50 %) at the suction. It is based on the concept of phasic volume fraction. Volume fractions are assumed to be function of space and time and their sum is always equal to 1. A set of equations are obtained by deriving conservation equations for each phase. These equations are closed by using empirical information in the case of gas-liquid interaction. Three different types of models are available in FLUENT, namely the Volume of Fluid (VOF), mixture, and Eulerian model.

The Eulerian model is most complex of all and it involves a set of continuity and momentum equations for each phase and slip velocity. The Eulerian model was preferred to model the complex two phase flow behavior in the twin-screw pump.

7 FLOW VISUALIZATION AND DYNAMIC PRESSURE MEASUREMENT

A twin-screw pump with a clear acrylic casing manufactured by Bornemann is used for flow visualization and dynamic pressure measurement purpose. The pump is driven by a 10 HP motor. A 60 HZ VFD is used to control the speed of motor. Initial testing is done by using oil (Viscosity is 0.2 Pa-sec at room temperature, Density is 850 kg/m^3) and air as two phase mixture. A closed flow loop is formed by connecting inlet and outlet to the sealed separation chamber located 0.8 m below the pump suction. The pump assembly is shown in the figure 7.1.

Figure 7.1: Twin-screw pump with clear casing

Flush mount dynamic pressure probes are used to track dynamic pressure. As shown in the Figure 7.1 probes are horizontally located while another three are vertically located with axial offset equals half the helix to get better understanding in the fluid pockets. An optical type of tachometer is used for speed measurement. A rotameter is used to supply fixed amount of air while a turbine flow meter is used to track the flow rate of the liquid. Flow visualization is performed using high speed camera as shown in Figure 7.2. A Phantom v711 camera is used to capture the flow. It has 1280*800 resolutions at 7530 FPS.

Figure 7.2: Phantom v711 High Speed Camera

8 EXPERIMENTAL EVALUATION OF TWIN-SCREW PUMP

Experimental testing involves investigation of steady state as well as of transient behavior of the twin-screw pump. Testing is subjected to different parameters actually occurring at well head conditions. Section 1 describes the steady state analysis which includes evaluation of different efficiencies as a function of pressure, temperature and GVF. Transient analysis is discussed in section 2 with comparison of two different sealflush recirculation systems. Transient analysis also undertakes pump behavior with change in viscosity. The test matrix for steady state and transient testing of the Colfax twin-screw pump is shown in Table 8.1.

Table 8.1: Test Matrix for Colfax Mr-200 Twin-screw Pump

Speed	GVF	Suction Pressure	Differential Pressure
RPM	%	PSI	PSI
900	50	15	0
1350	70	50	50
1800	90	75	100
	95	100	150
	98		200
	99		250
	100		300

8.1 Seal flush recirculation for optimum efficiency of Colfax twin-screw pump

Twin-screw pumps employ clearances between the rotor-rotor and rotor-liner which causes backflow which is mainly a function of pressure differential. Quality of multiphase mixture varies from time to time and critical parameter affecting the performance of the pump. Most of the multiphase twin-screw pumps employ the constant cross section which ensures the smooth delivery of the flow minimizing the GVF effect on backflow and pressure distribution on the rotor. Such design makes it difficult to pump the fluid if it is only gas and there is the possibility of the flow being chocked due to pressure differential between two subsequent chambers. To reduce this leakage flow, it is required to run with some quantity of liquid in addition to gas. Common conceptions assume the centrifugal action to cause the liquid to be thrown out and occupy the clearances. This action locks the gas in the pockets and therefore effectively pumping the multiphase mixture with theoretically only liquid back flow.

Multiphase pumps and their mechanical seals encounter large variation in load based on fluid composition, temperature and pressure variation, and erosive media. Mechanical seals on the screw shaft need to be capable of handling different parameters. In order to help them work efficiently seal faces need to be kept clean, cool and lubricated. Existing seals uses both buffer and barrier seal flush recirculating systems. Buffer media between the product and atmosphere prevents any environmental and human contact, while barrier media is the positive seal flush fluid which isolates the seal from product with poor lubricating properties or corrosive properties. Liquid used for barrier seal flush system is exhausted into the suction of the pump. This fluid is

important while pumps work at high GVF, close to 100% for the purpose of sealing the gas. If liquid required for sealing the gas is not enough, performance of the pump degrades drastically, this makes the sealflush flow very important while working on the reservoir with wet gas production.

Optimum seal flush recirculation can be calculated by plotting the energy imparted to the gas against the liquid recirculation. Energy imparted to the gas is defined in term of system efficiency which is represented by amount of power spent to transport the gas volumetric flow rate.

$$\eta_{system} = \frac{P_{gas}}{P_{drive}} \times \frac{V_g}{V_{th}} \qquad 8.1$$

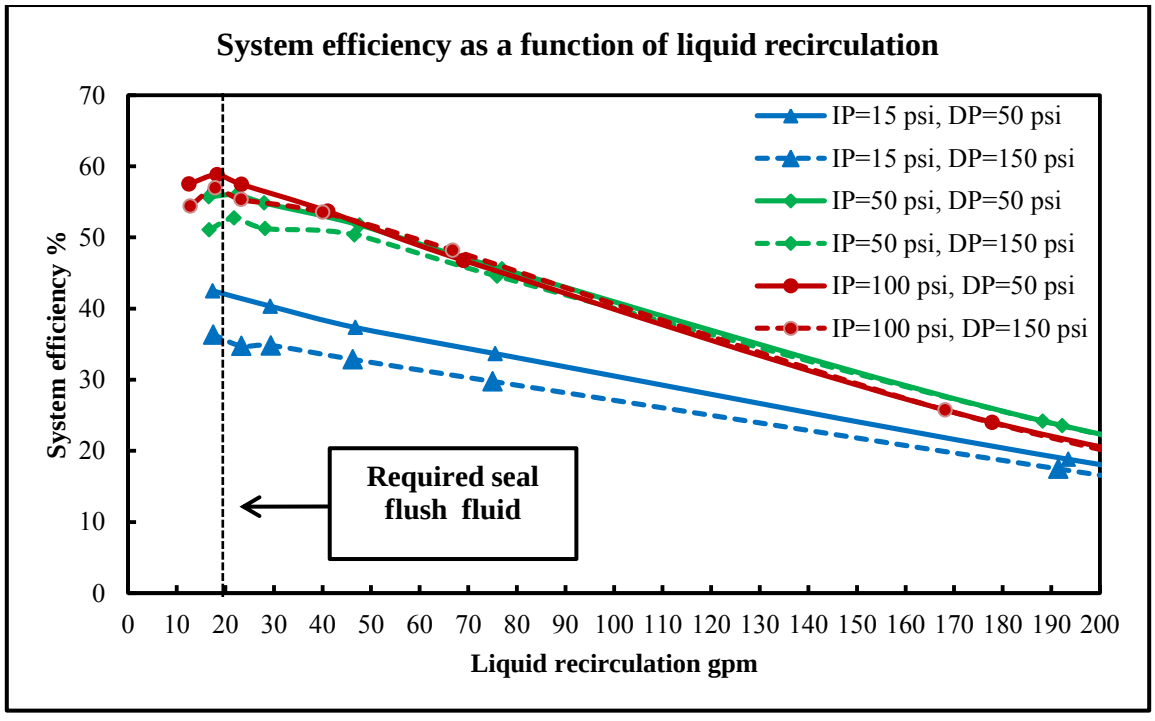

Figure 8.1: Optimum seal flush fluid requirement for effective working of the Colfax twin-screw pump

Figure 8.1 represents the system efficiency with change in liquid recirculation. The trend of system efficiency is upward with decrease in liquid recirculation; however, system efficiency starts breaking down for liquid recirculation below 20 GPM. Gas leakage flow goes up with the further decrease in liquid recirculation due to insufficient sealing. Power lost in gas leakage flow starts increasing and power imparted to move the mixture decreases. From the plot it is evident that at least 20 GPM of sealflush recirculation is necessary for wet gas conditions to achieve the optimum performance. In addition to two phase flow rate sealflush fluid of 17 gpm was always supplied from external source and considered in the evaluation. However, for convenience GVF will be denoted based on the net flow rate at the pump inlet.

8.2 Power consumption

Power consumption by the pump was directly measured by the VFD and used as input power for the evaluation of mechanical efficiency. This section discusses the factors affecting the power input to the multiphase pump. Figure 8.2 shows the effect of the speed on power consumption with the rise in pressure differential at 50 GVF and 50 psi suction pressure. Increase in load is linear with differential pressure with almost negligible variation in the slope. Increase in friction losses due to increased speed result in higher power consumption. Intercepts in the equation represent the frictional losses during no load condition.

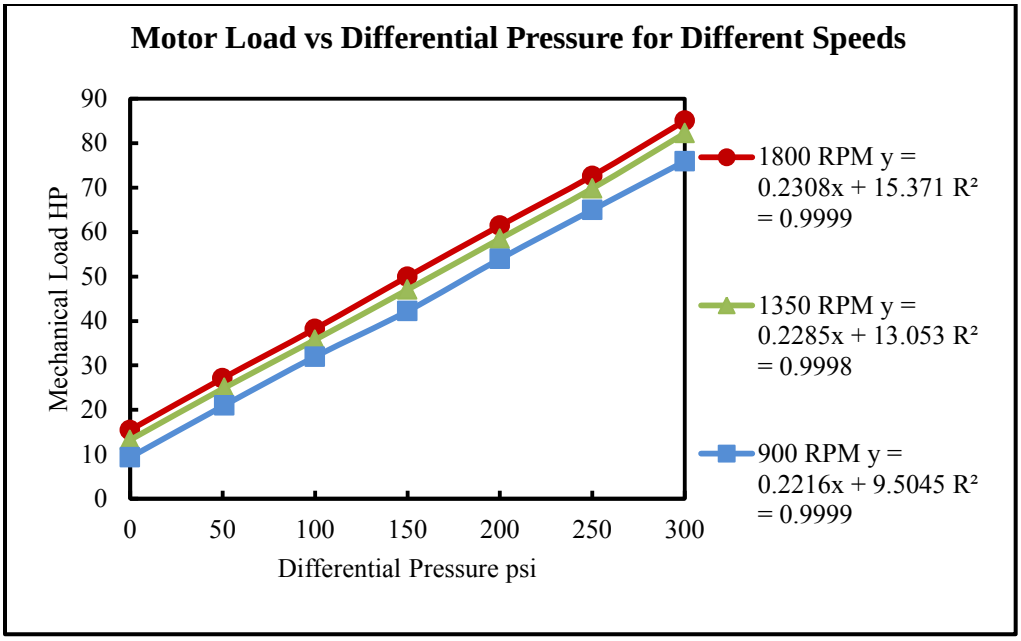

Figure 8.2: Variation in motor load with different speeds at 50% GVF and 50 PSI inlet pressure

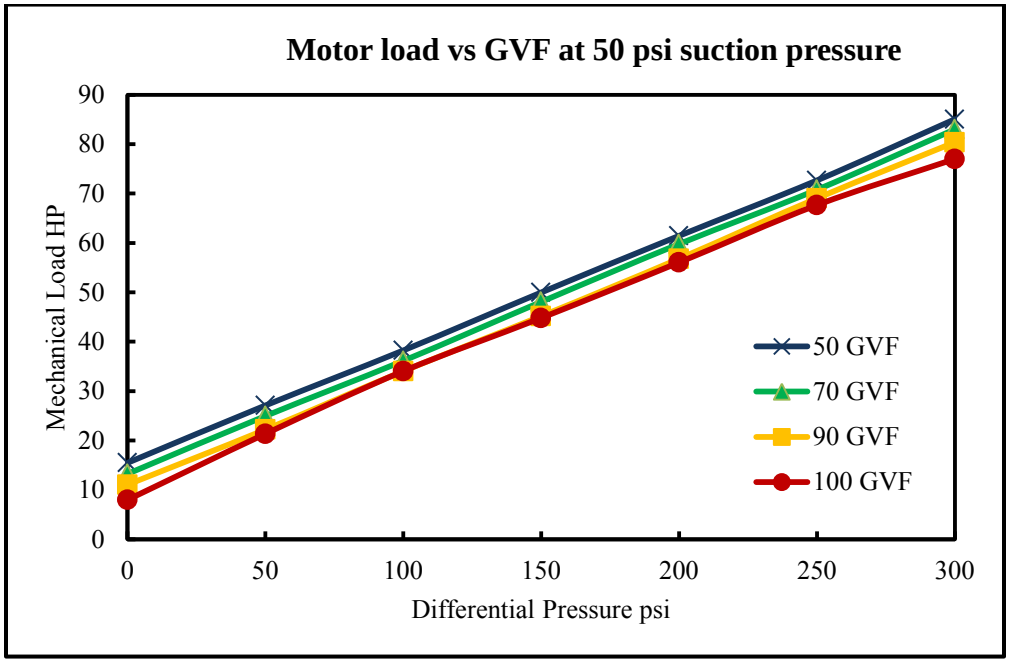

Figure 8.3: Effect of GVF on motor load at 50 psi suction pressure at 1800 rpm.

Dynamic resistance at zero differential pressure is composed of friction offered by different moving parts of the pump and the power lost in leakage flow and turbulent effects. Figure 8.3 shows the change in power consumption with GVF at 50 psi inlet pressure. Results contradicts the theoretical approach which says friction capacity of the liquid filled gaps, bearings, seals and on the gear wheels is the same pumping both liquid and mixtures (Karge 1988), As a result it should be independent of the mixture. However, power consumption for the present pump is decreased with increase in GVF. This effect can be attributed to the decreased viscous losses and drag friction due to decreased water quantity and increased air bubbles in the clearances. Pressure drop due to this friction loss is not visible as the location of pressure measurement is different than the inlet of the screws. Pressure at the inlet of the screws is lower than the pressure at the existing location, the inlet of the chamber due to suction effect created by screw rotation. Same might not be true for similar type positive displacement pumps such as progressive cavity pump which employs interference fit between rotor and rubber housing.

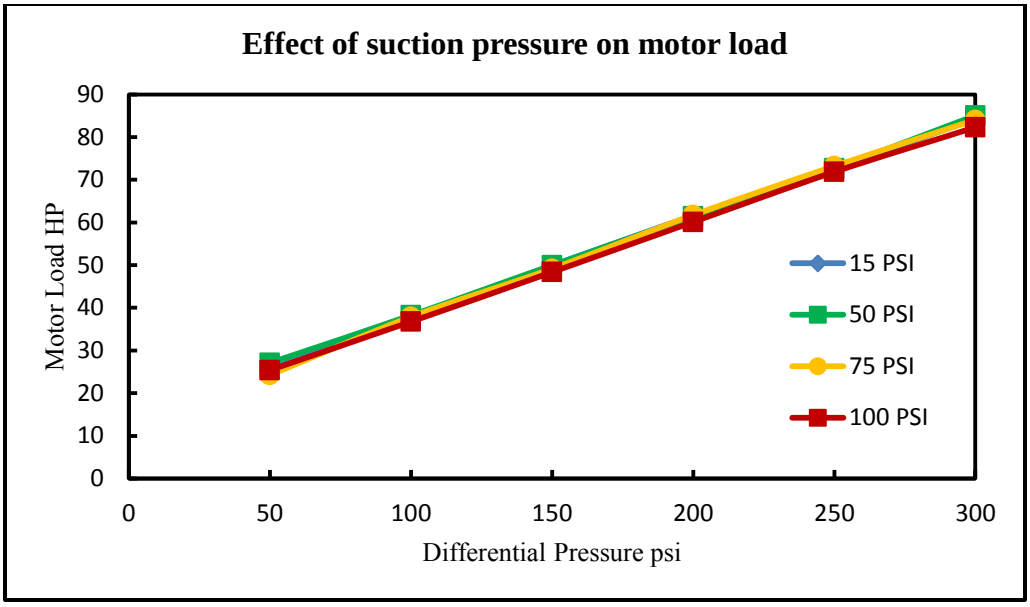

Figure 8.4: Effect of suction pressure on motor load at 50 GVF and 1800 RPM

Figure 8.4 shows plot of motor load against differential pressure for suction pressures ranging from 15 to 100 psi at 50 GVF and 1800 RPM. Twin-screw pumps are volumetric type of pumps and power input is independent of the suction pressure. With increase in suction pressure, the pump's capacity to deliver more mass flow rate increases due to higher density gas, however, it doesn't affect the power input. This can be seen in the above plot.

In brief, power input is primarily a function of pressure differential. Change in speed and GVF secondarily affect the power requirement.

8.3 Volumetric flow rate capacity of the pump

Volumetric flow rate of the pump is based on rated theoretical capacity of the pump. Theoretical capacity is the function of geometrical parameters; however, due to the clearances there is leakage flow from exhaust to inlet, and it is a function of differential pressure, speed and GVF. The current pump under investigation is the Colfax MR-200 multiphase twin-screw pump with theoretical capacity of 633 gpm.

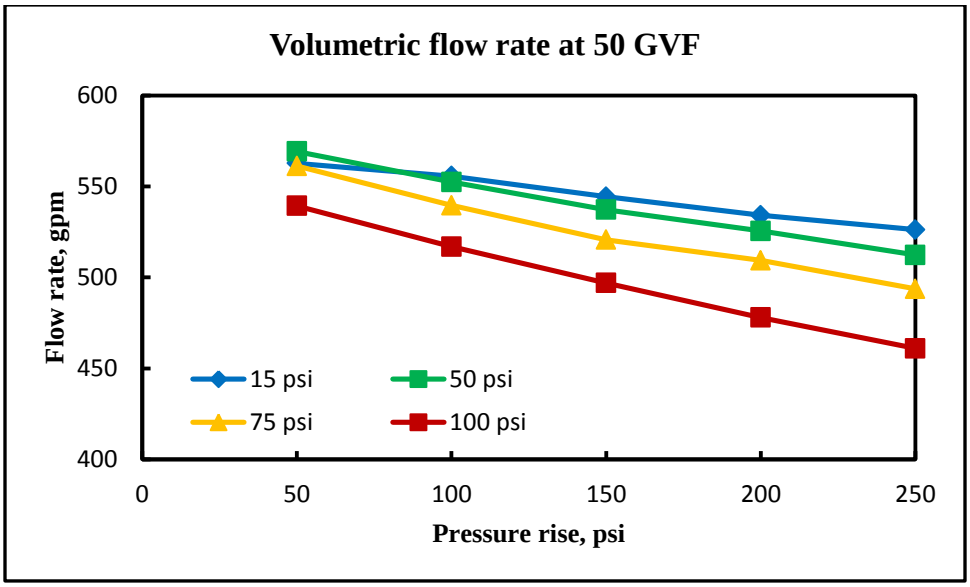

Figure 8.5: Volumetric flow variation at inlet of the pump with different suction pressures at 50 GVF, 1800 RPM.

As discussed previously, the non-contact design of the pump connects exhaust to inlet chamber via clearances between rotors and liner. Figure 8.5 shows the effect of differential pressure at 50 GVF for different suction pressures. There is linear decrease

in the inlet volumetric flow rate with rise in pressure differential. Leakage flow is lowest at 15 psi suction pressure and increased with increase in suction pressure with highest leakage flow occurring at 100 psi inlet pressure.

With the liquid being incompressible, if it is assumed that at low GVF there is only liquid leakage due to centrifugal action, the steady rise in the pressure differential would cause linear increase in leakage flow, however, nature of compression of gas in exhaust chamber varies with different suction pressure which may compromise this assumption.

Increase in pressure causes air density to rise at the pump inlet resulting in less separation between the phases. Leakage flow is higher with rise in suction pressure, compared to the rise with the pressure differential. Leakage flow rise is 41 % from 15 psi to 100 psi suction pressure at 50 psi differential pressure while leakage flow rises by 12% from 50 psi DP to 100 psi DP at 15 psi suction pressure. However, this rise is higher with greater suction pressure. At 100 psi suction pressure leakage flow rise is 21%, which indicates the effect of back flow pressure due to increased density at suction chamber even though the density rises by more than 4 times in the case of 15 psi suction pressure and 50 DP while it is just 1.5 times in case of 100 psi suction pressure and 50 psi pressure rise.

Back pressure is higher for higher suction pressures as the leakage flow rate from exhaust chamber to adjacent chamber goes up due to increased density of the air.

Energy generated in compressing the air at high pressure and same volume is released in the form of heat, however, due to higher heat capacitance of the water total temperature rise of multiphase mixture is negligible in case of 50% GVF.

Figure 8.6 show air and water flow rates. Volumetric flow rates of the air as well as the water decrease due to increase in suction pressure and differential pressure. With increased pressure pump transfers more mass flow rate but with increased mass flow rate there is increased leakage of air volumetric flow rate along with water leakage.

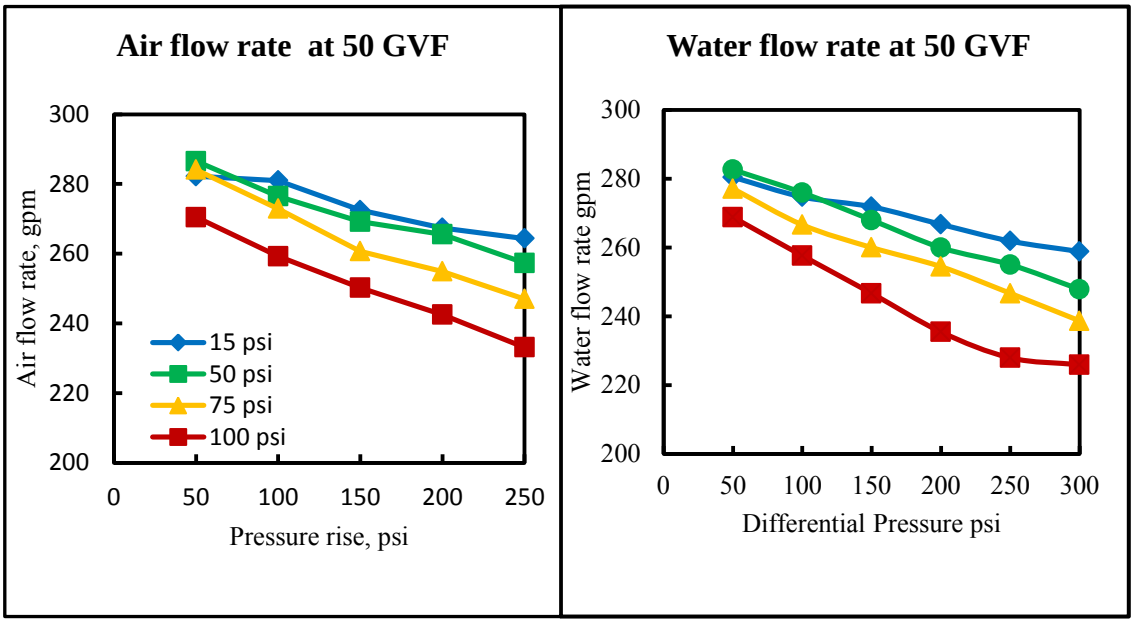

Figure 8.6: Volumetric flow rate of water at 50% GVF and different suction pressures

Effect of GVF with increased suction pressure on the leakage flow of the pump at the inlet can be seen in Figure 8.7. Leakage flow here is defined as Theoretical flow

rate minus the actual flow rate. Flow difference with increase in suction pressure is highest at 50 GVF (Figure 8.5) and it goes down and distributes evenly with increase in GVF due to increased leakage flow of the gas. Leakage flow rate is lowest at 50 PSI and 90 GVF and it is also observed that there is shift in minimum leakage flow with change in GVF for same pressure differential.

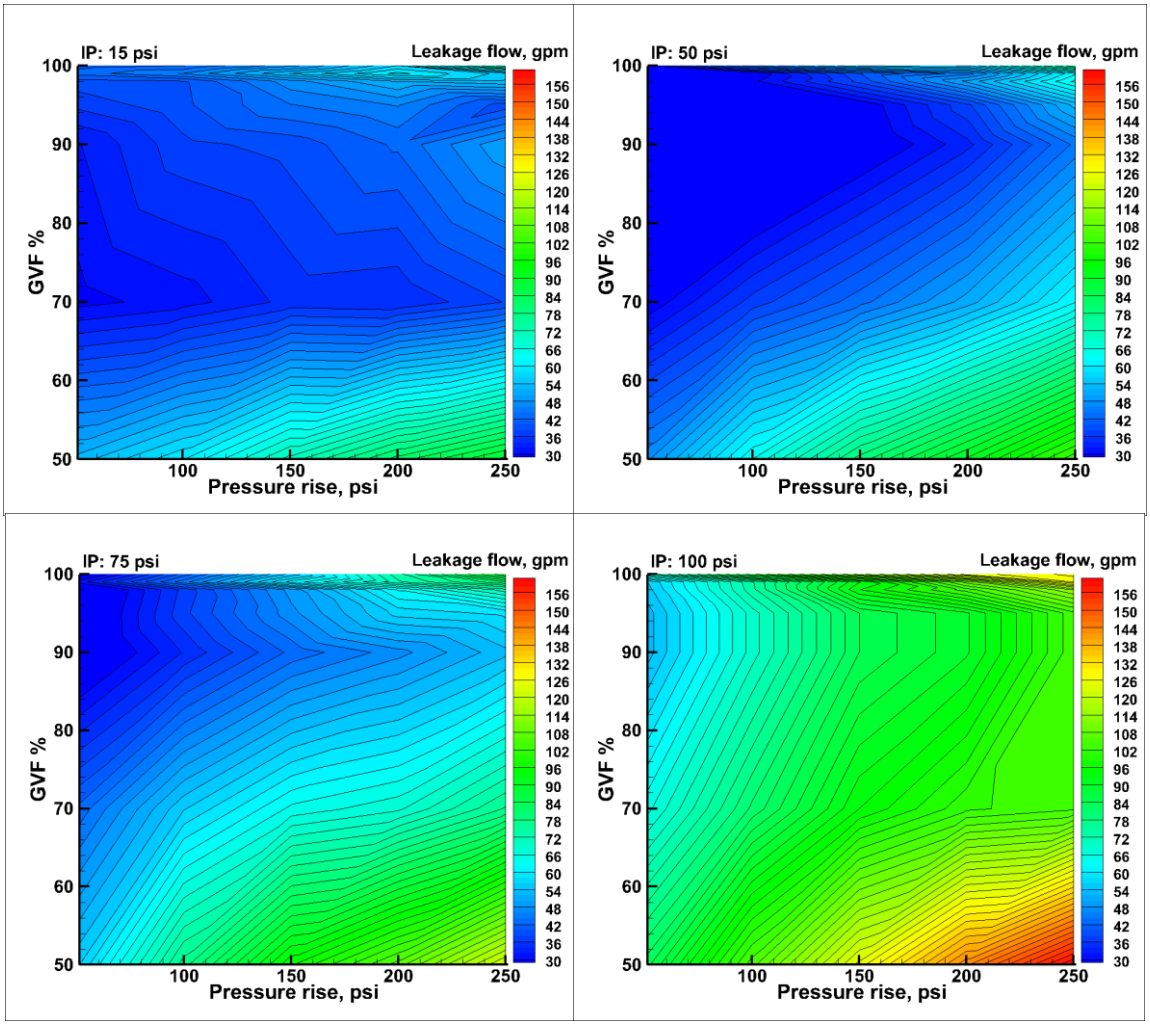

Figure 8.7: Counters showing effect of suction pressure on leakage flow

At 100 PSI inlet pressure, and 100 GVF sealflush circulation system could supply only 10 to 12 GPM which was less than the required seal flush recirculation causing higher than usual leakage flow rate.

At low GVF due to higher liquid content, it can be held valid that there is only liquid leakage to suction at low suction pressures due to efficient separation of two phases, however, pressure drop across the first chamber and suction chamber is higher for low GVF due to higher liquid content resulting in higher leakage flow rate. While with the rise in GVF if the liquid available is enough to seal the gas, the gases are not exposed to exhaust pressure until before opening of the last chamber to the exhaust chamber resulting in very small pressure drop across the first chamber formed between screws and the suction chamber compared to the pressure drop across the last chamber and small pressure drop causes low leakage flow. This holds true for GVF with enough liquid available to seal the pockets of gases. According to Wincek this limit is around 85%. As the GVF rises further, liquid becomes insufficient to seal the gas in the chamber, leading to well mixed leakage flow. With increased infiltration of the gas, the pressure drop across all the chambers tends to be equal resulting in higher leakage flow. The overall axial pressure profile follows linear to parabolic path from 0 to 90 GVF and again back to linear from 90 to 99 GVF (Xu 2008).

From justification above and the Figure 8.5, it can also be predicted that the pressure profile should vary from parabolic to linear with increase in suction pressure at same pressure rise and GVF.

It is also seen from the Figure 8.7 that the point of minimum leakage flow rate varies with GVF for different suction pressures. Leakage flow is lowest at 70 GVF for 15 psi suction pressure while it shifts to 90 GVF at 50 psi, 90~92 GVF at 75 PSI and 95 GVF at 100 psi suction pressure although it should be noted that total leakage flow rate goes up with increase in suction pressure at any particular GVF as discussed before. Minimum flow rate indicates the major portion of the leakage is liquid or liquid only while the condition of optimum sealing seems to vary with suction pressure. At low suction pressure, phase separation is effective due to large density difference but even with small path available to escape may result in higher gas leakage flow rate even though mass flow rate is less and hence for low suction pressure more liquid is required to seal the gases. Optimum sealing for 15 psi suction pressure occurs around 70 GVF, with increase in GVF beyond 70~75, leakage flow goes up due to increased gas leakage. Increased suction pressure homogenizes the flow. Due to increased volume of the gas more liquid flows back to the suction and point of optimum sealing occurs at the intersection of minimum gas leakage flow and maximum liquid leakage flow with minimum pressure drop across the suction chamber and first chamber. So there is shift in the optimum sealing towards higher GVF with increase in suction pressure.

Suction pressure and GVF affects the leakage flow significantly, and results do not quite agree with previous work especially the conventional views at 50 GVF which acknowledges liquid only leakage flows. Condition of optimum sealing varies with suction pressure which was vaguely addressed before.

Effects of GVF and suction pressure on volumetric efficiency at 1800 rpm are shown in Figure 8.8. Efficiency is lower at 50 GVF and 100 psi suction pressure condition while it is higher at 50 psi suction pressure and GVF ranging from 70 to 90.

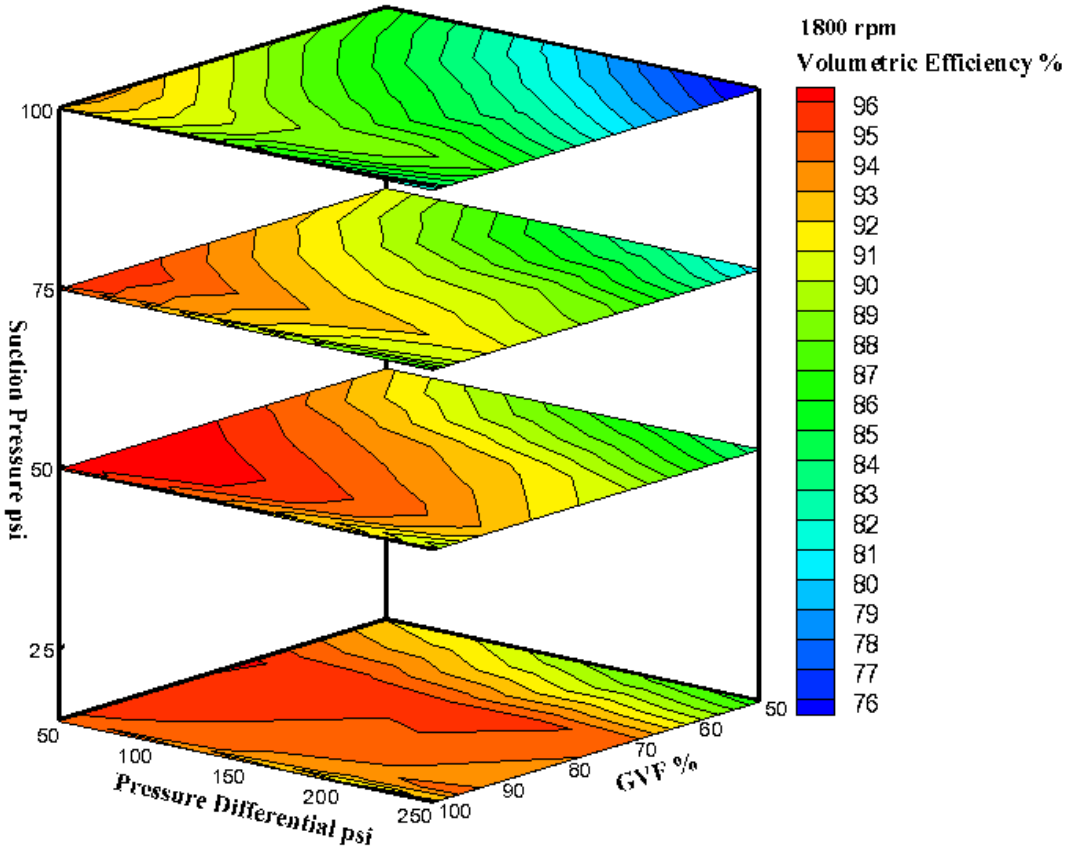

Figure 8.8: Counters of volumetric efficiency

8.4 Leakage flow variation with speed

Speed is an important factor affecting the performance of twin-screw pump. Volumetric flow rate is proportional to the speed of the pump; however, speed also affects the leakage flow through clearances. The parameters induced by speed affecting the performance are tangential or rotational velocity of the screws on the fluid in clearances, axial velocity of the pockets formed and the phase separation due to centrifugal effect. Pockets move from inlet to exhaust with the axial velocity proportional to the rotational speed of the screws. The component of back flow velocity in the clearances near the flights, flanks and root of the screws, which moves with rotational speed according to zero slip, affects the shear stress between screws and the liner.

Components of leakage flow through clearances can be expressed as

$$Q_l = Q_p + Q_r \qquad 8.2$$

where Q_p is leakage due pressure difference. This component is constant for all the speeds in case of single phase flow. Q_r is the leakage due to rotation of the screws and it is different in the different clearances. Leakage flow due to rotation of the screw in the circumferential clearances can be viewed as couette-flow. The Component of leakage flow velocity due to rotation is orthogonal to the screw flight and directed towards suction. The velocity induced due to pressure difference across the clearances is constant. Leakage flow through the root and flank clearance is similar except for the pressure and velocity profile which changes due to counter rotation of the screws and the geometry.

The component of leakage flow due to pressure difference is constant, however the component of leakage flow due to rotation of the screws increases with increase in screw speed, hence the total leakage flow rate increases with increase in speed in case of single phase flow. It is confirmed by experimental results as shown in Figure 8.9.

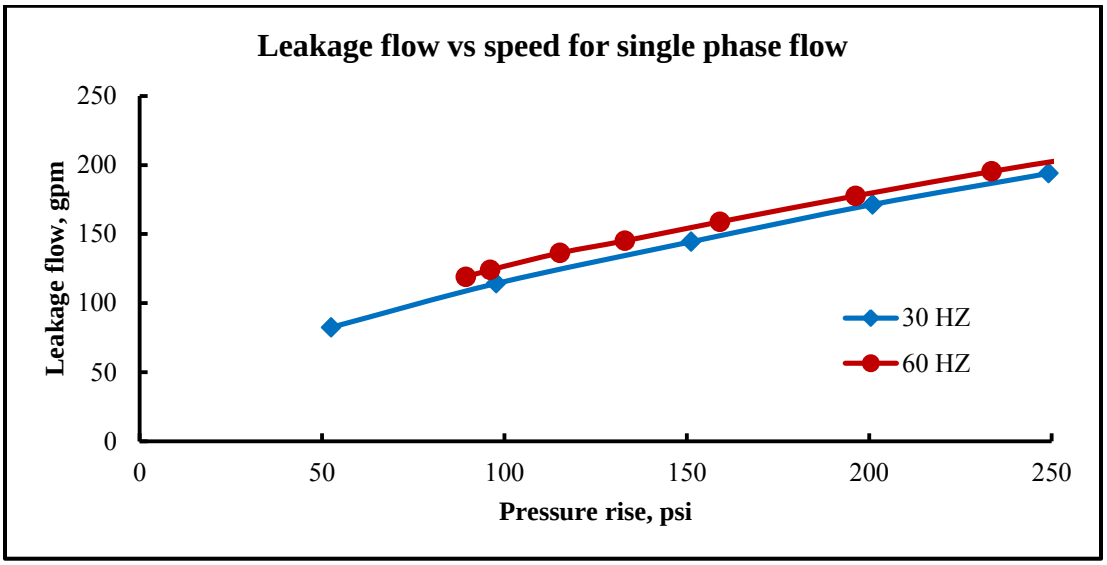

Figure 8.9: Single phase leakage flow as a function of speed

The following section discusses the two phase leakage flow as a function of speed for different GVF's and suction pressures. Figure 8.10 and figure 8.11 shows the leakage flow behavior for 15 psi and 100 psi suction pressure respectively at different speeds. Leakage flow increases with decrease in speed for all multiphase flow conditions.

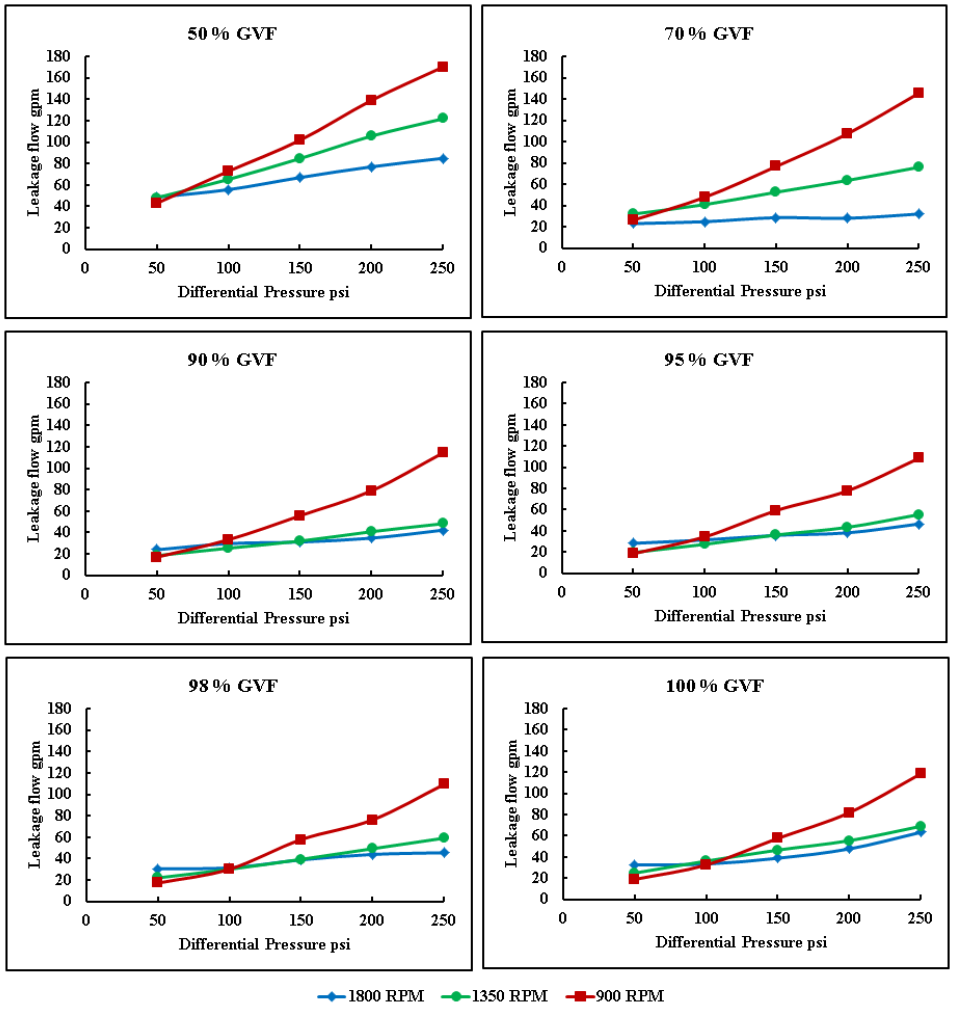

Figure 8.10: Effect of speed on leakage flow for different GVF at 15 psi inlet pressure

At low suction pressure and low differential pressure leakage flow is lower for lower speed as the component of leakage flow due to circumferential speed of the screw is dominant and effect of component of leakage flow due to pressure difference is very small due to very small pressure difference across the first chamber and suction chamber. With increase in pressure differential centrifugal effect becomes more dominant due to higher speed and leakage flow goes down with increase sealing of the

gas. With increase in suction pressure (Figure 8.11) the component of leakage flow due to pressure difference becomes predominant due to increased density and homogenization of multiphase mixture. Outcome is increased leakage flow rate with increase in pressure rise at lower speed. At 50% GVF the difference between the leakage flows for different speeds is not very significant but with increase in GVF from 70% to 95% difference becomes wider and again becomes narrower above 98% GVF.

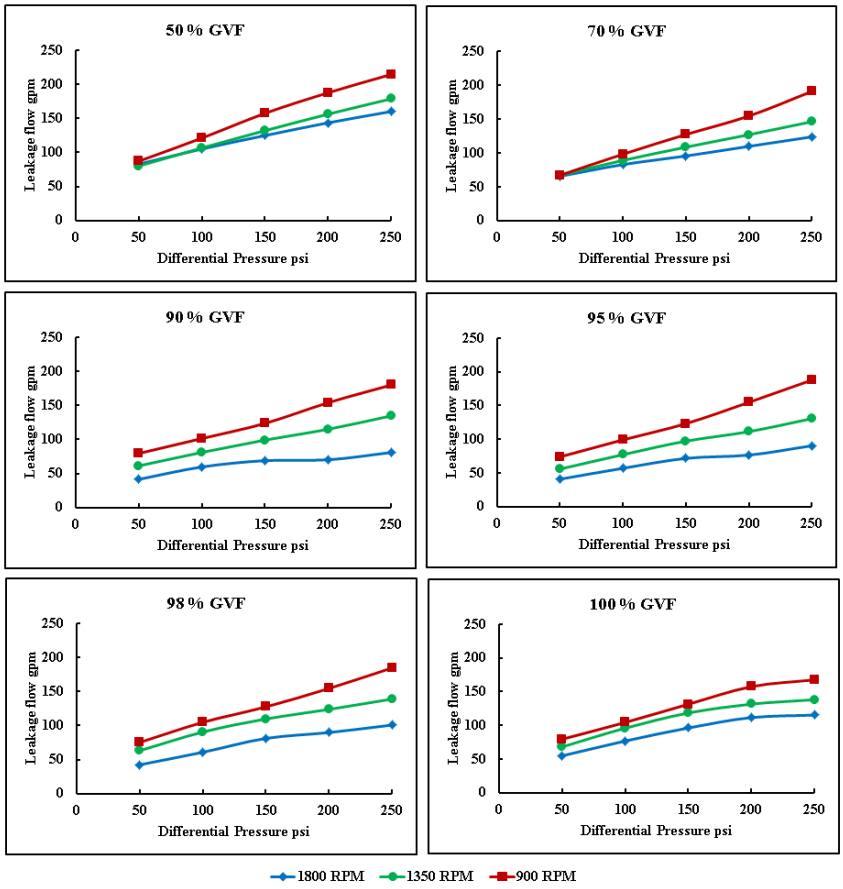

Figure 8.11: Effect of speed on leakage flow for different GVF at 100 psi inlet pressure

Figure 8.12 and 8.13 shows the volumetric efficiency of the twin screw pump at 15 psi and 100 psi suction pressure operating over same range of conditions. Volumetric efficiency decreases with decreasing the pump speed. Condition of optimum GVF varies with speed and it is different for different suction pressures. At 15 psi suction pressure maximum efficiency for 1800 rpm occurring around 70 GVF, 90 GVF for 1350 rpm and around 95 GVF for 900 rpm. With decreased speed, volumetric efficiency decreases due to increased air infiltration.

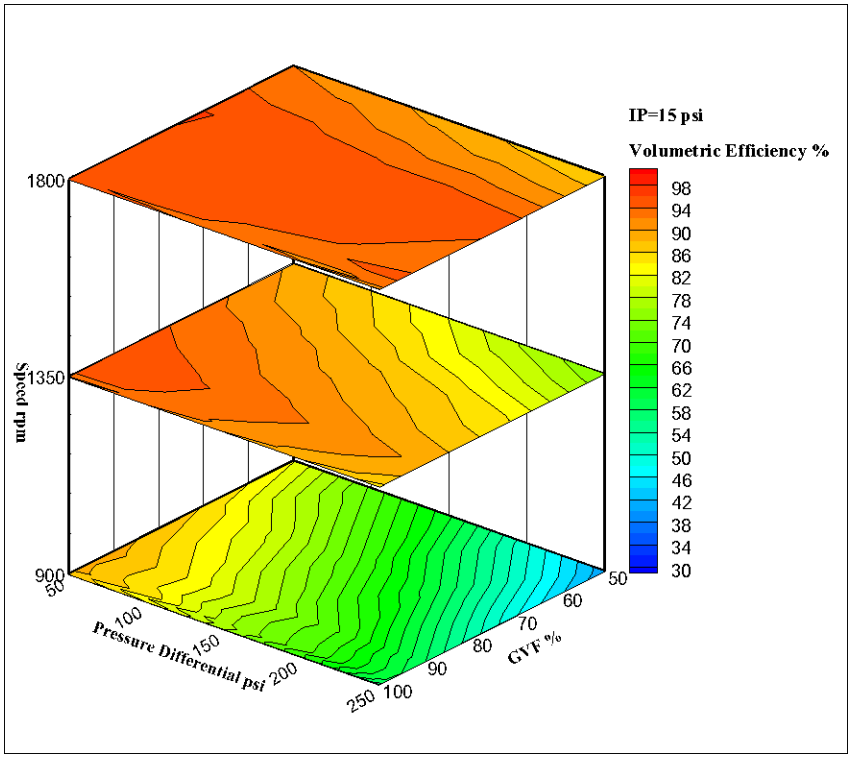

Figure 8.12: Volumetric efficiency at 15 psi suction pressure for 900 rpm, 1350 rpm and 1800 rpm

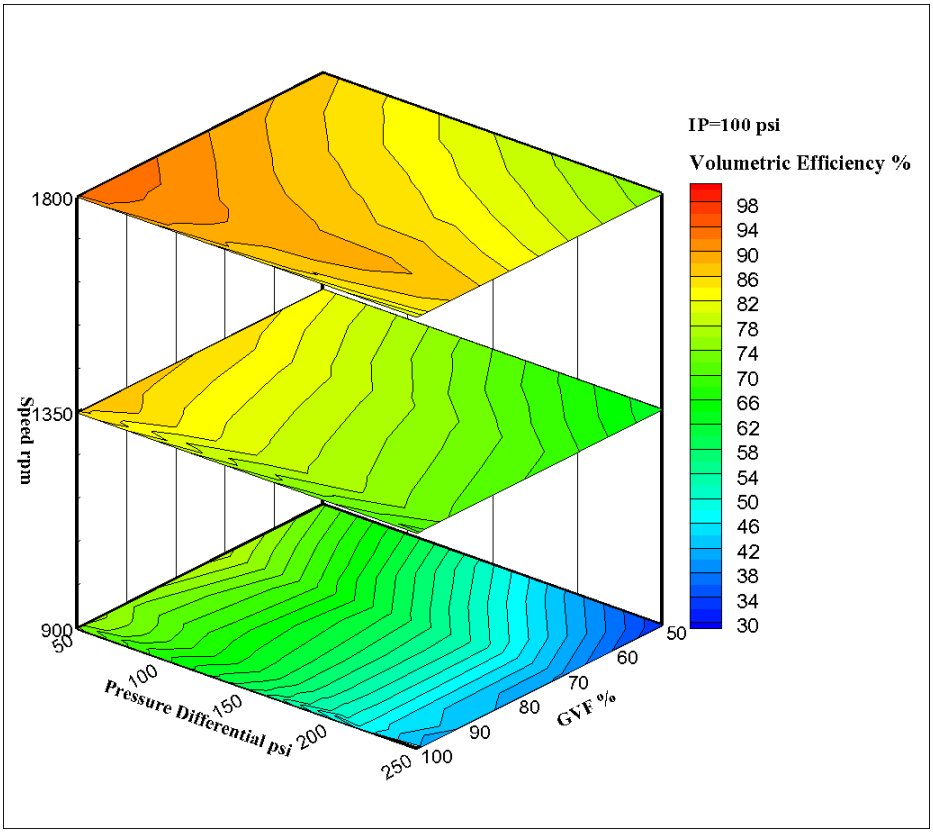

Figure 8.13: Volumetric efficiency at 100 psi suction pressure for 900 rpm, 1350 rpm and 1800 rpm

8.5 Effectiveness, process efficiency and mechanical efficiency

In the oil and gas industry, multiphase pumps are often compared with conventional multiphase systems due to their low installation and maintenance cost and smaller footprint. This comparison can be extended further based on the performance of multiphase pump for the same operating conditions. It has been proven from the previous studies that multiphase pump works better with higher GVF and currently are being used with oil well with similar production. One of the major issues with the production line is slug flow; fluctuations occur due the pressure variation which makes

separation of multiphase flow very difficult and sometimes causes plant shutdowns. When sized and designed properly, multiphase pumps can handle wide range of GVF and to the some extent can mitigate this problem.

Theoretical efficiency of the compression for the specific process can be derived from the theory of thermodynamics. This will represent the best possible performance of the device and one common tool to compare the compressor in the multiphase system with the multiphase pump. Actual efficiency of the pump will be lower due to friction losses and leakage flow. The hydraulic power represented in equation 4.13 is the power imparted to the fluid in an ideal condition and represents the best performance a pump may achieve for the same volumetric flow rate when flow is compressed.

The compression process of multiphase flow is mainly affected by GVF and the design of the pump. With 0% GVF to low GVF, the process where power imparted to the fluid can be regarded as isothermal as the liquid capacitance is very high and it absorbs all the heat generated due to compression of the gas. Equation 3.15 can be rewritten as

$$P_{isothermal} = Q_l \cdot \Delta p + p_{inlet} V_{inlet} \ln\left[\frac{p_{outlet}}{p_{inlet}}\right] \qquad 8.3$$

As the GVF increases, thermal capacitance of the liquid is not enough to absorb all the heat and process becomes polytropic in nature and it varies between isothermal to isentropic process ($n = k = C_p/C_v$). Temperature of the mixture increases and rises towards the highest gas temperature for isentropic case. Equation 3.13 can be rewritten as

$$P_{poly} = Q_l \cdot \Delta p + \frac{n}{n-1} p_{inlet} V_{inlet} \left[\left(\frac{p_{outlet}}{p_{inlet}} \right)^{\frac{n-1}{n}} - 1 \right] \quad 8.4$$

The efficiency of a gas compressor in the conventional multiphase system can be defined as ($P_{compressor}/P_{drive}$). $P_{compressor}$ is the power imparted to the gas and it follows isentropic compression and can be represented by

$$P_{compressor} = \frac{k}{k-1} p_{inlet} V_{inlet} \left[\left(\frac{p_{outlet}}{p_{inlet}} \right)^{\frac{k-1}{k}} - 1 \right] \quad 8.5$$

A typical gas compressor has an isentropic efficiency of 70% and multiphase pump operating at 100% GVF may approach the same efficiency, however the efficiency of the multiphase pump may be significantly different as compared to isentropic efficiency of the compressor.

Effectiveness represents the decreasing ability of the pump to compress the multiphase fluid with increase in gas as compared to the power imparted to the liquid with same volumetric flow rate, inlet pressure and pressure differential.

$$\eta_{effectiveness} = \frac{P_{pump}}{P_{hydraulic}} \quad 8.6$$

where $P_{pump} = P_{isothermal}$ or $P_{polytropic}$

The liquid portion of the multiphase fluid has higher thermal capacitance compared to the gas. Hence heat generated during the compression of gas is absorbed by the liquid with least increase in the temperature. Due to this energy added to the gas is decreased and always less than energy added in case of isentropic process which follows

ideal compression and is a measure of energy imparted in the case of isentropic compressor.

Process efficiency is the measure of actual power imparted to the multiphase fluid to the power imparted for the case of isentropic process. This is solely based on the thermodynamic process and represents the upper limit of pump performance.

$$\eta_{process\ efficiency} = \frac{P_{pump}}{P_{isentropic}} \qquad 8.7$$

where $P_{pump} = P_{isothermal}$ or $P_{polytropic}$

The question here is whether the isentropic process truly represents the desired process. Energy imparted to the fluid by compressors or multiphase pumps is desired when all the energy imparted is converted to the pressure energy, however, apart from boosting the pressure thermodynamic processes discussed above also increases the temperature by means of increase in internal energy. If this rise in temperature is not desired and must be removed by mean of heat exchanger then this additional energy is actually a waste of energy. If this heat rise must be eliminated then in the actual installation the cost of a heat exchanger must be included. The basic definition of efficiency is what is desired and what it costs, so this can vary based on device and purpose that is if temperature rise is useful or not. In this case, it is not and elimination of this energy reduces the total useful energy and adds the cost of installing and running the heat exchanger.

Figure 8.14 and 8.15 represent how the compression process affects the effectiveness of the pump for same suction pressure, pressure rise and volumetric flow

rate. At low suction pressures there is significant difference in the density of the two fluids and the pumps ability to add energy decreases linearly from 100% to 10% with increase in GVF and pressure differential. The difference between isothermal and isentropic effectiveness decreases as the pressure differential increases.

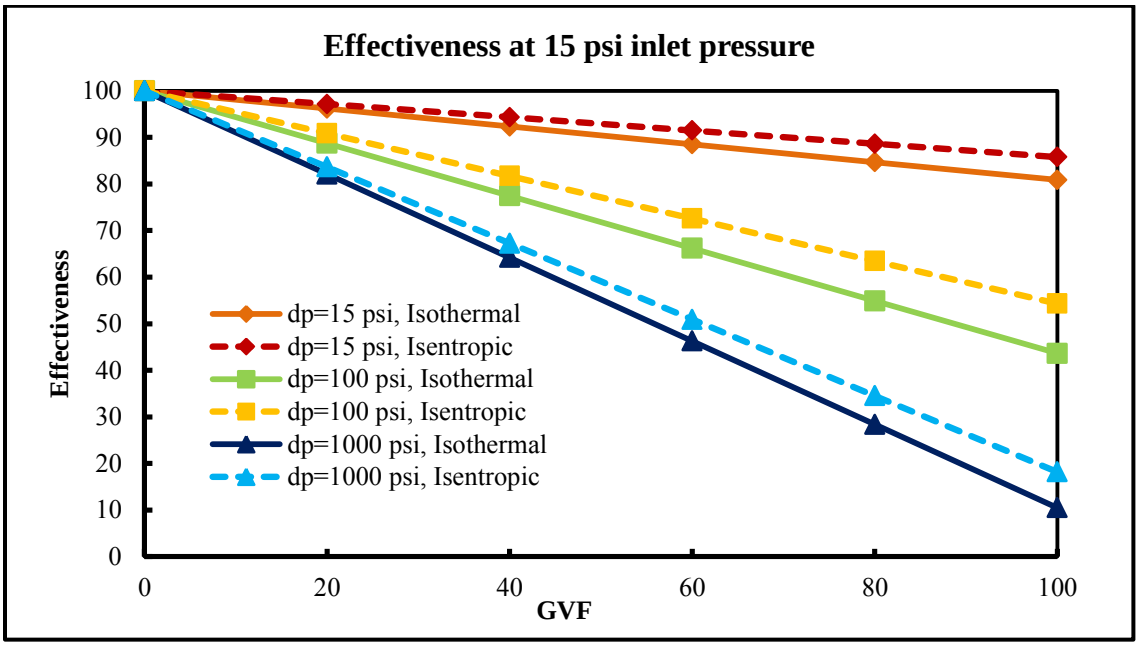

Figure 8.14: Effectiveness of the pump for 15 psi inlet pressure comparing isothermal and isentropic processes for 15 psi, 100 psi and 1000 psi pressure differential.

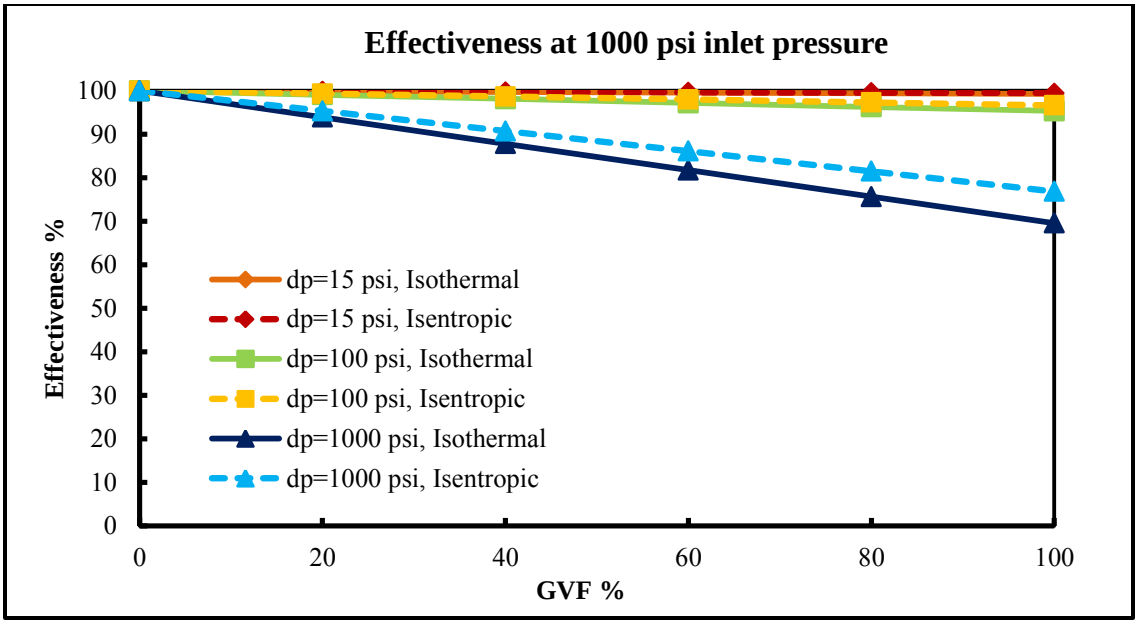

Figure 8.15: Effectiveness of the pump for 1000 psi inlet pressure comparing isothermal and isentropic processes for 15 psi, 100 psi and 1000 psi pressure differential.

Effectiveness increases greatly with increase in suction pressure. Figure 8.15 shows effectiveness at 1000 psi inlet pressure. Effectiveness is close to 100% at 15 psi pressure rise while it is more than 95% for 100 psi pressure rise. Difference between isothermal and isentropic effectiveness is minimal. There is a significant decrease in effectiveness at 1000 psi pressure rise. The difference between isothermal and isentropic is also widening with increased pressure rise. The effectiveness decreases as the gas density ration between the outlet and inlet of the pump increases. Minimum isothermal effectiveness is still around 70% for 1000 psi pressure rise. Figure 8.16 through Figure 8.18 shows contours illustrating how the pump effectiveness changes with GVF, pressure rise and index n for the polytropic process. Pump effectiveness decreases with increase in gas content and increases with increase in suction pressure. At 100 GVF and

15 psi suction pressure it is around 14% while at 1000 psi suction pressure effectiveness improves to 70%. The contours also illustrate the effect of polytropic index which has secondary effect upon effectiveness.

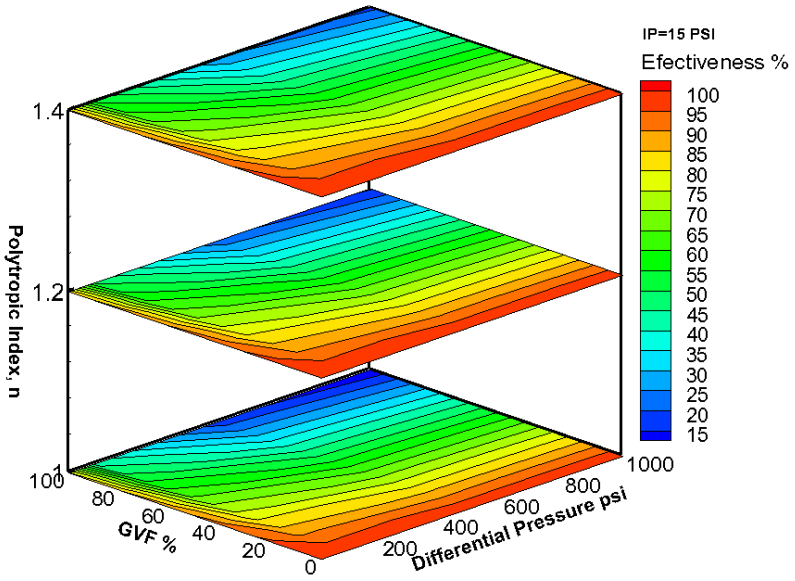

Figure 8.16: Polytropic pump effectiveness for P_{in}=15 psi

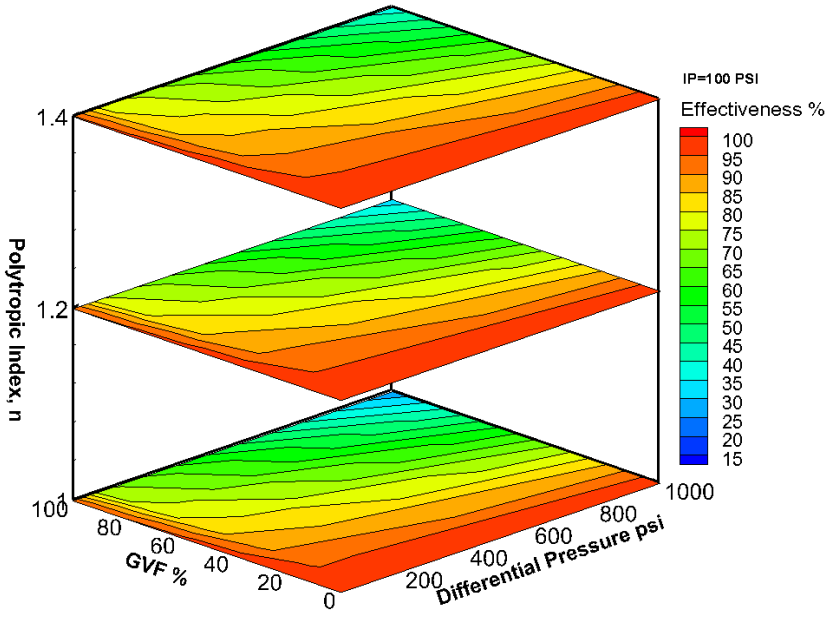

Figure 8.17: Polytropic pump effectiveness for P_{in}=100 psi

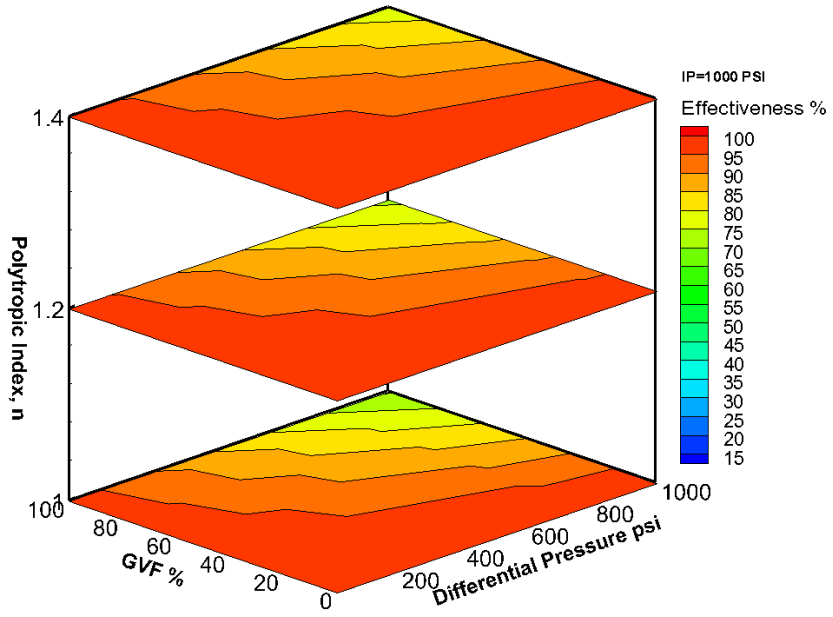

Figure 8.18: Polytropic pump effectiveness for P_{in}=1000 psi

The MR-200 multiphase twin-screw pump is evaluated at different operating conditions. Figure 8.19 shows isothermal effectiveness of the twin-screw pump for the inlet pressures of 15 psi, 50 psi, 75 psi and 100 psi, 50% to 100 % GVF and pressure differential varying from 50 to 250 psi. Results agree well with the theoretical analysis. Effectiveness is highest with higher inlet pressure, low GVF and differential pressure.

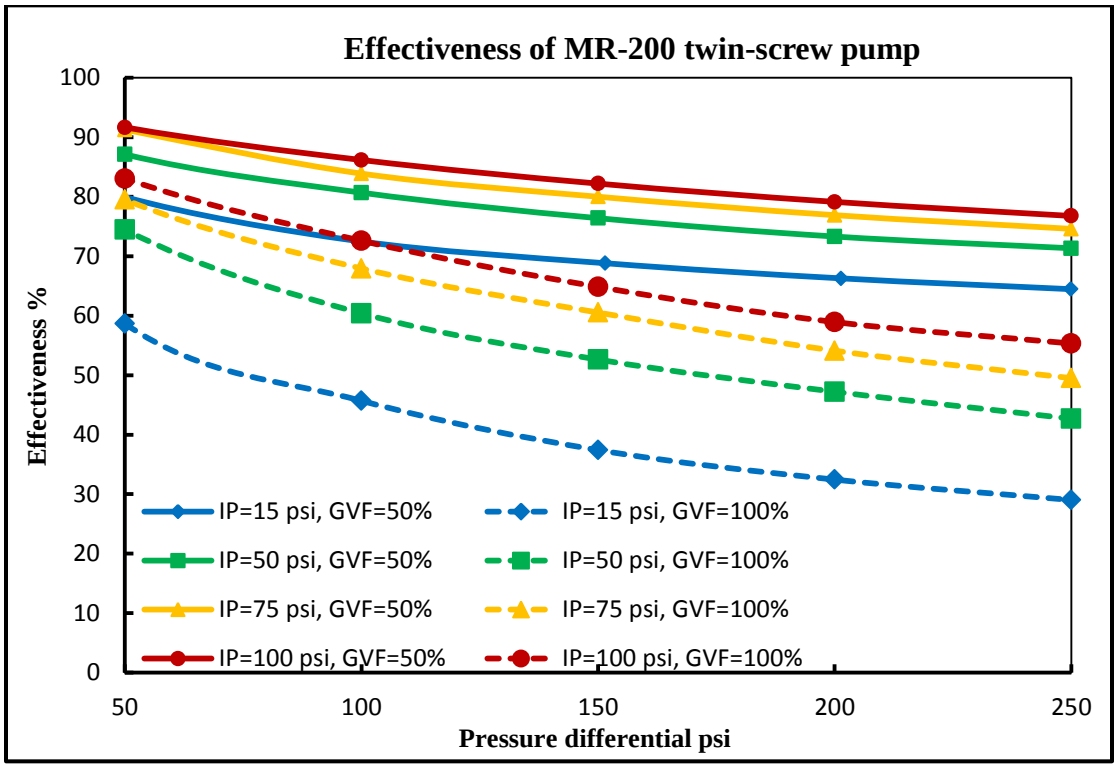

Figure 8.19: Effectiveness of MR-200 multiphase twin-screw pump

Figure 8.20 shows the effect of suction pressure on effectiveness of twin-screw pump in more detail. Stacked contours show the increase in effectiveness with increase in suction pressure.

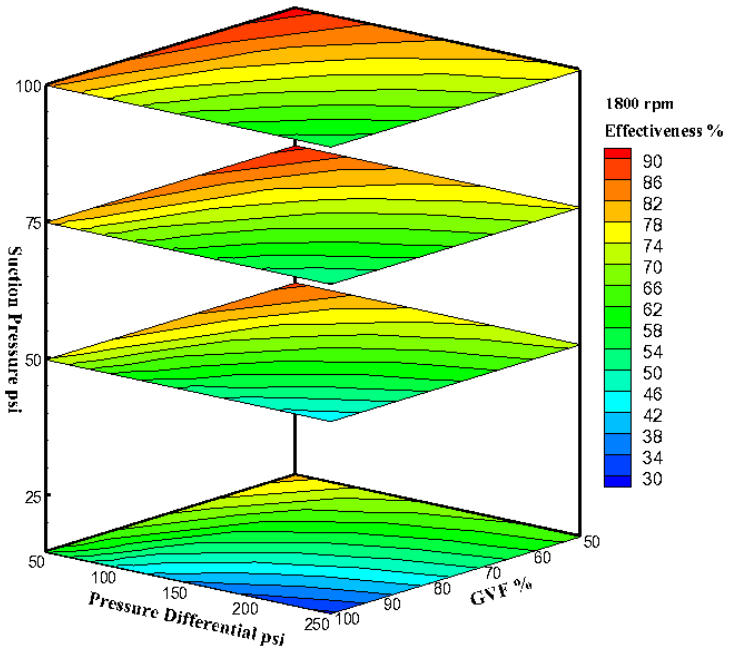

Figure 8.20: Effect of suction pressure on effectiveness of the twin-screw pump at 1800 rpm

Effectiveness is a purely theoretical term and the results discussed in the theoretical analysis should be consistent with the effectiveness derived from experimental data for the same operating conditions. Figure 8.21 shows the isothermal pump effectiveness for the inlet pressure 15 psi and 100 psi, GVF varying from 50% to 100% and pressure rise of 100 psi. Pump curve agrees well with theoretical prediction for given matrix and pump effectiveness increase with increase in suction pressure. This pump is good for 750 psi suction pressure but due to limitation in the facility resources it was limited to 100 psi, however, this plot will serve the good benchmark and can accurately predict the effectiveness for the higher suction pressure.

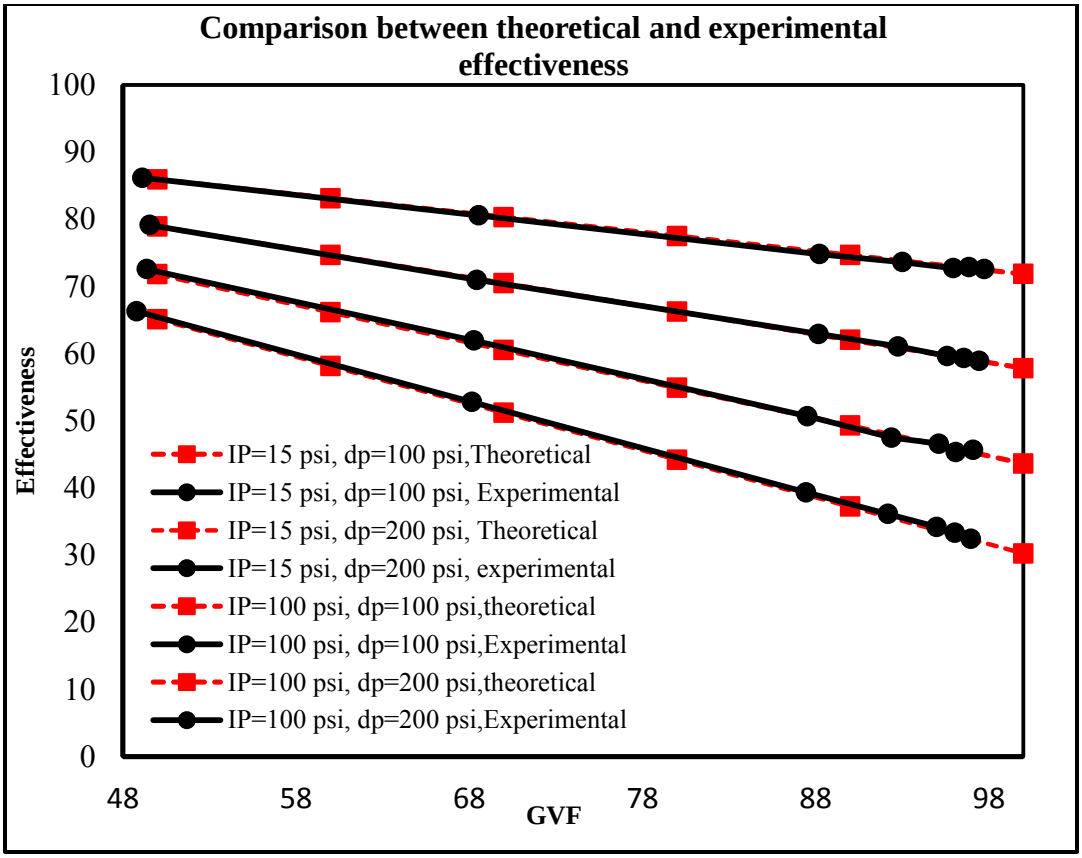

Figure 8.21: Comparison between theoretical effectiveness and effectiveness of twin-screw pump.

The pump was also tested for 3 different speeds, 900rpm, 1350rpm and 1800rpm. Figure 8.22 shows the effect of speed on pump effectiveness. Speed has a little effect on effectiveness of the pump with effectiveness mildly higher for low speed. This can be attributed to the increased water quantity compared to total mixture content due to same sealflush flow irrespective of the speed.

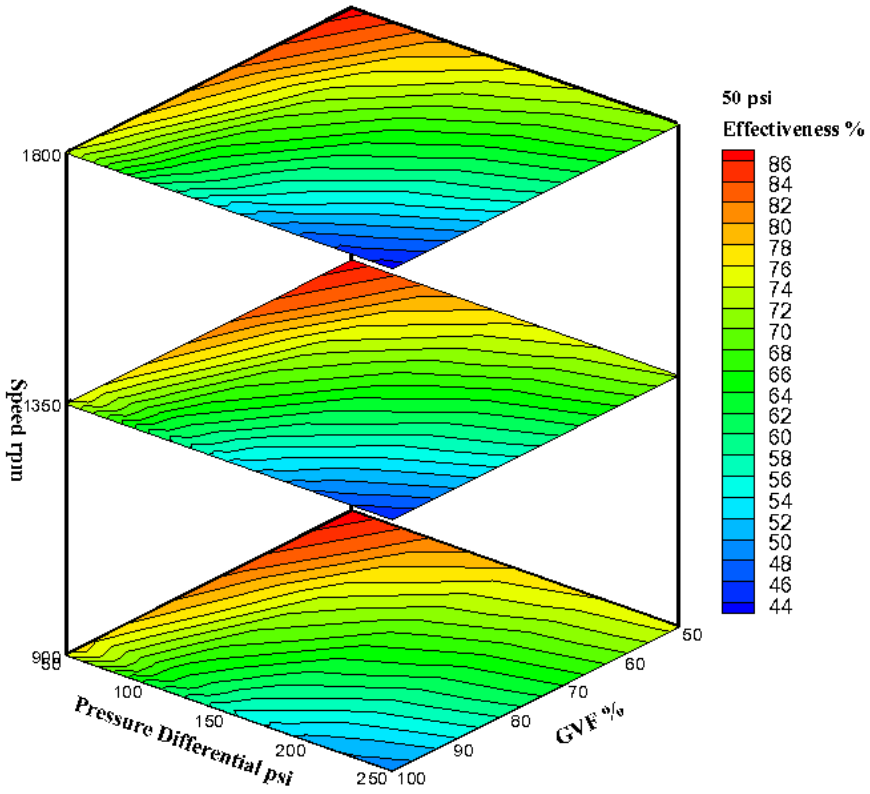

Figure 8.22: Effectiveness of the pump at different speeds

Another approach to compare the pumps ability to handle gas with theoretical maximum power is theoretical Process efficiency. The value of process efficiency goes up with increase in polytropic index. So in the case of two phase flow, the largest effect is present when the process is isothermal and theoretical maximum power added is lowest due to quenching of the air. Figure 8.23 shows the isothermal process efficiency for different pressure conditions. Process efficiency is 100% at 0% GVF due to absence of compression and once the flow becomes multiphase, process efficiency decreases with increase in GVF and becomes lowest at 100 % GVF. However, the effect of suction

pressure on process efficiency is significant and with increase in suction pressure effect of GVF and pressure differential becomes minimal.

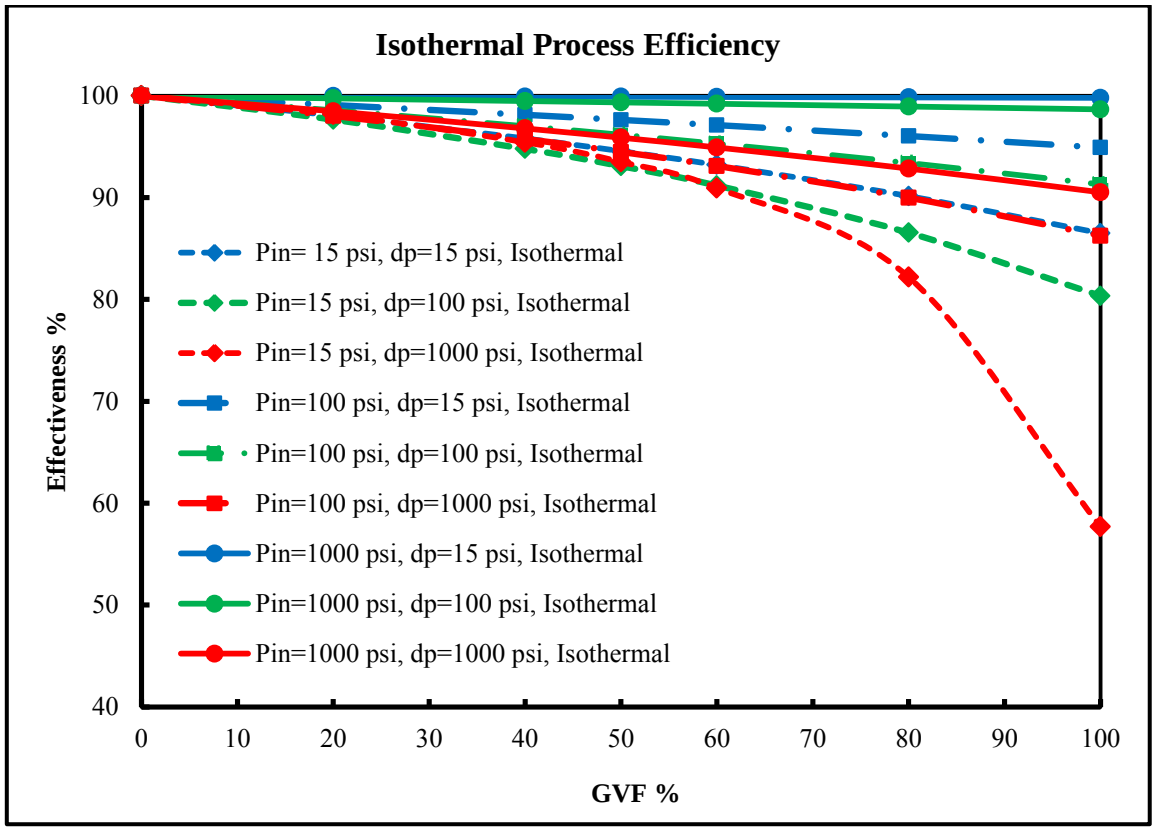

Figure 8.23: Process efficiency for isothermal processes at 15 psi, 100 psi and 1000 psi inlet pressures.

Isothermal process efficiency is the lowest value the device can achieve which represents the desirable work done in the case of multiphase pumps. The component of total work done in raising the heat is represented by polytropic index. The following Figures from 8.24 to 8.26 show the effect of polytropic index on process efficiency. Each figure shows effect of polytropic index at one suction pressure. Three contours are

presented with polytropic index of 1, 1.2 and 1.4. Efficiency drops from 100% to 56% at 15 psi as the GVF increases from 0 to 100%. Process efficiency gradually increases and becomes100% for index 1.4 as it is the isentropic process. As expected with increase in suction pressure, process efficiency increases with pressure rise becoming less steep. At 100 psi suction pressure minimum process efficiency is 70% for 100% GVF at 1000 psi pressure rise. The minimum process efficiency rises to 91% for 1000 psi suction pressure, 100 GVF and1000 psi pressure rise for isothermal compression. These figures indicate the total loss occurred compared to isentropic compression decreases from 44%, 30% to the 10% with increase in suction pressure from 15 psi, 100 psi to 1000 psi.

If heat of compression is not desirable and those losses are acceptable then this factor should be included in the analysis while comparing the multiphase pump with conventional multiphase system which consist of liquid pump, separator, compressor and lot of extra piping compared to multiphase pumps. Additionally if the separated phases are again mixed together in to the same pipeline then resulting outcome received by host platform is same as that of outcome from multiphase pump eliminating any additional energy added to the gas by isentropic gas compressor.

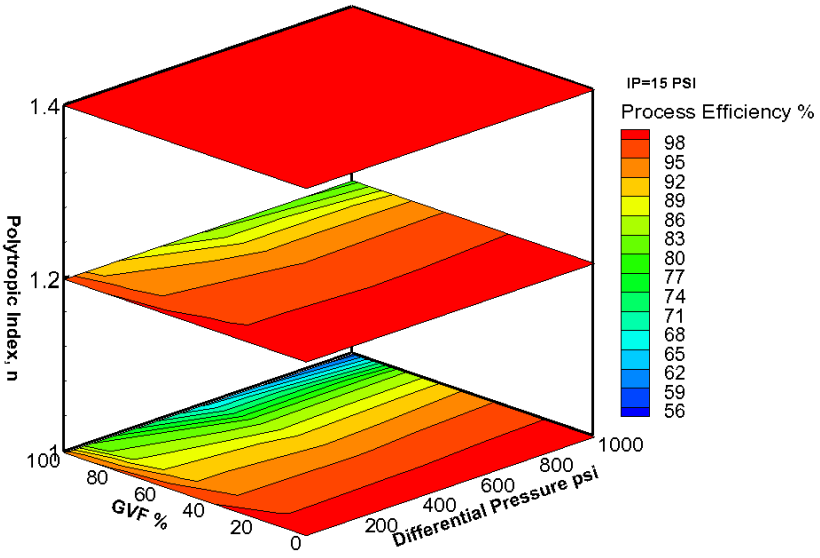

Figure 8.24: Process efficiency for polytropic process with index 1, 1.2 and 1.4 for 15 psi suction pressure

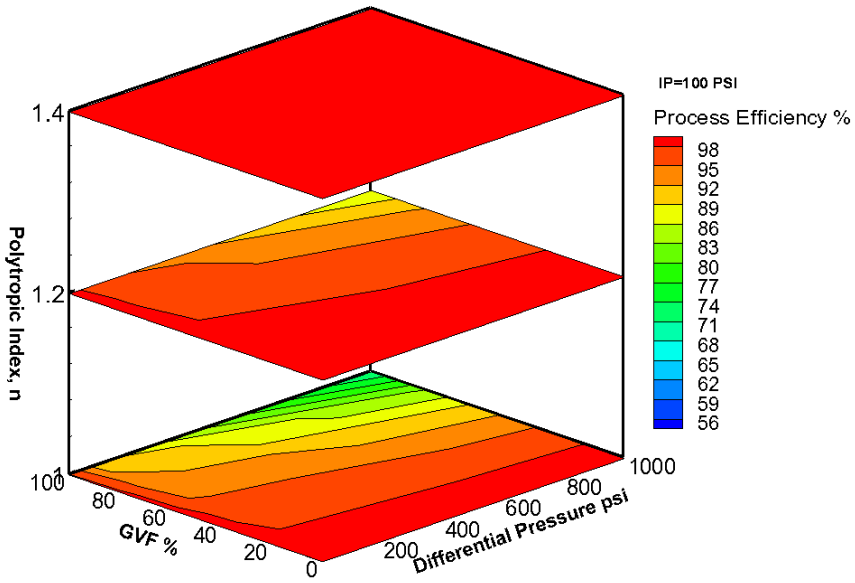

Figure 8.25: Process efficiency for polytropic process with index 1, 1.2 and 1.4 for 100 psi suction pressure

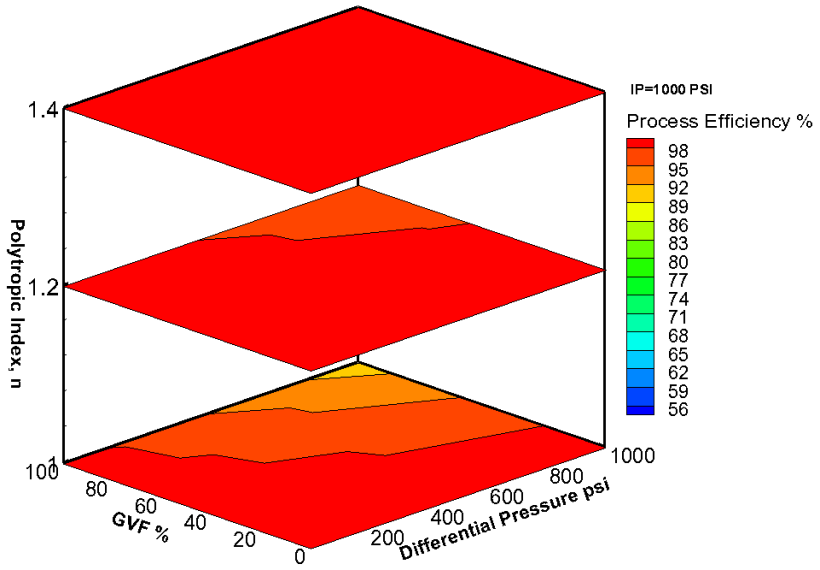

Figure 8.26: Process efficiency for polytropic process with index 1, 1.2 and 1.4 for 1000 psi suction pressure

Mechanical efficiency is a measure of how effectively the multiphase pump turns shaft energy into desired energy. Figure 8.27 shows the variation of power imparted to the gas and liquid with Input power. Input power linearly increases with the pressure rise as does the power imparted to the liquid and much higher than the gas HP. The power imparted to the gas depends on the suction pressure and increase with the increase in suction pressure. However, with increase in mass flow rate of the air there is increased leakage flow of the liquid due to increased pressure difference between first chamber and the suction chamber which reduces the liquid HP with increase in the suction pressure. While with 90 GVF total HP is mainly influenced by gas content and liquid HP has a very small share (Figure 8.28).

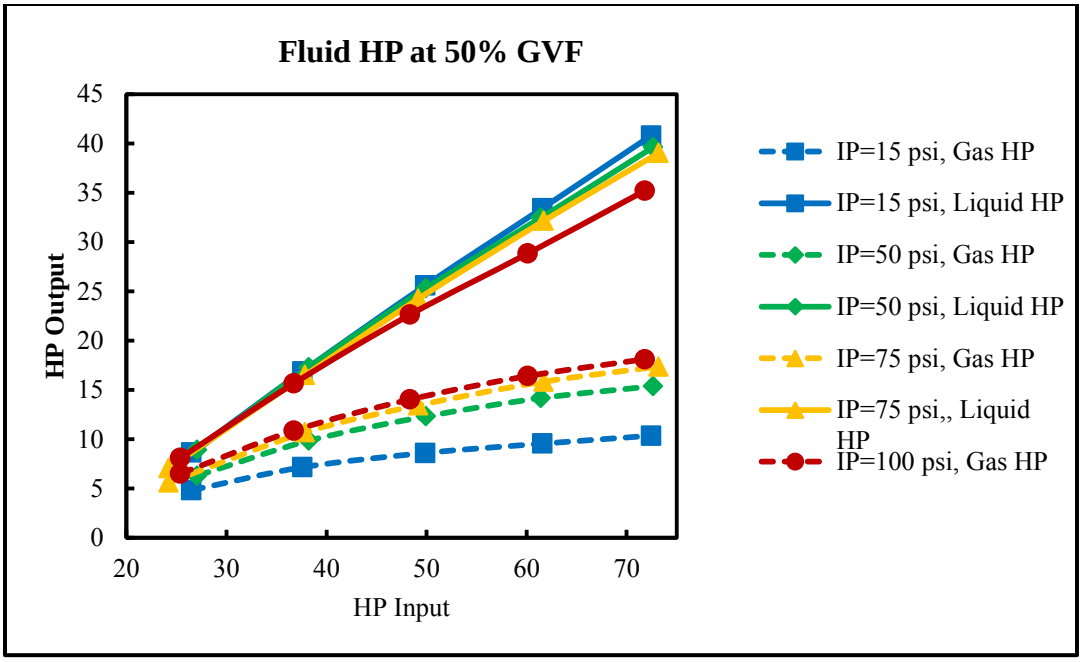

Figure 8.27: Variation of fluid HP with Input power at 50% GVF and 1800 rpm

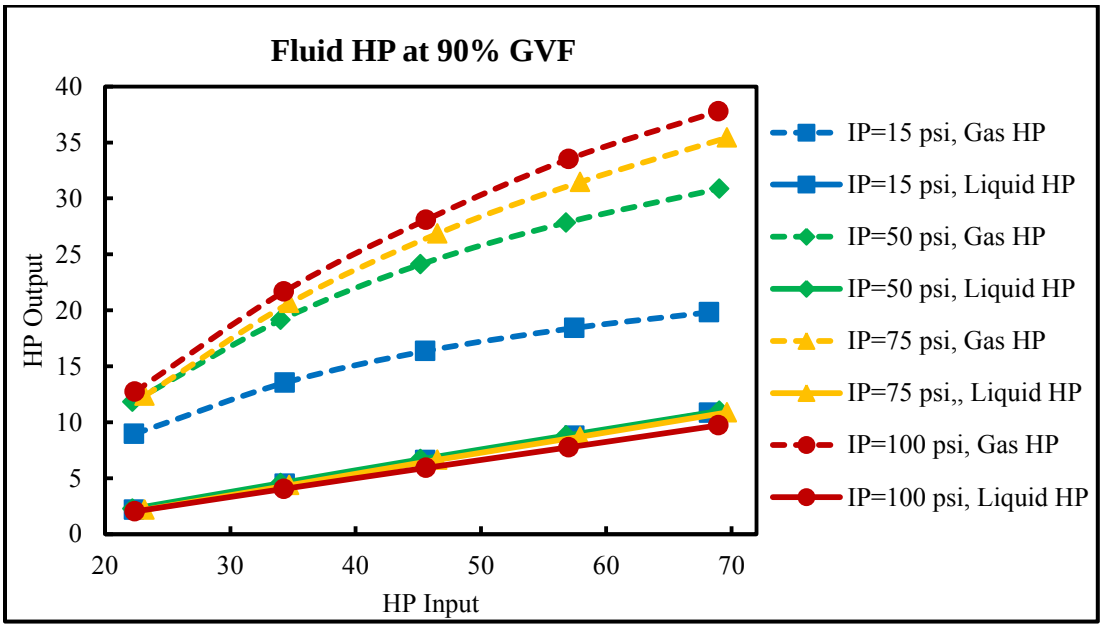

Figure 8.28: Variation of fluid HP with Input power at 90% GVF and 1800 rpm

Figure 8.29 shows the dependence of mechanical efficiency upon suction pressure and pressure rise for the GVF varying from 50% to 100% at 1800 rpm. Mechanical efficiency for 50 GVF is mainly driven by liquid content in the mixture. Efficiency is lower at 15 psi suction pressure but further increase in suction pressure from 50 psi to 100 psi does not make significant change in the mechanical efficiency. This observation can be attributed to the losses incurred due to density difference. Suction pressure significantly affects the mechanical efficiency at high GVF (90% and 100%) due to higher gas content. There is a steady increase in mechanical efficiency with increase in suction pressure due to net increase in net mass flow rate. The peak of the efficiency cause varies with the GVF with it occurring at higher differential pressure at lower GVF, while with increase in GVF peak shifts to lower pressure rise.

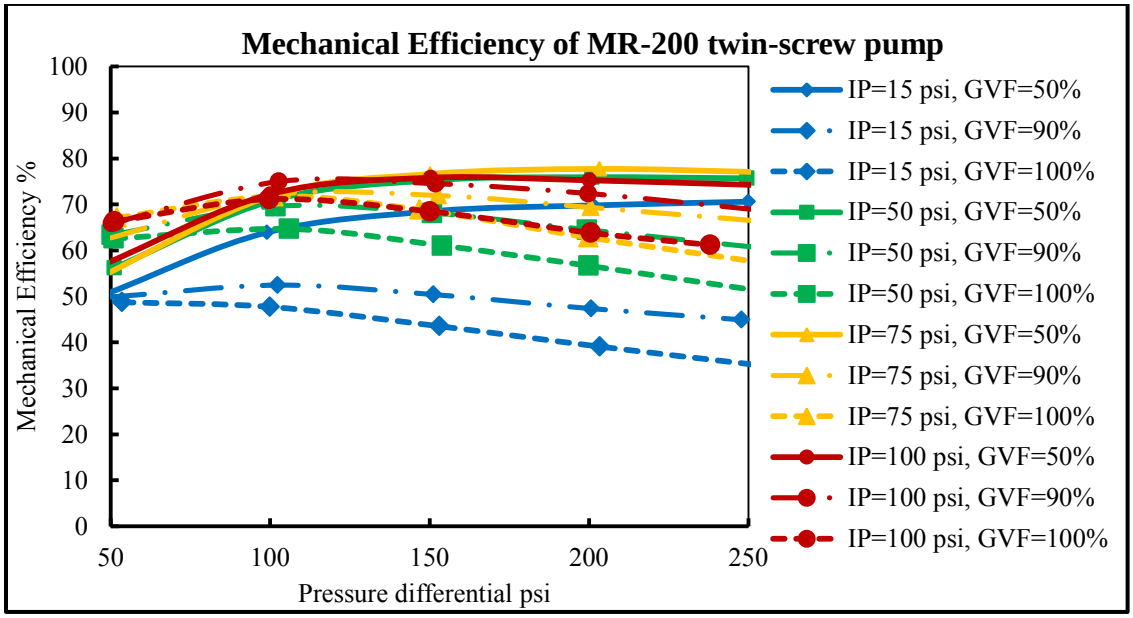

Figure 8.29: Mechanical efficiency of the twin-screw pump for different suction pressures at 1800 rpm

Figure 8.30 shows the contours illustrating the effect of suction pressure upon mechanical efficiency with different GVF and pressure rise. The efficiency is relatively constant with pressure rise but decreases with increase in GVF. Mechanical efficiency is higher with higher suction pressure due to increased gas density and increased workdone.

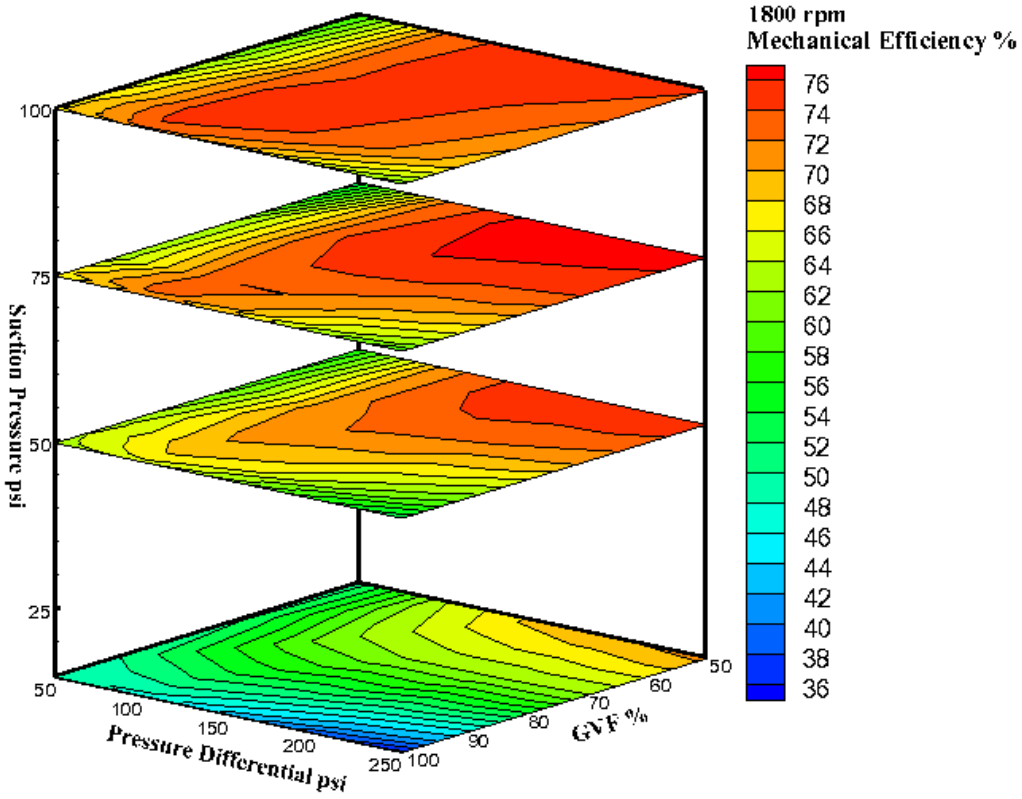

Figure 8.30: Effect of suction pressure on mechanical efficiency of twin-screw pump.

The pump performs optimally at full speed due to its design considerations, however in actual practice as the reservoir depletes the watercut and gas to oil ratio

increases resulting in lower wellhead pressures, so the pump needs to be operated at reduced speed to maintain the constant pressures, so this makes it important to understand the behavior of the pump at lower speed.

Figure 8.31 shows the variation of power imparted to gas and liquid with input power. Unlike full speed, power imparted to the liquid is no more linear as it starts decreasing after achieving the peak at around 200 psi pressure rise for all suction pressures. This can be attributed to ineffective separation in case of lower speed that results in power lost in increased leakage flow. While the power imparted to the gas increases with increase in suction pressure but total gas HP is less than total liquid HP.

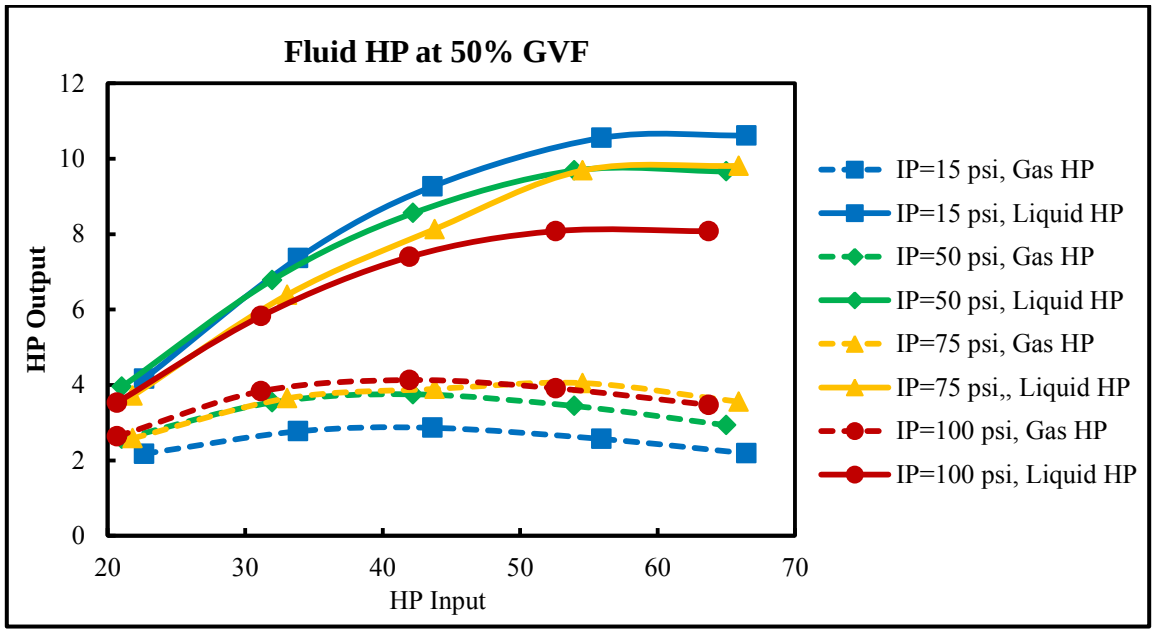

Figure 8.31: Variation of fluid HP with Input power at 50% GVF and 900 rpm

Figure 8.32 shows the variation of mechanical efficiency for different suction pressures at 900 rpm at GVF of 50%, 90% and 100%. It follows the similar trend except the efficiencies are much lower for low speed due to power lost in leakage flow. Figure 8.35 shows the effect of speed on mechanical efficiency in detail. Pump efficiency was highest at 1800 rpm, gradually decreases with decrease in speed and lowest at 900 rpm.

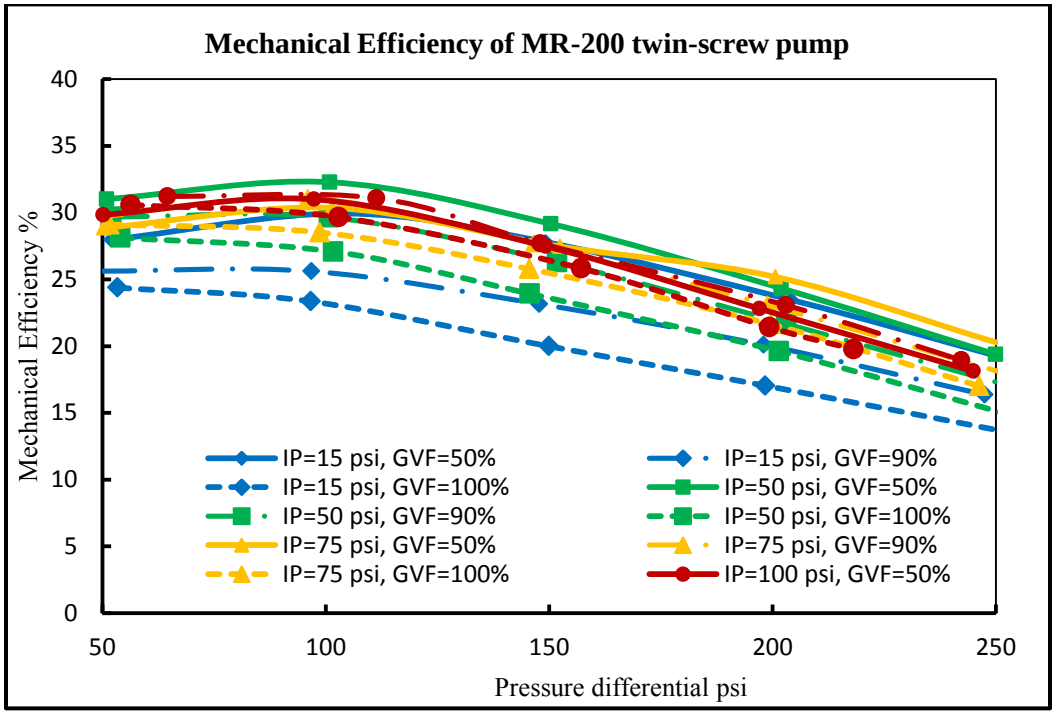

Figure 8.32: Mechanical efficiency of the twin-screw pump for different suction pressures at 900 rpm

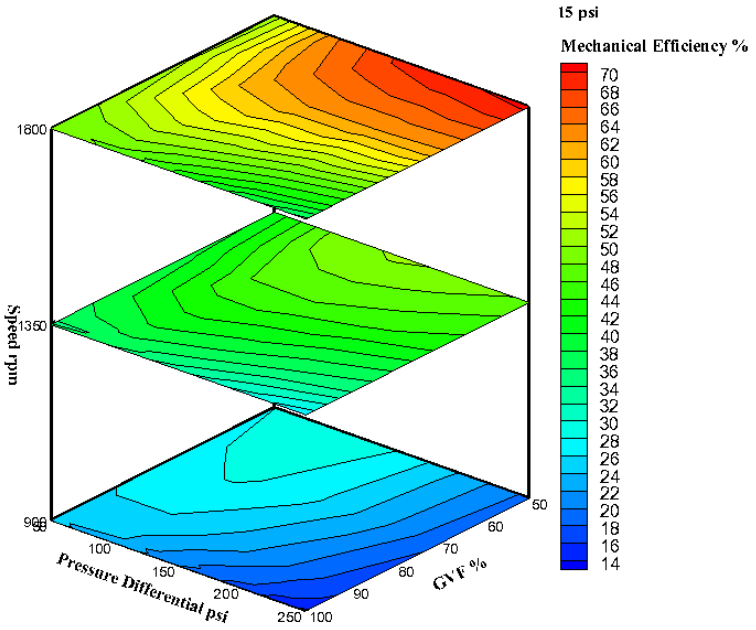

Figure 8.33: Variation of mechanical efficiency with speed 900 rpm, 1350 rpm and 1800 rpm at 15 psi Inlet pressure

8.6 Comparative study of isothermal twin-screw pump and isentropic compressor

Comparison is often made between a compressor and the twin-screw pump regarding their performance and efficiencies. Compressors follow isentropic compression and their efficiency is typically around 70%. Efficiency evaluation of the twin-screw pump is not straight forward and performance varies based on GVF, pressure rise and suction pressure. Theoretically the compression process should vary from isothermal to isentropic based on GVF. In order to run the pump efficiently, there should always be some quantity of water with gas to prevent it from leaking through different clearances. This presence of liquid changes the compression process and a twin-screw pump is not able to achieve isentropic compression which is the highest power output.

The efficiency of a compressor is evaluated based on isentropic compression. So the present argument about low efficiency of the pump compared to the compressor is not valid, since it does not compare both the systems on the same platform.

Present analysis compares the two systems based on the standard evaluation parameters currently being used in the industry. Power imparted to compress the multiphase mixture is assumed to follow isothermal compression, which is the desired energy and can be calculated based on energy added to raise the pressure. Efficiency of the compressor is considered 70% based on isentropic compression. Power output from the compressor is calculated based on the same electrical power input. Power input per kg of gas was first calculated.

$$\dot{P}_{in-total} = \frac{P_{ele}}{\dot{m}_{gas}} \qquad 8.8$$

Figure 8.34 shows the total power input per unit mass of gas for suction pressure of 15 psi, 50 psi, 75 psi, and 100 psi and differential pressure of 50 psi, 150 psi and 250 psi. Power input is higher with lower suction pressure due to higher $\left(P_{exhaust}/P_{suction}\right)$. Power required pumping the multiphase mixture decreases considerably with increased suction pressure due to decreased outlet to inlet pressure ratio and density difference.

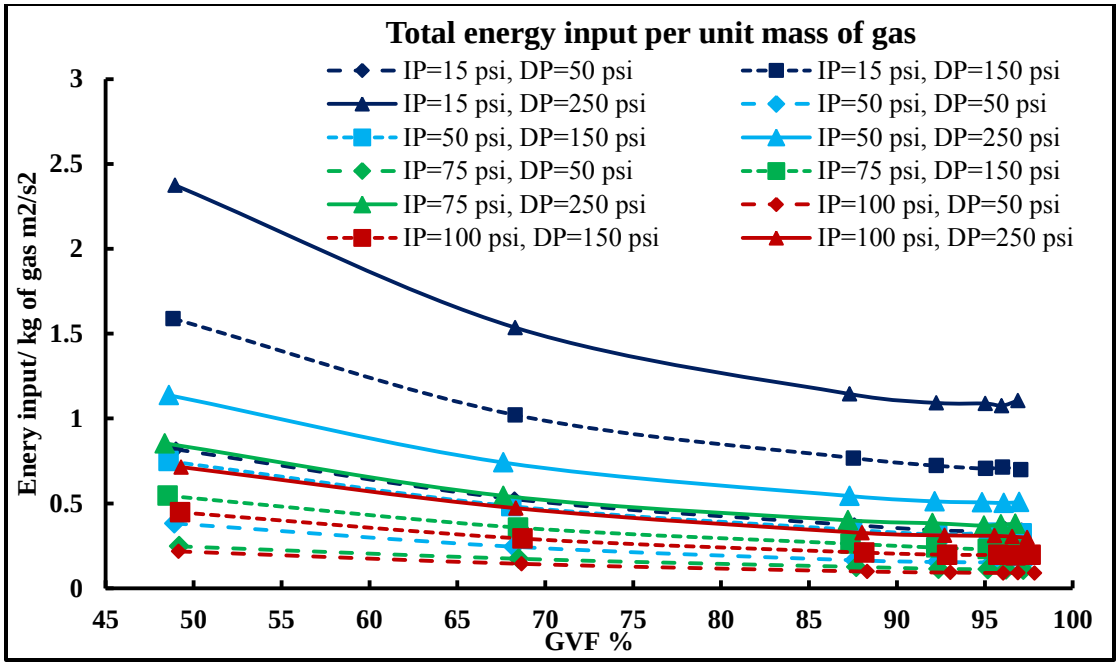

Figure 8.34: Total power input per unit mass of the gas at different suction pressures, pressure rise and GVF

The twin-screw pump is a positive displacement type of pump and the power input is theoretically only a function of pressure rise across the pump. Figure 8.35 shows that the power input as measured for the Colfax pump is independent of suction pressure and it has only a small dependence on GVF. Slop of load variation with pressure rise is same for all the GVF's.

Based on these results, power input to the gas can be calculated by multiplying GVF with total power input per kg of gas. Therefore, power input to the gas per unit mass of the gas in the case of twin-screw pump is given by

$$\dot{P}_{in-gas} = GVF.\frac{P_{ele}}{\dot{m}_{gas}} \qquad 8.9$$

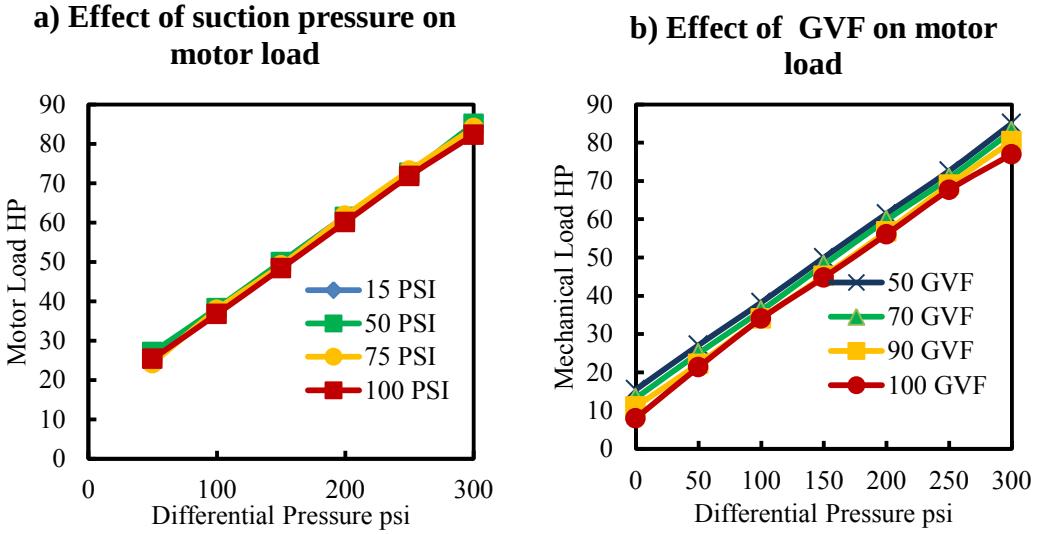

Figure 8.35: a) Effect of suction pressure on motor load at 50 GVF and 1800 RPM, b) Effect of GVF on motor load at 50 psi suction pressure and 1800 rpm.

Power required to pump the gas for same pressure rise is higher for lower suction pressure as shown in figure 8.36.

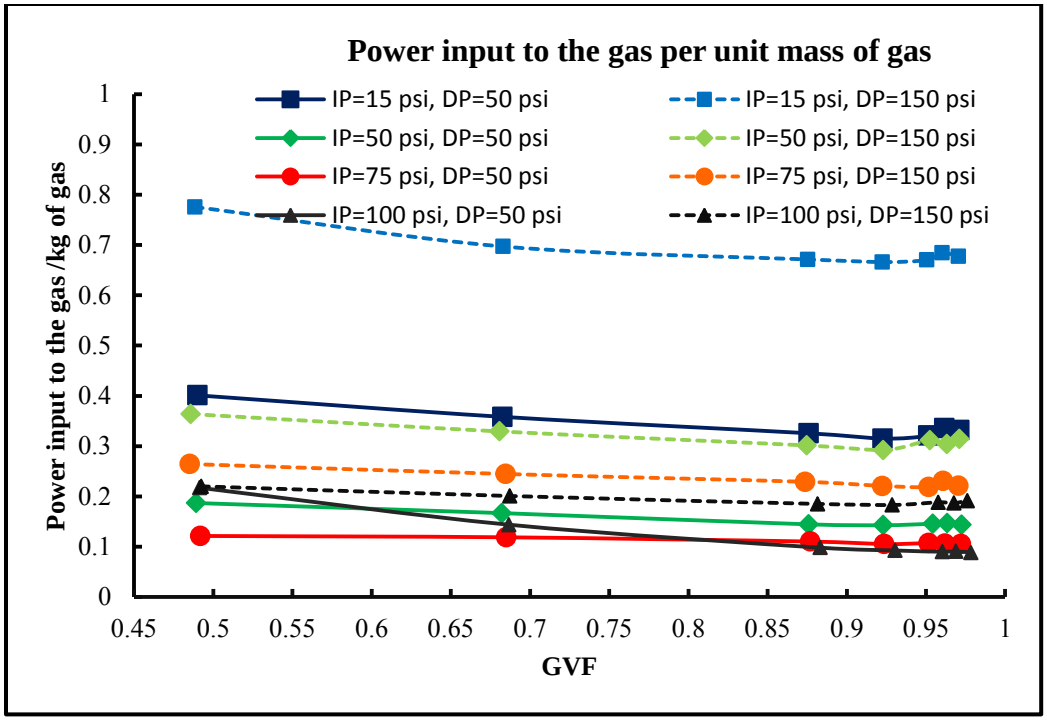

Figure 8.36: Power input to the gas at different suction pressures, pressure rise and GVF

Power imparted to the gas depends on pressure rise across the pump as well as the suction pressure at the inlet. With increase in suction pressure, power imparted to the gas increases due to increased density, however, it is independent of GVF. Figure 8.37 shows the justification.

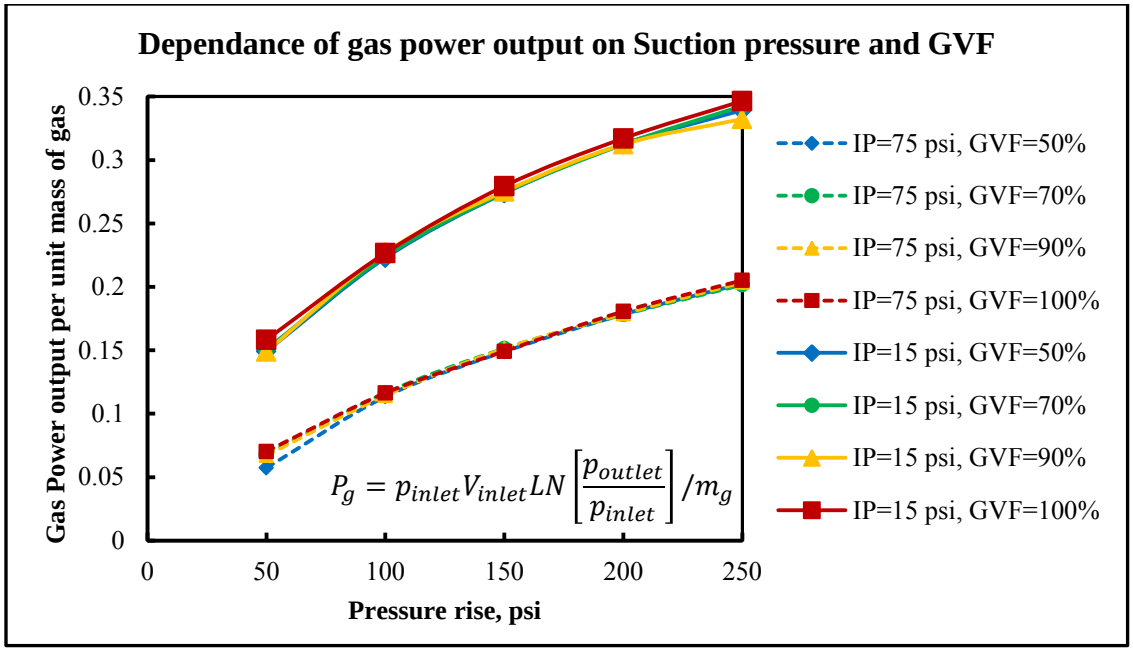

Figure 8.37: Dependence of gas power output on Suction pressure and GVF

Therefore, gas output power per kg of gas in case of twin-screw pump can be calculated by multiplying total power output with the GVF.

$$\dot{P}_{output-gas} = GVF.\frac{(P_l + P_g)}{\dot{m}_{gas}} \qquad 8.10$$

Power output per kg of gas from the gas compressor can be calculated by multiplying efficiency of the compressor to the power input to the gas.

$$\dot{P}_{output-compressor} = 0.7 * GVF * \frac{P_{ele}}{\dot{m}_{gas}} \qquad 8.11$$

Figure 8.38 and Figure 8.39 show the comparison between power output from the twin-screw pump and the compressor at 50 psi and 150 psi pressure rise respectively. Output power is higher at lower GVF due to the effective sealing and transfer of the

gases. Compressor output is significantly higher than for the twin-screw pump (TSP) at low suction pressure; however, this difference decreases with increase in suction pressure and pressure rise. At 15 psi suction pressure, 50 psi pressure rise and 95% GVF, the compressor output is 31% higher than TSP output, while TSP output is 7% higher than compressor output at 100 psi suction pressure, 150 psi pressure rise and 50 GVF. The power difference between the two compression devices at higher suction pressure, pressure rise and GVF is almost negligible.

This analysis indicates how the individual performance of the twin-screw pump and the compressor differ. Even though the TSP output is evaluated based isothermal compression, difference between output powers is insignificant at higher suction pressures. Pump performance degrades significantly at low suction pressure and lower than the compressor output, however assumption of 70 % compressor efficiency at low suction pressure need to be validated.

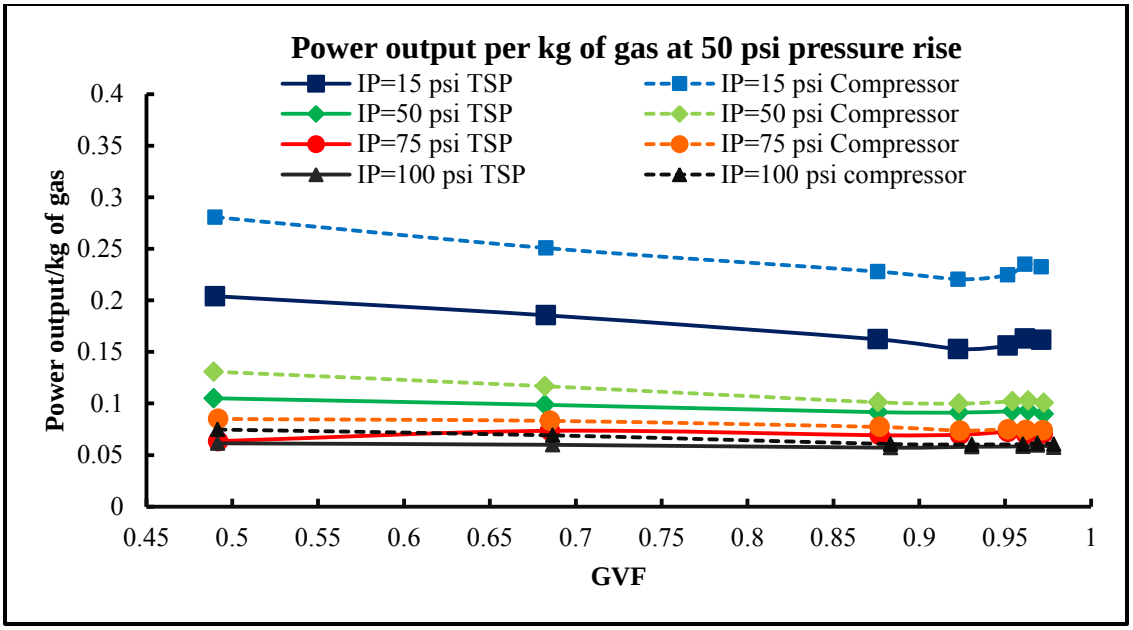

Figure 8.38: Power output per unit mass of gas at different suction pressures, GVF and 50 psi DP.

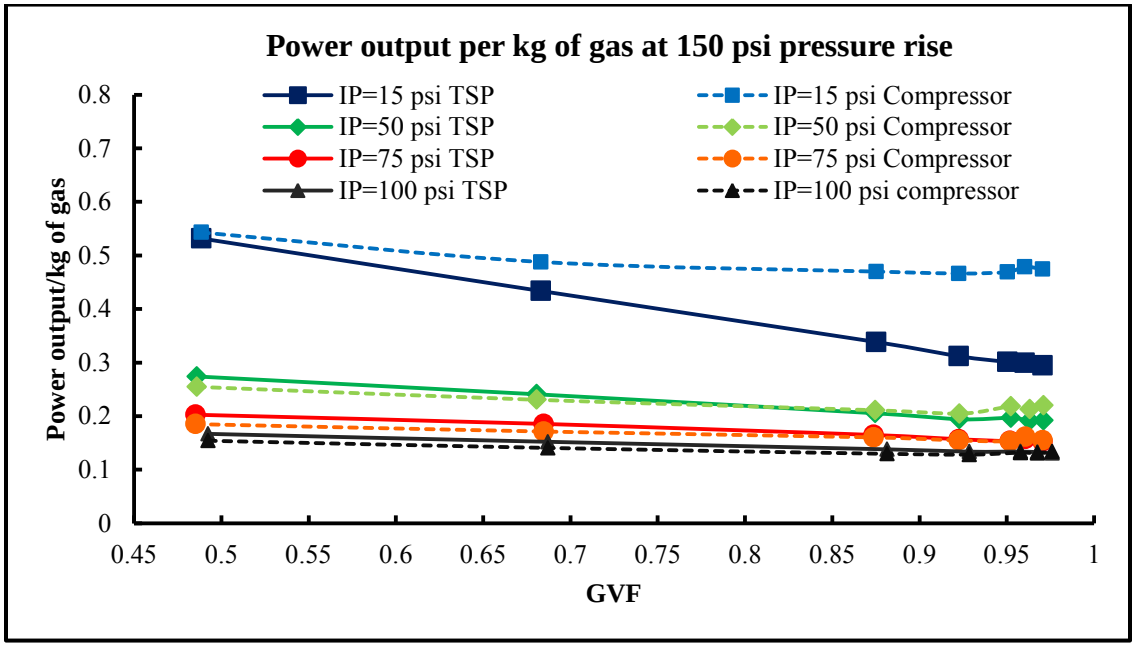

Figure 8.39: Power output per unit mass of gas at different suction pressures, GVF and 150 psi pressure rise.

Process efficiency is the measure of the true performance of the pump/compressor compared to the isentropic performance of the pump. In order to compare them effectively on the basis of isothermal compression which is the desired output, Compressor efficiency is multiplied by the process efficiency to get the isothermal efficiency of the compressor.

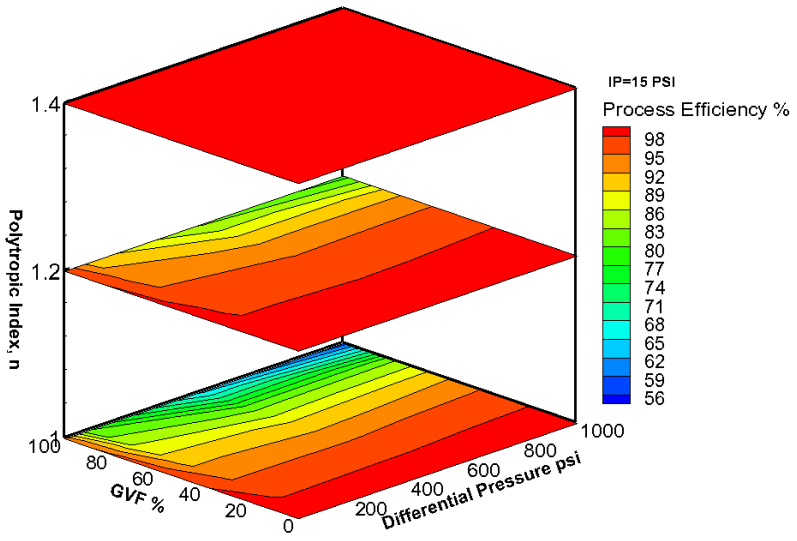

Figure 8.40: Process efficiency for polytropic process with index 1, 1.2 and 1.4 for 15 psi suction pressure

Figure 8.40 shows that the process efficiency for isothermal compression varies from 92% for 50% GVF to 73% for 100 GVF for the pressure rise of 200 psi with 15 psi suction pressure. If it is considered that gas compressor has a mechanical efficiency of 70% based on isentropic compression then multiplying this value with theoretical process efficiency will estimate the isothermal mechanical efficiency of the compressor.

So the efficiency of the compressor varies from 64% to 51 % for the GVF varying from 50% to 100%, while the isothermal mechanical efficiency of the twin-screw pump for the same operating condition is measured to be 69% and 39%. Value at 50% GVF is higher than compressor efficiency while it degrades rapidly and becomes lower than compressor efficiency at 100% GVF. However, those values represent the lower limit of the multiphase pump.

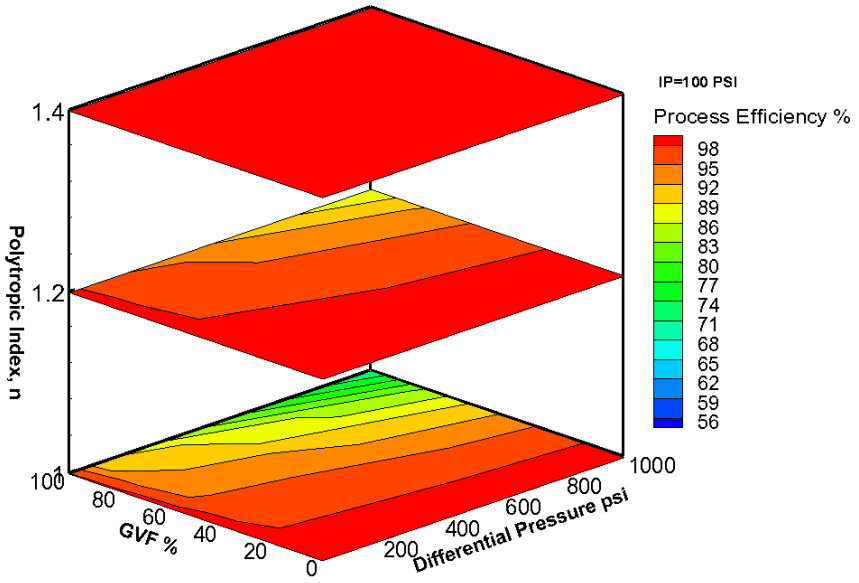

Figure 8.41: Process efficiency for polytropic process with index 1, 1.2 and 1.4 for 100 psi suction pressure

If the process efficiency values shown in Figure 8.41 are multiplied to the isentropic compressor efficiency for 100 psi suction pressure, the isothermal compressor efficiency varies from 66% to 60% while isothermal efficiency for multiphase twin-

screw pump varies from 75% to 63% with the same operating condition. Results are shown in Figure 8.42.

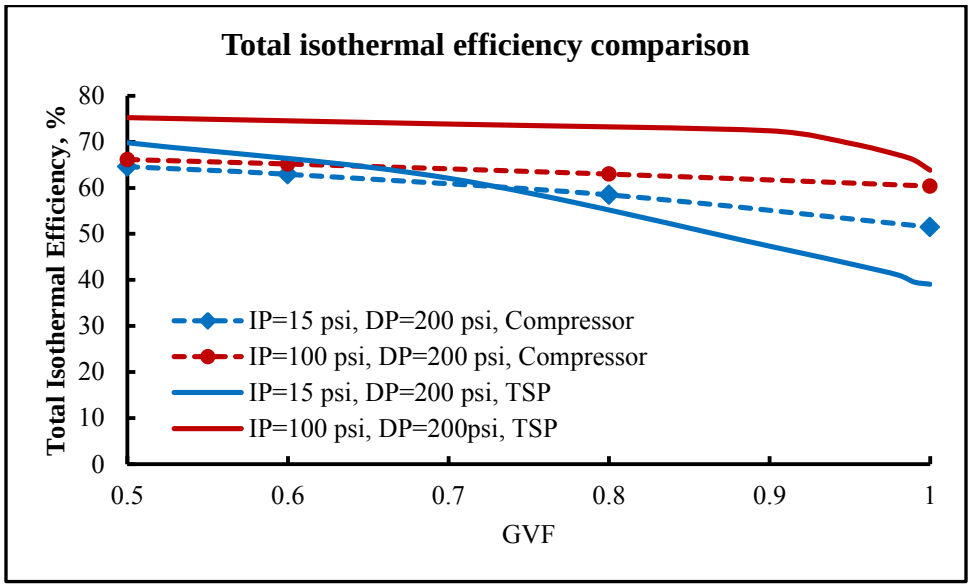

Figure 8.42: Total efficiency comparison between compressor and TSP based on isothermal compression at IP=15 psi, 100 psi, DP=200 psi

From the analysis of theoretical effectiveness it can be predicted that mechanical efficiency will further increase with increase in suction pressure as the power input is independent of suction pressure.

This comparison is based on theoretical and experimental analysis of the twin-screw pump and the assuming certain performance criterion of the compressor based on standard benchmarks. Further analysis should be carried out by treating the twin-screw pump as liquid pump for low GVF. Efficiency of conventional multiphase system should be calculated based on total efficiency of compressor, separator and the liquid pump as a

one unit. Inclusion of the efficiencies of liquid pump and separator will result in further reduction in the efficiency of conventional multiphase systems.

8.7 Transient analysis of Leistritz pump

8.7.1 Effect of temperature rise on pump performance at high GVF

Twin-screw pump operating at high gas volume fraction behaves like compressor and pumping action becomes thermodynamic issue due to nature of compression of gas. Compression follows isothermal to isentropic path depending on variation of GVF. In the existing systems, at high GVF, sealflush recirculation liquid is used to seal the chambers and thereby medium to absorb the heat of compression. The Leistritz pump employed a close loop recirculation design with 4% to 6% sealflush liquid supplied from a 50-gallon boot tank driven by exhaust pressure. Multiphase mixture from the exhaust first passes through this tank which has an inbuilt separator and strainer to separate the liquid in case of high GVF. This liquid is supplied as barrier fluid for the cooling of seals and to pump the gases effectively. However, heat generation due to the compression of the gas is diverted back to the inlet through sealflush liquid. As the liquid capacitance is very high as compared to the gases, additional energy component at the inlet adds up an extra burden on the pump in term of increased internal energy thereby reducing the effective workdone by the pump. To understand the performance quantitatively, pump was set to run till 180 F exhaust temperature and then quenching of the sealflush fluid was achieved by the means of a heat exchanger (Copper tube air-cooled heat exchanger driven by 60HZ motor) which is connected at the inlet of seal flush to the pump skid.

Figure 8.43 represents the variation in the sealflush temperature and exhaust temperature at 150 psi and 250 psi pressure rise. Temperature increase is the function of pressure rise across the pump and exhaust temperature was rising towards the adiabatic temperature of compression. Difference between the exhaust temperature and sealflush temperature is constant throughout the test cycle. The Heat exchanger was started when the temperature at the exhaust was reached 180F. There was sharp drop in the temperature after the heat exchanger started.

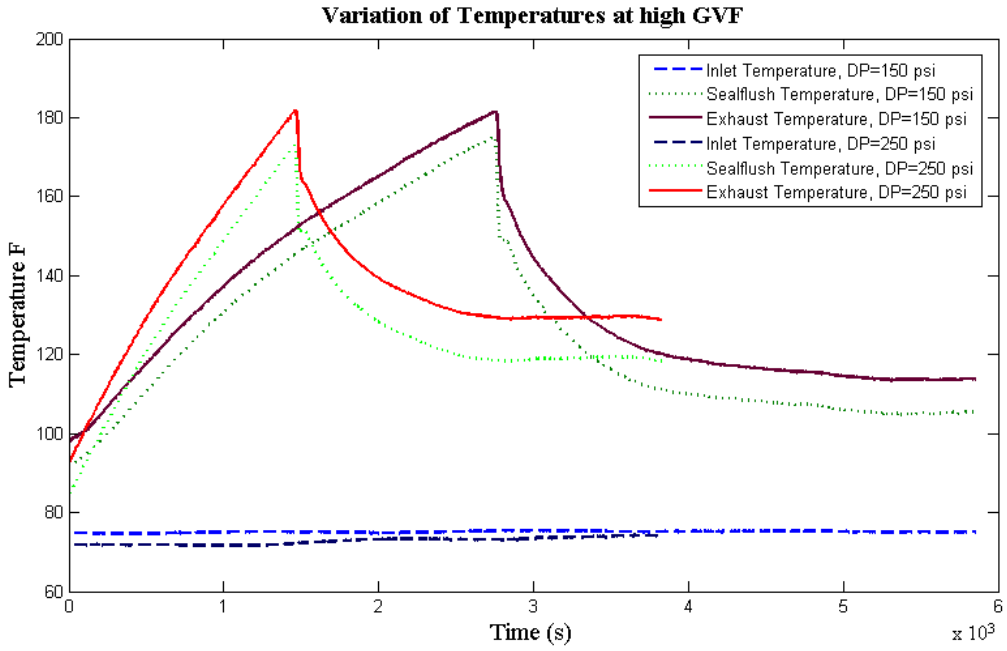

Figure 8.43: Temperature variation at different pressure rise

Figure 8.44 represents the transient response of the pump at 10 psi inlet pressure and 150 psi pressure rise. Volumetric Efficiency here referred to the actual capacity of

the pump to transport the gas against the required pressure rise. Gas volumetric efficiency of the pump decreased drastically from 75% to 52% with rise in temperature from 98 F to 180 F during the operating time of 45 minutes. With the heat exchanger turned on, the volumetric efficiency increased to 75% with temperature decreasing from 180F to 113F during the testing of next 45 minutes. Mechanical Efficiency of the pump was relatively constant for the entire testing except for sight variation during the initial testing due to fluctuation in the suction pressure. Mechanical Efficiency was evaluated based on total energy output, which can be evaluated considering polytropic compression. Results show small difference in the mechanical efficiencies based on isothermal compression and polytropic compression. This is true for the low suction pressure only.

These results indicate the impact of sealflush fluid recirculation on the volumetric flow capacity of the pump even though it is only 4 to 6% of the total flow rate. The liquid absorbs heat generated due to the compression of the gas at the outlet. The liquid with increased internal energy is feed back to the inlet, increasing the temperature of gases mixing at the inlet making it difficult for the pump to compress the gases for the same pressure rise thereby reducing the useful energy. This causes the volumetric efficiency reduction by 30% with increase in temperature from 100F to 180F. Change in the screw rotor and deflection due to temperature rise affects the volumetric capacity of the pump and is unknown in this case.

With very small increase in mechanical efficiency due to increased internal energy (which is undesirable anyway), there is a significant loss of volumetric efficiency

which causes significant degradation of the pump performance. To conclude, existing design of Leistritz pump necessitates the heat exchanger to cool down the sealflush recirculation liquid in order for the pump to run effectively and to ensure the safety of the seals.

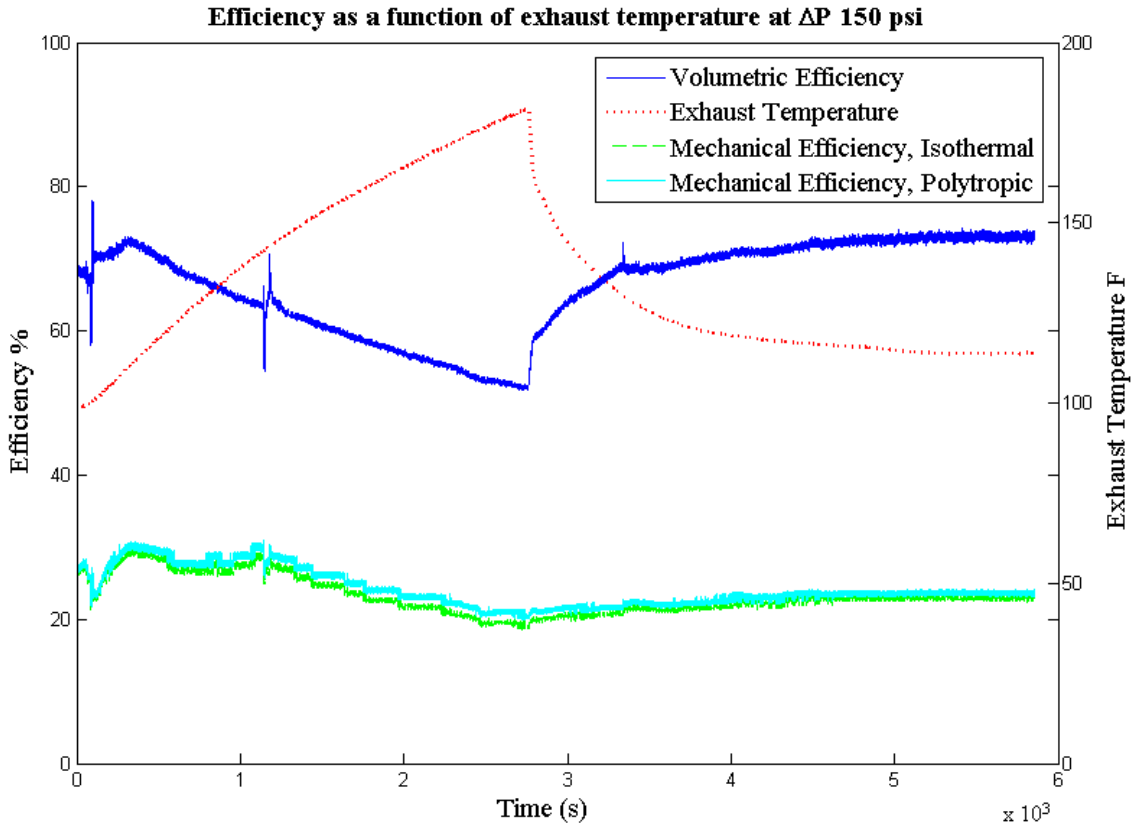

Figure 8.44: Transient Response of Screw Pump Using Heat Exchanger

8.7.2 Effect of viscosity on the pump performance

Singh 2003 and Martin 2003 presented the evidence of increasing the efficiency of the pump with increase in viscosity of the liquid phase; however, testing conducted by Chan 2006 does not confirm the earlier finding especially at high GVF. To check the effect of viscosity on the pump performance at wet gas compression, further tests are conducted for 100% GVF entering the Leistritz pump skid with recirculation fluid bearing 10cp and 20cp viscosity. Guar gel from Halliburton was used to artificially increase the viscosity of the liquid captured for sealflush recirculation. Desired apparent viscosity of the fluid was obtained by mixing the recommended amount of guar gel in to the water. Guar gel is non-Newtonian pseudoplastic fluid and viscosity of the fluid decreases with increase in shear rate. The small size of the clearances and the pressure differential across them produces high shear rate decreasing the effective viscosity of the fluid. However, even though the viscosity reduces with shear rate, it is still greater than viscosity of water and should have some effect on pump performance.

Figure 8.45 represents the transient performance of the pump under the influence of different viscosity liquid recirculation. Sealflush recirculation was maintained constant for the different viscosity tests. Experimental results by Chan 2006 reports at high GVF, viscosity is not the dominant parameter, however, efficiency does increases at low GVF with increase in viscosity. Results agree well with the prediction from the Chan 2006 for high GVF tests. Volumetric efficiency of the pump was decreased with increase in viscosity. There was significant decrease in the efficiency from 1cp to 10cp. Efficiency difference for 10cp and 20cp was insignificant. Mechanical efficiency of the

pump was constant regardless of the viscosity of the fluid. From the present experiments on high GVF, it can be concluded that with high viscosity, fluid becomes insufficient to seal the gases due to decreased fluidity enabling more gases to escape through clearances. Instead increasing the viscosity, it would be interesting to see the effect of friction reducer or surfactant mixed with sealflush fluid recirculation at high GVF.

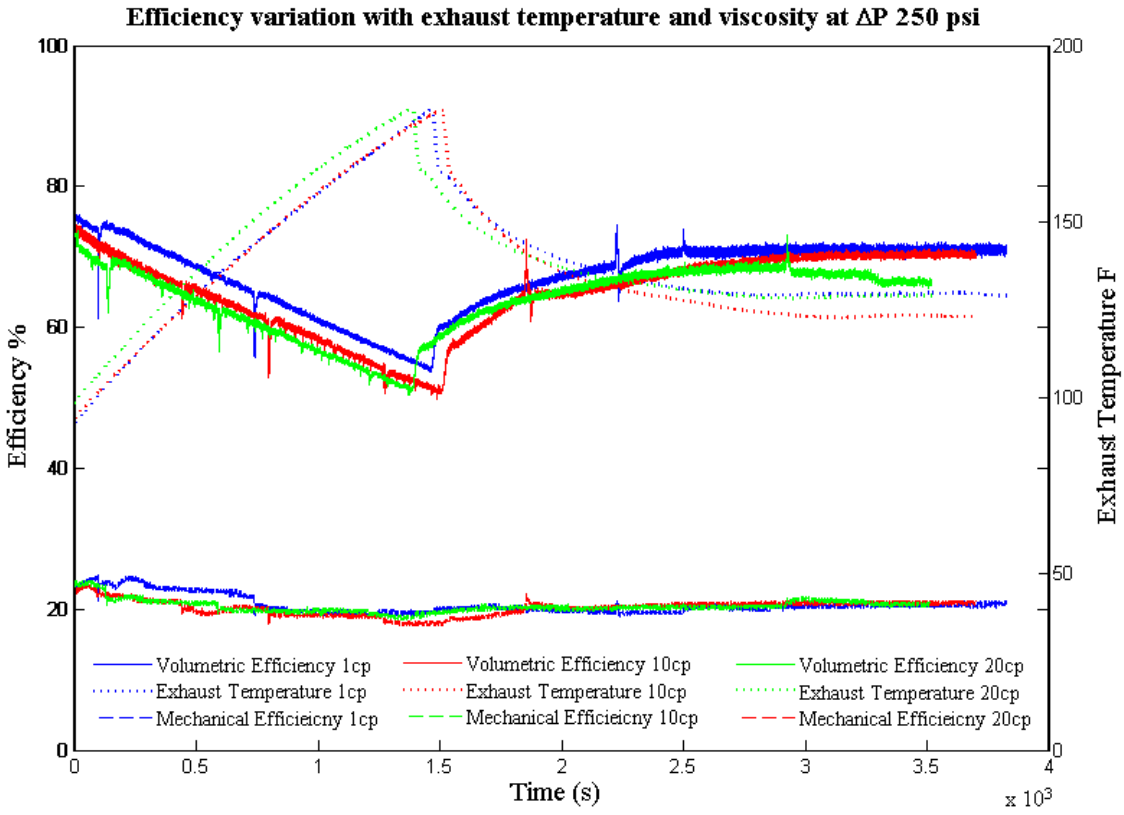

Figure 8.45: Effect of viscosity on transient performance of twin-screw pump

8.8 Performance comparison of twin-screw pumps with different volumetric capacity

Steady state analysis was performed on two different twin-screw pumps with different flow rate capacity and design. Volumetric Efficiency of the Colfax pump was consistently higher than the Leistritz pump. One interesting observation about the Leistritz pump was it does not confirm the conventional norms about dependence of volumetric flow rate on the GVF. With increase in GVF volumetric efficiency decreased. At high GVF, there was increase in volumetric efficiency with increase in pressure rise beyond 150 psi. This can be attributed to the seal flush recirculation which is proportional to the pressure rise, effectively sealing the gases thus increasing the overall flow rate. Smart sealflush recirculation design system actually increases the performance of the pump at high pressure rise; however, the total volumetric efficiency was far less than the Colfax pump (Figure 8.46). Information about design parameters was not available for the Leistritz pump, but from the experimental testing it is evident that design of the screw rotors, clearances and scaling has a significant effect on the performance of the pump.

Effectiveness of the pumps is shown in the Figure 8.47. Difference in the effectiveness of the pump is insignificant for both the pumps. Effectiveness of the pump to work as a compressor is decreased with increase in GVF and pressure rise as discussed in previous section.

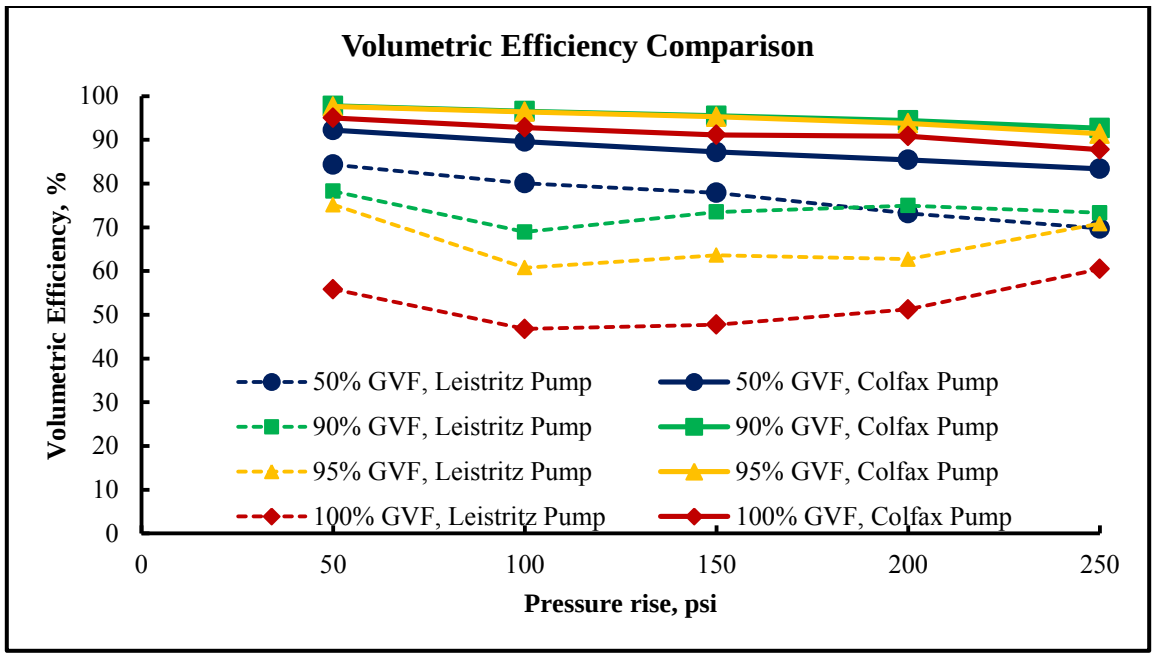

Figure 8.46: Volumetric efficiency of two different pumps with different capacity

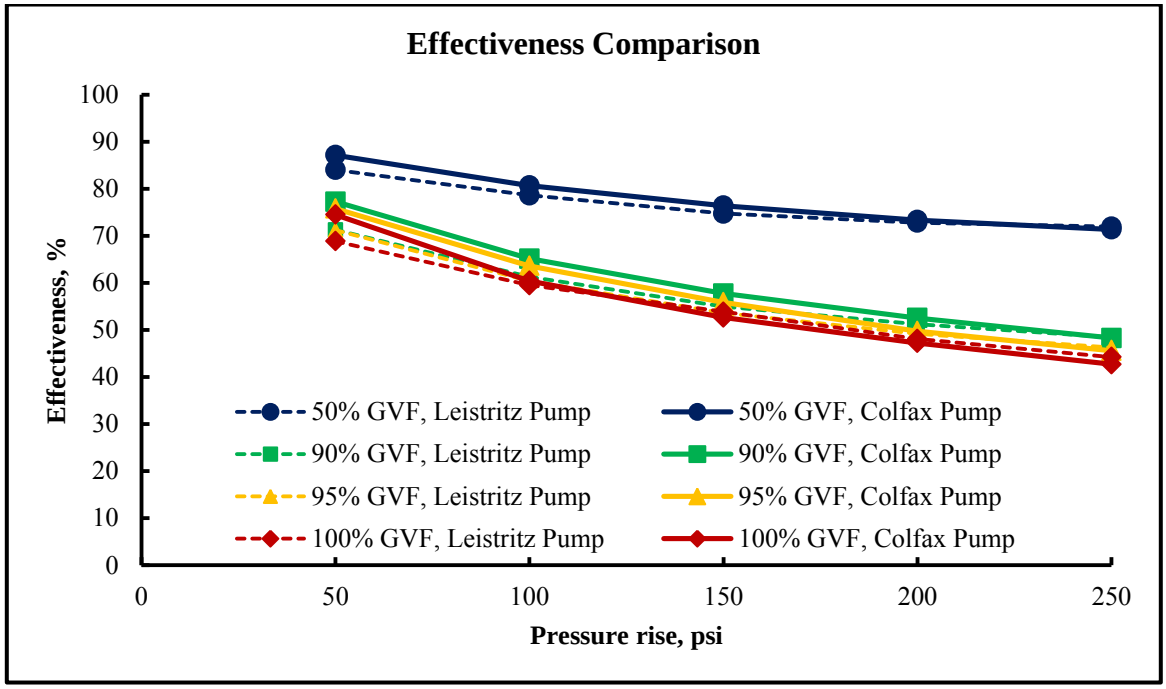

Figure 8.47: Effectiveness comparison of twin-screw pumps with different capacity

Mechanical Efficiency of the Colfax pump was higher than Leistritz pump for the entire GVF and pressure rise as shown in Figure 8.48. Power imparted to the multiphase mixture was significantly lower in case of Leistritz pump due to the higher leakage flow rate. Self-sufficient design of Leistritz pump is good fit for the current requirement of the oil and gas industry, however, the design parameters such as clearances, and the scaling has a significant effect on the performance of the pump. To effectively compare both the pumps, it would be interesting to see the performance of the Colfax pump for close loop recirculation system.

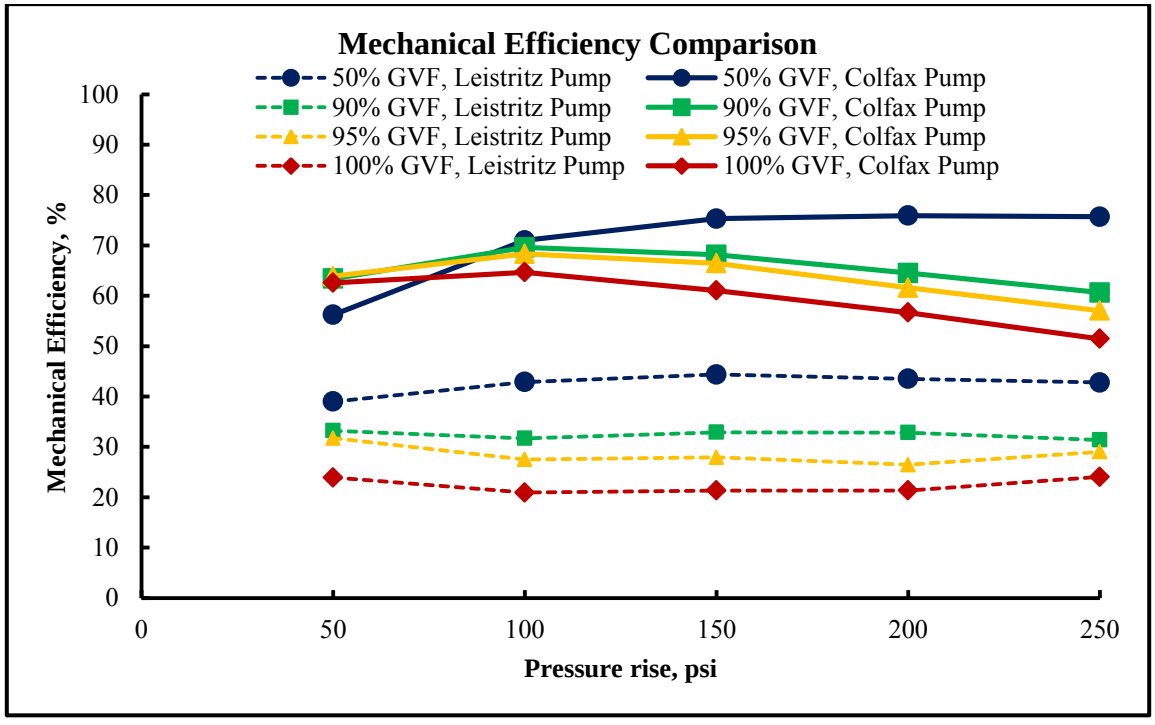

Figure 8.48: Mechanical efficiency comparison of twin-screw pumps with different capacity

9 COMPUTATIONAL FLUID DYNAMICS OF TWIN-SCREW PUMP

9.1 Single phase CFD simulation of twin-screw pump

This section represents the CFD simulation of twin-screw pump for single phase flow. Solid geometry of the pump was provided by the pump manufacturer. However, a new geometry was created with 0.1% larger volumetric capacity to match modifications made to the pump. Meshing was performed using the Gambit meshing tool. A grid independence study was performed to justify the number of nodes created are sufficient and further increase in node has no effect on the results. The small size of the clearances compared to the fluid pockets complicates the flow behavior and it is somewhat analogous to labyrinth seals. Recommended y* for standard wall function should be less than 300 for accurate turbulent flow representation. Current meshing without adaption employs all hexahedral elements with very fine mesh in the clearances. However, mesh is relatively coarser in the pockets. y* is highest at the inlet and exhaust of the screws before forming the pockets due to higher turbulent kinetic energy in the suction and discharge chamber. Grid size near to the root of the rotor is relatively coarser which result in higher y* value. y* values for base models are shown in Figure 9.1.

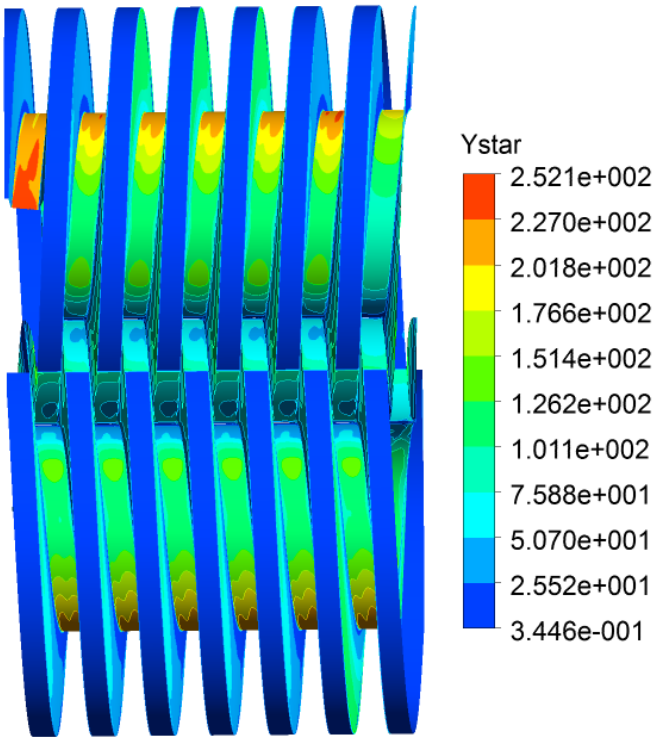

Figure 9.1: The y* value at the wall of screw rotors.

The model created without adaption has y* value of 252. Mesh adaption was carried out for 150, and 50 y* value and the number of nodes created are shown in the Table 9.1

Table 9.1: Number of nodes for different models

	Model 1	Model 2	Model 3
y*	252	150	50
No. of nodes.	6.76 million	7.02 million	14.4 million

Figure 9.2 shows the percentage change in the leakage flow as a function of grid size. There was maximum difference of 0.5 % in leakage flow between model 1 and model 3 which has 14.4 million nodes. Difference between model 1 and model 2 was 0.07%.

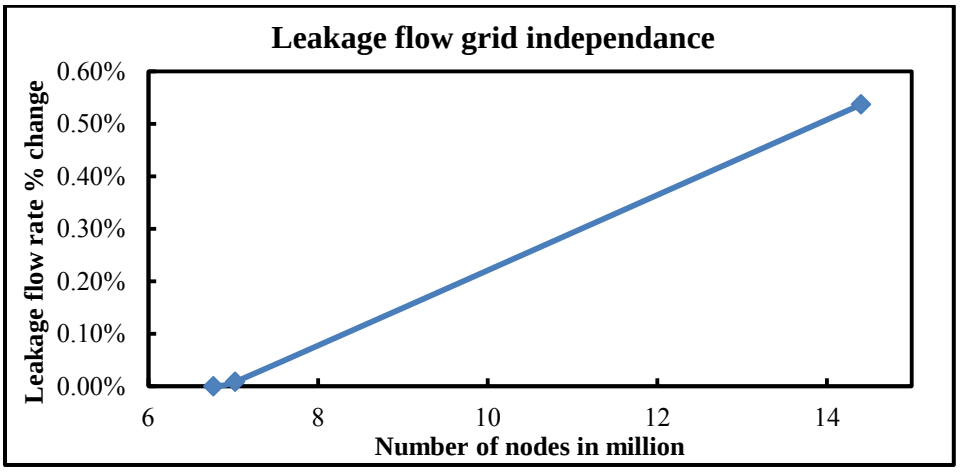

Figure 9.2: Mesh independence study for leakage flow rate

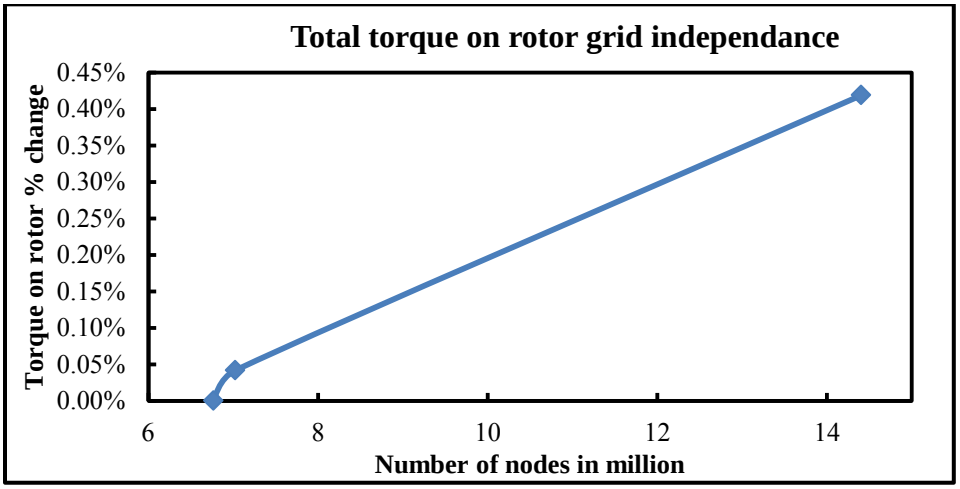

Figure 9.3: Mesh independence study for total torque on the rotors.

Similar results are seen in the Figure 9.3 for the torque required to rotate the screws with maximum difference of 0.43%. Basic model without grid adaption was chosen for the analysis.

This simulation assumes there is no change in the clearances due to the radial loading. Moving reference frame was used to simulate the rotation of screws. This was chosen to simplify the pump simulation. For the time dependent pump rotation case, the sliding interfaces of the rotors require continuous mesh adaption in very tight clearances. The pump is classified as a positive displacement pump whose leakage into and from each individual cavity (pocket) formed by the screws is what must be determined to calculate the actual displacement of the pump. Since the screws moves slowly compared to the fluid leakage velocity, a quasi-steady state assumption is made. This assumes that the flow field for each fixed angle of the screws will be the same if calculated using steady state moving reference frame compare to the time dependent solution obtained for the same angular position. The moving reference frame simulation is then used to determine the leakage flow rate, pressure and GVF distribution inside the pump. The calculated leakage rate is then subtracted from the theoretical flow rate based on pump geometry to obtain the pump actual flow rate. Figure 9.4 shows the justification. Position A refers to the pocket formed at left screw and pocket is in the process of formation in the right screw. Position B represents pocket formed at right screw and in the process of formation in the left screw. Leakage flow rate from the first pocket to suction chamber depends on pressure which varies with the rotation, however both the screws are aligned

such that the leakage flow from one pocket is balanced by leakage flow from other pocket and resultant leakage flow from both the screws is constant.

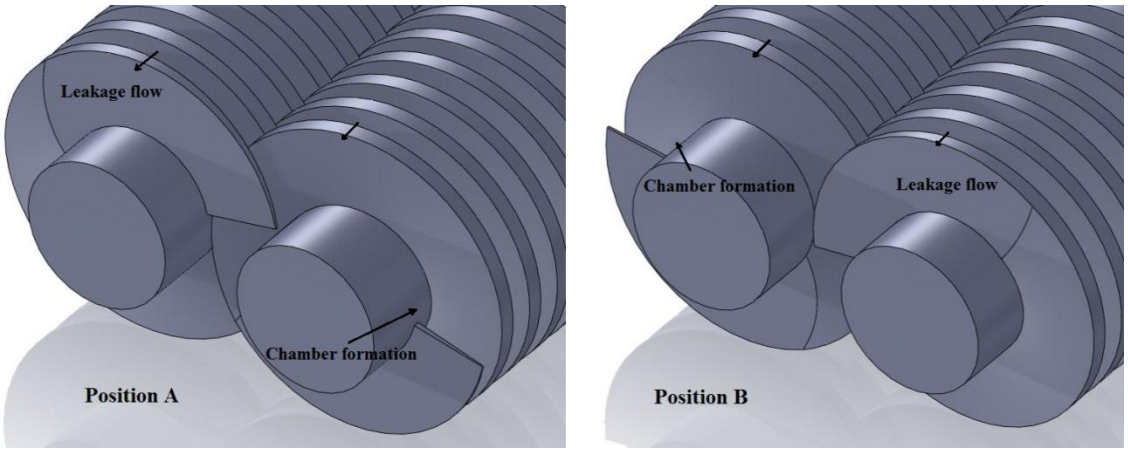

Figure 9.4: Leakage flow independence on the position of screw rotors

There is loss of pressure head between the inlet of the manifold (point of measurement) and the screw inlet due to suction effect. GVF may vary from the inlet of the manifold to the inlet of the screw depending on this loss. However, this study assumes that GVF is unchanged from the point of measurement to the screw inlet.

Since this is positive displacement type of pump, Actual flow rate is theoretical flow rate minus the leakage flow rate. Leakage flow rate is the function of geometrical parameters, rotational speed and the pressure difference across the chambers. So the pressure inlet and pressure outlet condition was specified for the single phase simulation. Pressure profile obtained with steady state analysis is presented in Figure 9.5. Plot of variation of the pressure along the liner is shown in the Figure 9.6. Pressure in the

chamber is relatively constant along the axis due to very small axial velocity of the chamber. There is a sudden drop in the pressure due to sharp transition from chamber to the clearance, followed by linear pressure decrease across the clearance incurred due to friction loss. The pressure becomes constant again in the next chamber towards the inlet.

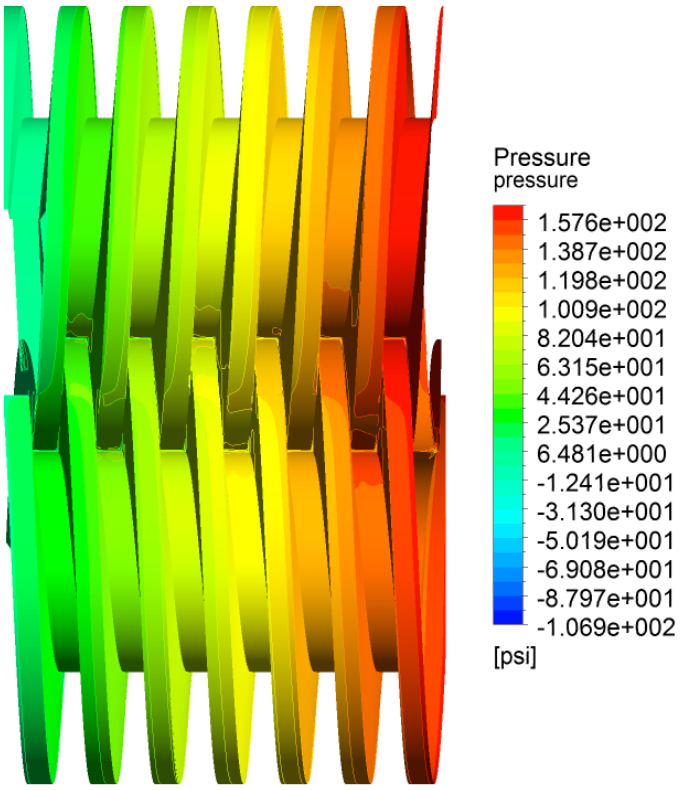

Figure 9.5: Static pressure distribution along the twin-screw rotors.

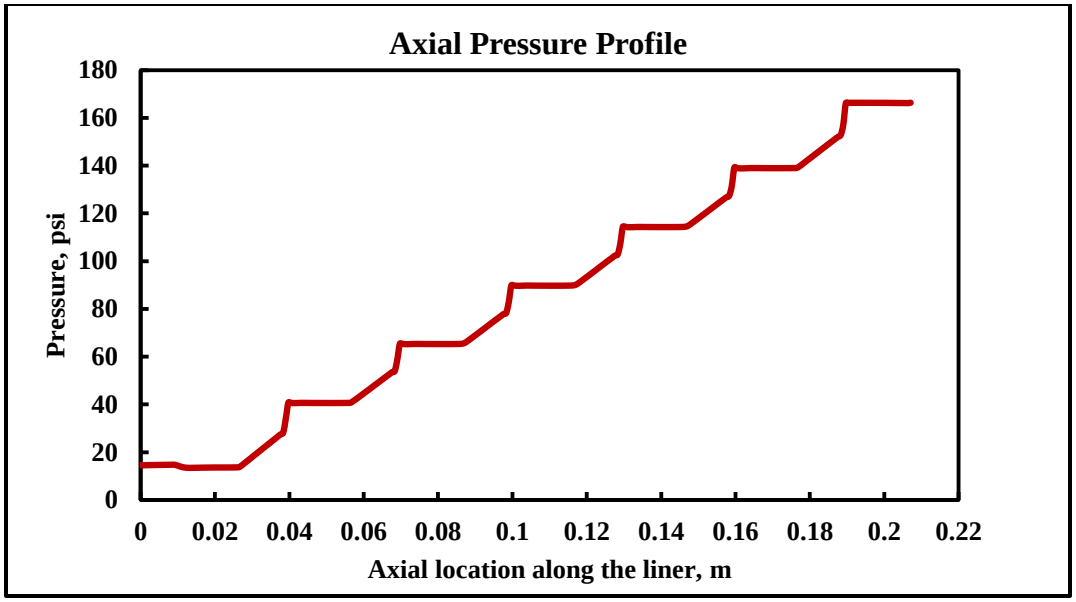

Figure 9.6: Pressure distribution along the circumferential clearance

Figure 9.7 shows the axial pressure distribution along the flank and root of the right screw. Root clearance is formed between root of one screw and the crown of other screw, so it separates the two chambers of the same screw. From the pressure distributions it is seen that there is sharp localized reduction in the pressure at the root clearance of both the screws. A sudden increase in momentum is seen due to the reduction in the area and the pressure difference across the two chambers formed across one screw rotor. Pressure falls below the absolute zero pressure at the center of root in the chamber near to the suction, increases as the fluid expands and becomes constant. In reality, the fluid would cavitate producing the pockets of gas at this location. However, cavitation model is not included in this study which causes pressure to fall below absolute zero. If the inlet pressure were increased, all of these pressure would also be

increased as well and eliminate the cavitation. Here it should be noted that the direction of rotation of the screws is opposite to the direction of flow. A plot of the static pressure for 15 psi inlet pressure at different root clearances from inlet to exhaust is shown in the Figure 9.8. It is observed from the figure that pressure is not entirely constant in the chamber. Interestingly it is seen that the pressure in the leg of the "C" shaped chamber on the exhaust side is little bit lower than the pressure in leg on the other side of the chamber. Pressure is lower in the leg where the fluid is leaking in from the previous chamber which is at higher pressure and momentum of the fluid coming in to the chamber reduces the pressure while high pressure region is the outlet of the chamber and this extra increase in the pressure is realized due to the back flow. The same can be seen from the velocity streamline shown in the Figure 9.9 b) where the velocity streamline are directed towards the circumferential clearance from root clearance due to the suction effect while a vortex is created in the outlet section of the chamber due to the back pressure.

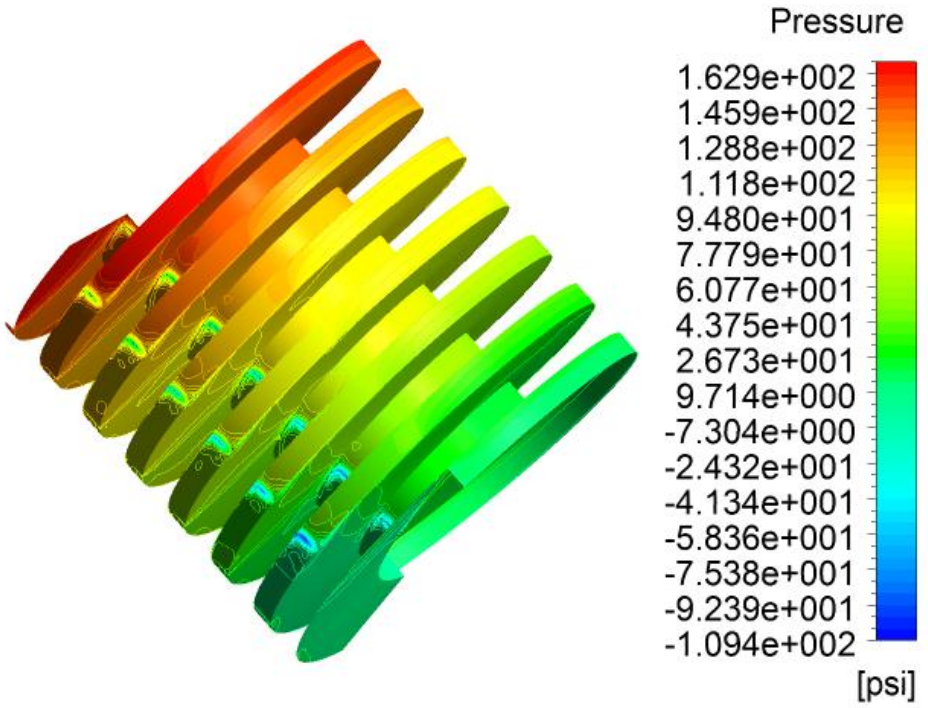

Figure 9.7: Pressure distribution across the right sided screw rotor.

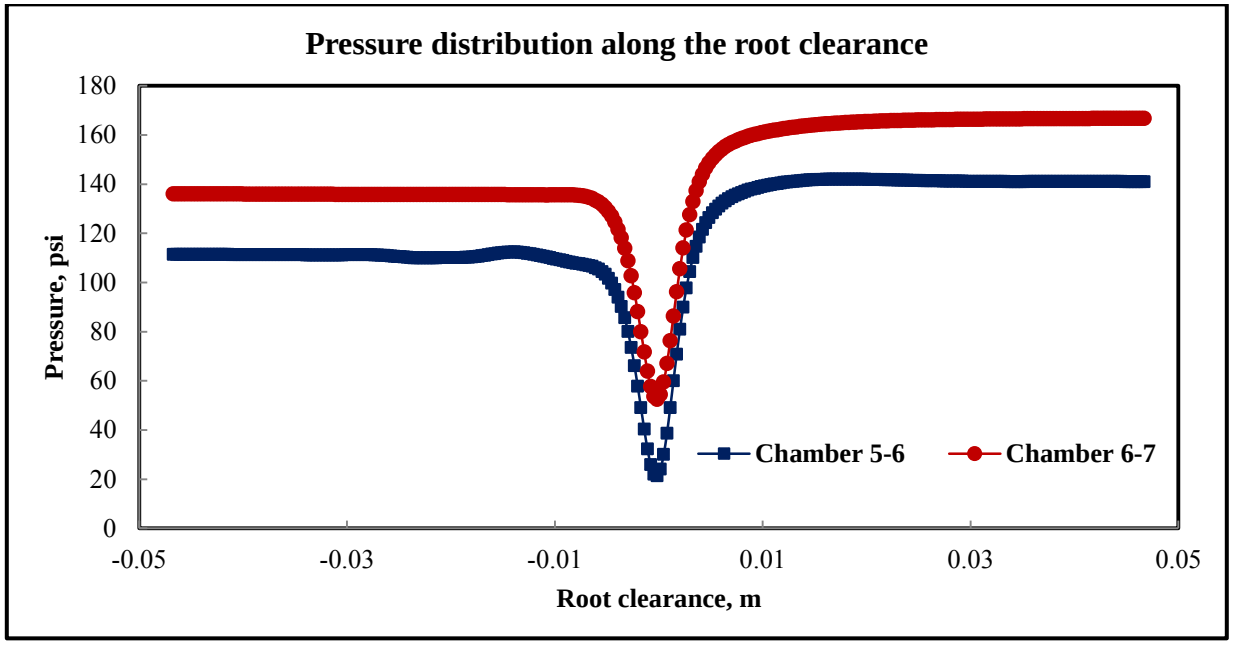

Figure 9.8: Pressure distribution along the root clearance

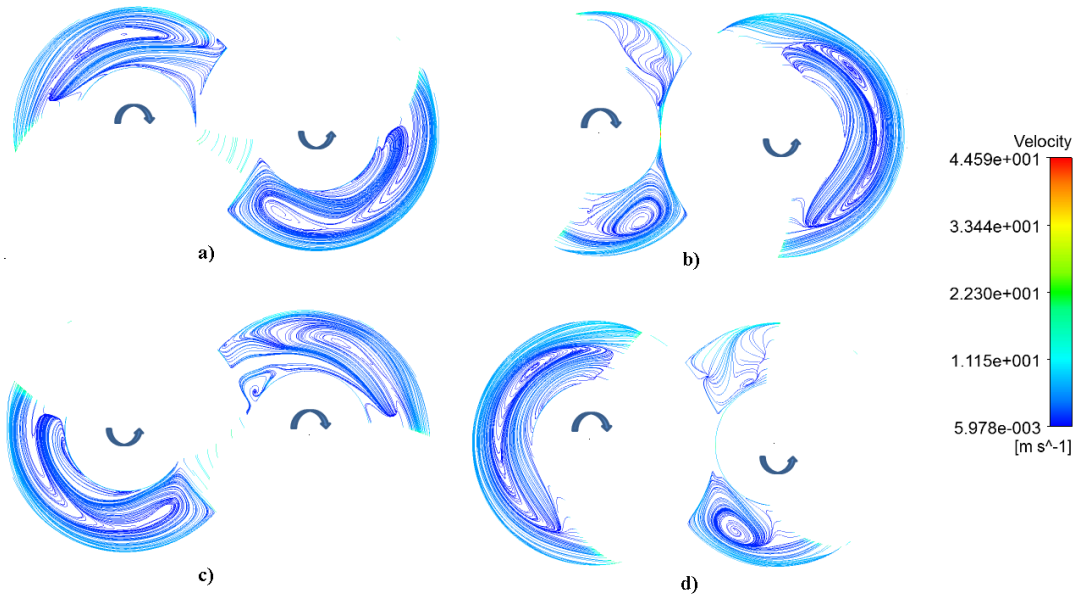

Figure 9.9: Streamlines showing the variation of the velocity for the one rotation of the screw ($\theta=90^0$)

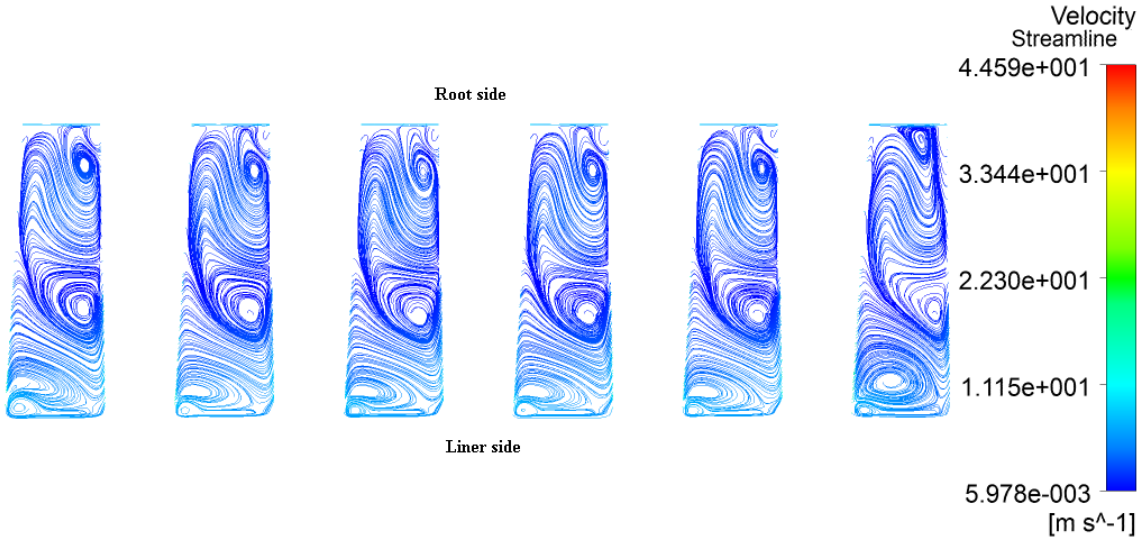

Figure 9.10: Velocity streamlines in the chamber across axis of the screw

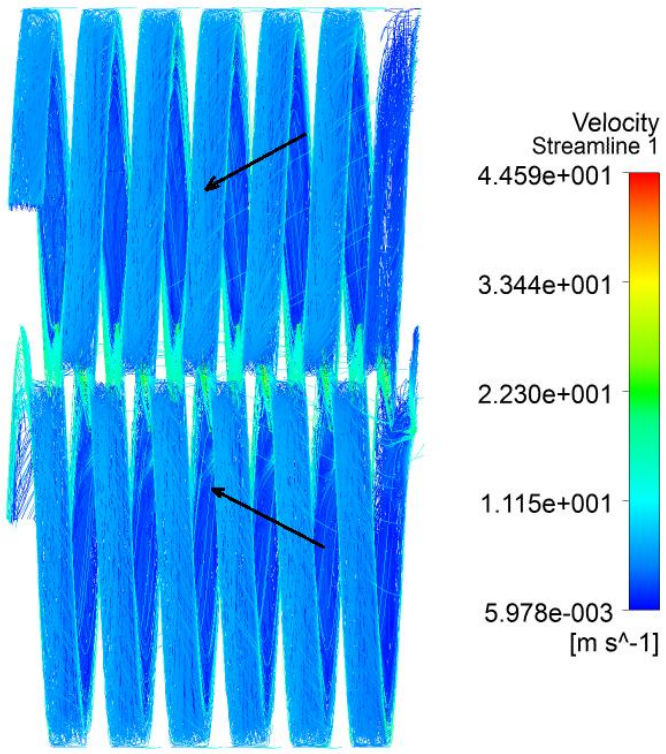

Figure 9.11: Streamlines showing the direction of leakage flow along circumferential clearances.

Figure 9.9 a) ($\theta=0^0$) , b) ($\theta=90^0$), c) ($\theta=180^0$), and d) ($\theta=270^0$) shows the fluid behavior for one apparent rotation of the rotor. There is very small variations in the average velocity in the pocket with the velocity profile the same at every pitch distance along the axis of the screw. The velocity is highest in the different clearances due to the reasons explained above.

Velocity streamline in the pockets along the axial direction are shown in the Figure 9.10. Fluid flow is driven by pressure differential across the circumferential clearance. Vortices are generated at the inlet of the clearances indicating the velocity inlet loss due to sudden reduction in the area and acceleration of the fluid inside the

clearance. As the driving force is constant for all the clearances, magnitude of the vortex is constant at every pitch distant along the axis of the screw. There is minimal variation in the vortex between the first and last chamber due their exposure to the inlet and exhaust. Figure 9.11 shows the direction of the leakage flow along the circumferential clearances which is the resultant of the tangential velocity due to the direction of rotation of the screw and the pressure differential along the screw.

Table 9.2: Percentage distribution of leakage flow through one side of the screw pump

Pressure rise psi	$leakage_{cc}$ gpm	$leakage_{fc\&rc}$ gpm	$leakage_{cc}$ %	$leakage_{fc\&rc}$ %
50	32.67543	7.862148	0.759386529	0.240613471
100	45.76812	10.84518	0.763040634	0.236959366
150	55.39258	13.04323	0.76453112	0.23546888
200	64.11863	15.11899	0.764202912	0.235797088
250	71.36645	16.90196	0.763166622	0.236833378

Table 9.2 shows the percentage distribution of leakage flow through the circumferential clearance, flank clearance and root clearance. For the single threaded pump cross section area of circumferential clearance is much larger than the flank and root clearances. 76% of total leakage flow occurs through the circumferential clearances, while around 20% of leakage flow is contributed by flank clearance. Root clearance contributed only 4% of total leakage flow.

Effect of speed on leakage flow is shown in Figure 9.12. As discussed in the experimental evaluation, leakage flow rate is higher for higher screw speed due to

increased component of tangential velocity in the axial direction. CFD result agrees with experimental data.

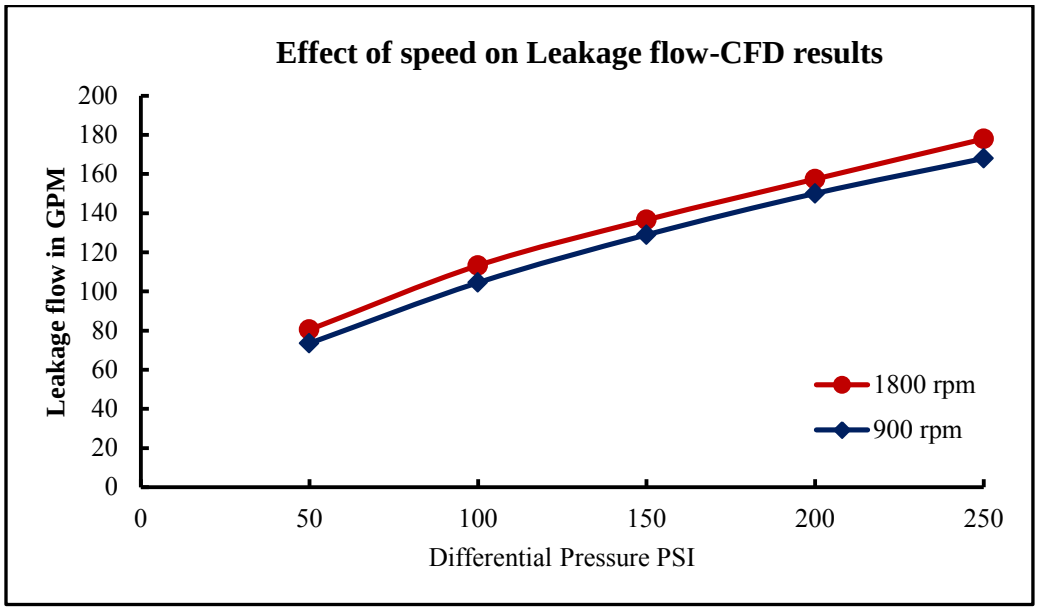

Figure 9.12: Effect of speed on single phase leakage flow of the pump

The pump is also tested for 0% GVF for the purpose of validation. It has been shown from previous studies that leakage flow for single phase can be correctly represented by analytical equations. Leakage flow rate is calculated using this approach to validate the CFD results for single phase flow. Total leakage flow was derived by separately calculating the leakage flow induced due to pressure differential and leakage flow induced due to rotation of the screws. Leakage flow induced due to pressure differential is calculated using following method

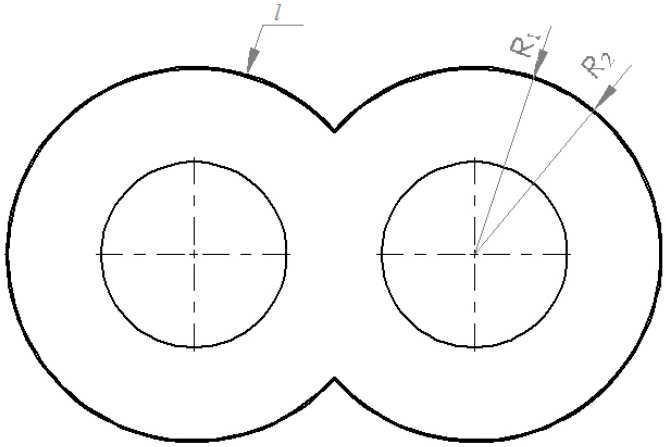

Figure 9.13: Circumferential clearance flow path

Due to the small clearance to screw diameter ratio (Figure 913), the circumferential clearance between the screw outer diameter and the liner can be modeled as rectangular channel with length equal to the length of the helix described by the outside diameter of the screw, height $c = R_2 - R_1$, and B, width of the screw crown.

With this simplification, flow rate through the clearance can be modeled as flow through two parallel plates driven by pressure drop and the speed. Pressure drop can be calculated by using the definition of Darcy-Weisbach friction factor.

$$\nabla p = \frac{\lambda . \rho . B . v^2}{4c} \qquad 9.1$$

No information is available on the surface roughness so it is modeled using Fanning friction factor correlation C_f ($\lambda = 4C_f$) for pressure induced flow.

$$C_f = 0.066 . Re^{-0.25} \qquad 9.2$$

where

$$\mathrm{Re} = \frac{\rho . v . c}{\mu} \qquad 9.3$$

Knowing the fact that the pressure difference is linear along the circumferential clearance, average velocity was calculated by combining in Equations 9.2 and 9.3 with Equation 9.1. Slip rate was calculated using$Q_{slip} = v . c * l$. Actual flow rate was then calculated using Equation 4.3.

Leakage flow induced due to screw rotation was modeled as Couette flow and calculated using equation given by Vetter

$$Q_{couette} = c . l . \sin\alpha \, . \left(\frac{R_1^2 . \omega}{R_2 - R_1} \right) . \left[ln\left(\frac{R_2}{R_1} \right) . \left(\frac{R_2^2}{R_2^2 - R_1^2} - 0.5 \right) \right] \qquad 9.4$$

where l is length of circumferential gap, α is the helix inclination angle, ω is angular velocity in rad/s, R_1 and R_2 are the inner and outer radii of circumferential clearance. Figure 9.14 shows the plot of CFD prediction as well as analytical predictions for different pressure rise across the first chamber and suction chamber at 1800 rpm. Both results show good agreement for the specified pressure differential.

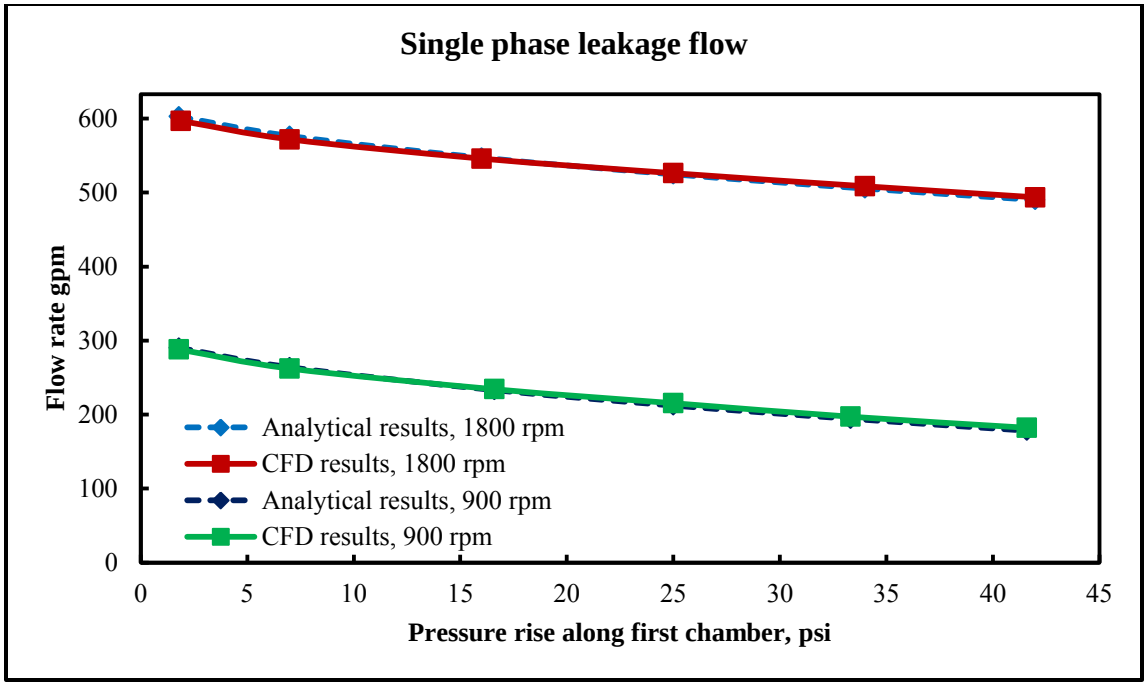

Figure 9.14: Flow rate prediction using CFD simulation and analytical approach.

Colfax twin-screw pump was run for single phase flow at different speeds and pressure rise conditions to validate the CFD simulation data. Figure 9.15 shows the total flow rate comparison between CFD data and experimental results. CFD results agree well with the experimental data. Maximum difference in total flow was around 5% at 200 psi for the 1800 rpm while this difference increased to around 15% at 250 psi pressure rise for the 900 rpm. CFD consistently under predicts the leakage flow for both the speeds. The difference in actual boundary conditions at the screws and the boundary conditions used for CFD may be major contributing factor for this discrepancy.

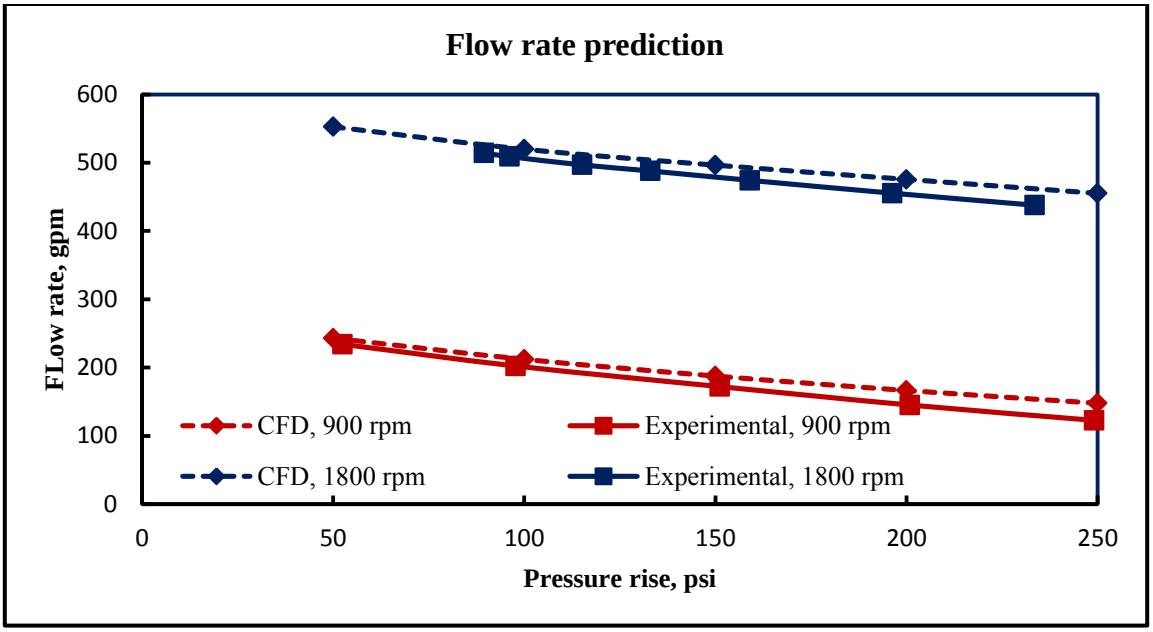

Figure 9.15: Leakage flow comparison using CFD and experimental data

9.2 Two phase CFD simulation of multiphase twin-screw pump

9.2.1 2D CFD simulation of rotating and translating cavities for two phase flow

Two-phase CFD simulations of the twin-screw pump were performed and results are validated with experimental data. To understand the 2 phase behavior under pure rotation and to validate the previous conventions, 2D CFD simulations were performed by assuming cavities as a fluid pockets between series of coaxial rotating discs translating from inlet to outlet at constant axial velocity (Figure 9.16). The simulation was performed for 15 psi suction pressure with pressure rise of 50 psi.

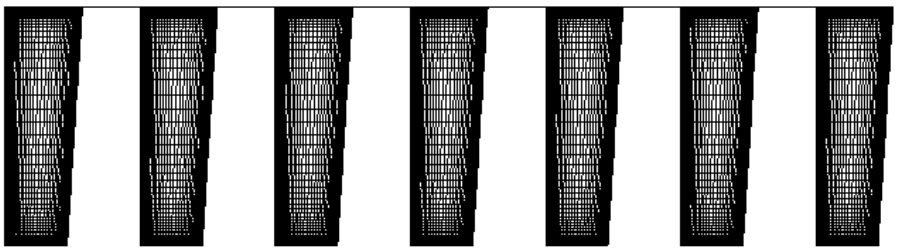

Figure 9.16: Mesh structure of 2D cavities

For single phase flow basic transport equations are given in the form of mass, momentum and energy conservation. These are local and instantaneous equations and can be applied to volume and time domain. However, for multiphase flow such local and instantaneous equations cannot be formulated without appropriate averaging.

The Euler-Euler formulation employs the concept of volume fraction which assumes it is meaningful to conceive a volume fraction of phase q in any small volume at any particular time. This means that at any time and certain position all the phases are available with certain volume fraction and there is no interface between the two phases. Consider two phase flow with phase p and q, the volume fraction of phase q is defined by

$$\sum_{q=1}^{n}(\alpha_q) = 1 \qquad 9.5$$

And the volume of phase q is

$$V_q = \int_V \alpha_q \, dV \qquad 9.6$$

Effective density of phase q is given by

$$\hat{\rho}_q = \alpha_q \rho_q \tag{9.7}$$

where ρ_q is physical density

Volume fraction of each phase is computed from the continuity equation

$$\frac{1}{\rho_{\gamma q}}\left(\frac{\partial}{\partial t}(\alpha_q \rho_q) + \nabla.(\alpha_q \rho_q \bar{v}_q) = \sum_{p=1}^{n}(\dot{m}_{pq} - \dot{m}_{qp})\right) \tag{9.8}$$

where $\rho_{\gamma q}$ is volume averaged density of the phase q. Right hand term represents the rate of mass transfer from phase p to phase q.

The conservation of momentum equation for phase q is given by

$$\begin{aligned}\frac{\partial}{\partial t}(\alpha_q \rho_q \bar{v}_q) + \nabla.(\alpha_q \rho_q \bar{v}_q \bar{v}_q) \\ = -\alpha_q \nabla p + \nabla.\bar{\bar{\tau}}_q + \alpha_q \rho_q \vec{g} \\ + \sum_{p=1}^{n}(K_{pq}(v_p - v_q) + \dot{m}_{pq}\bar{v}_{pq} - \dot{m}_{qp}\bar{v}_{qp}) + \vec{F}\end{aligned} \tag{9.9}$$

where $\bar{\bar{\tau}}_q$ is q[th] phase stress-strain tensor and $\vec{F}$ force vector representing the momentum due to granular multiphase flow. Pressure is shared by both the phases, and the significance of remaining terms is similar to the single phase flow.

Coupling is achieved through pressure and interphase exchange coefficients. The exchange coefficient in this case given by FLUENT is

$$K_{pq} = \frac{\alpha_q \alpha_p \rho_p f}{\tau_p} \tag{9.10}$$

where α_q, α_p, represents the fraction of fluid p and fluid q. f is the drag function and defined differently for different exchange coefficients. It is based on relative Reynolds number and differs among the exchange coefficient model. Fluent defines different models to evaluate drag coefficient for different conditions.

τ_p is the particulate relaxation time and defined as

$$\tau_p = \frac{\rho_p d_p^2}{18\mu_q} \tag{9.11}$$

where d_p is the diameter of the bubble of phase p.

Interphase momentum exchange term should include other relevant force, however in most cases drag force dominates other interphase forces such as lift force and virtual mass force hence they are not considered in this study.

Importance of surface tension is determined based on the value of Weber number when Reynolds number is greater than 1

$$We = \frac{\rho L U^2}{\sigma} \tag{9.12}$$

where U is free-stream velocity. Surface tension becomes important when We<<1. In the existing case higher tangential velocity in the clearances ensures the Weber number higher than 1. However, present model includes the effect of surface tension. Three different methods are provided by FLUENT to model multiphase turbulence model namely mixture model, disperse model and per phase model. Default mixture model was used which is applicable when phases separate and density difference is close to one. Mixture properties are used to capture the important features of the turbulent flow. It is sufficiently accurate with only moderate increase in the computational effort compared to the single phase simulation.

As the major portion of the two-phase mixture is occupied by water, it is assigned as primary phase. Air was assigned as secondary phase. In fluid-fluid flow each secondary phase is assumed to form droplets or bubbles. 2D CFD simulations are performed with the pressure inlet, pressure outlet boundary condition. GVF at the inlet

and outlet was calculated using ideal gas law. Simulation assumes continuous rotation of the fluid without any obstruction as opposed to the 3D model the screws meshing obstruct tangential cavity flow. Due to the annular shape of the cavity, the direction of rotation of the disc and the fluid is in the same direction which is not true in the case of actual 3D model.

Figure 9.17 shows the velocity contour in the direction of rotation (w) and the axial direction (u) at 15 psi inlet pressure, 50 psi pressure rise and 1800 rpm. The velocity field is strongly affected by the rotation of the screws, pressure differential across the cavity and the velocity gradient due to presence of liner and disc.

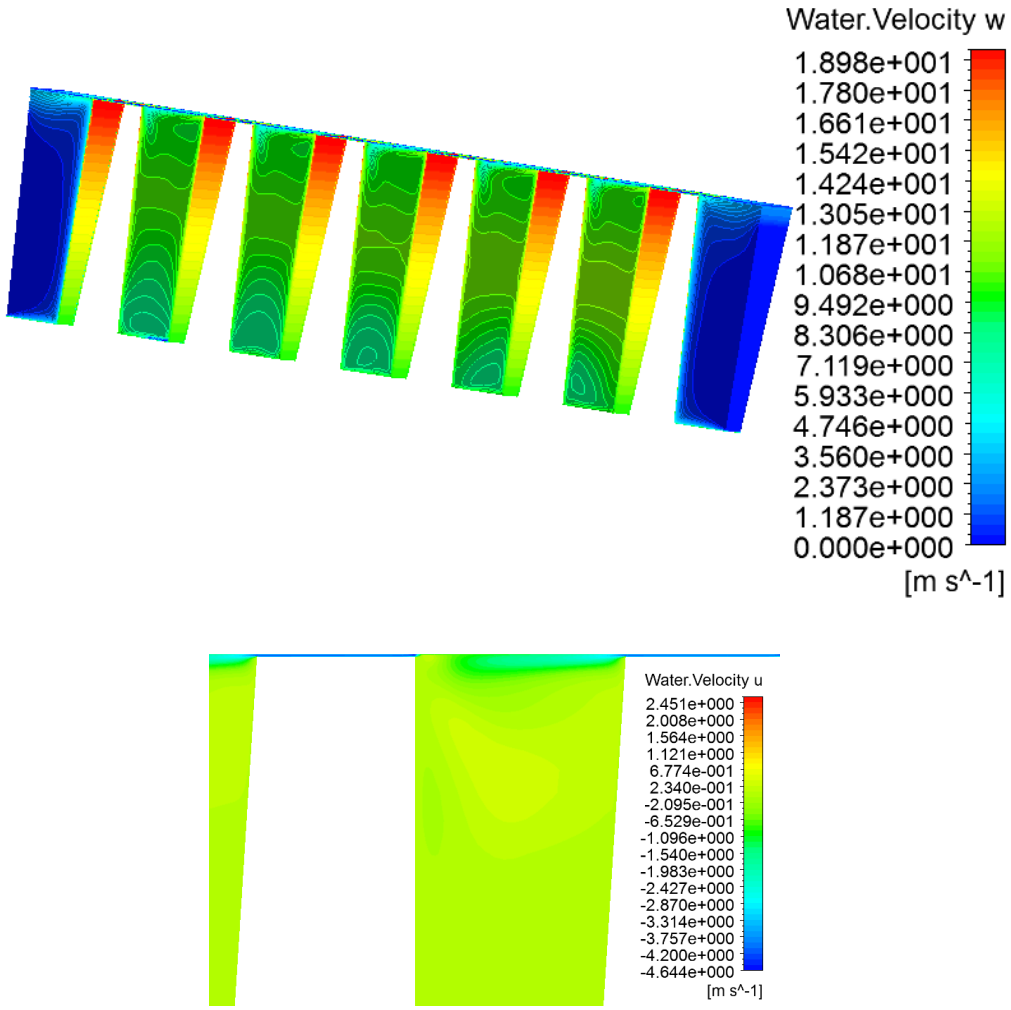

Figure 9.17: Velocity distribution in the direction of rotation (w) and axial direction (u) along the circular discs.

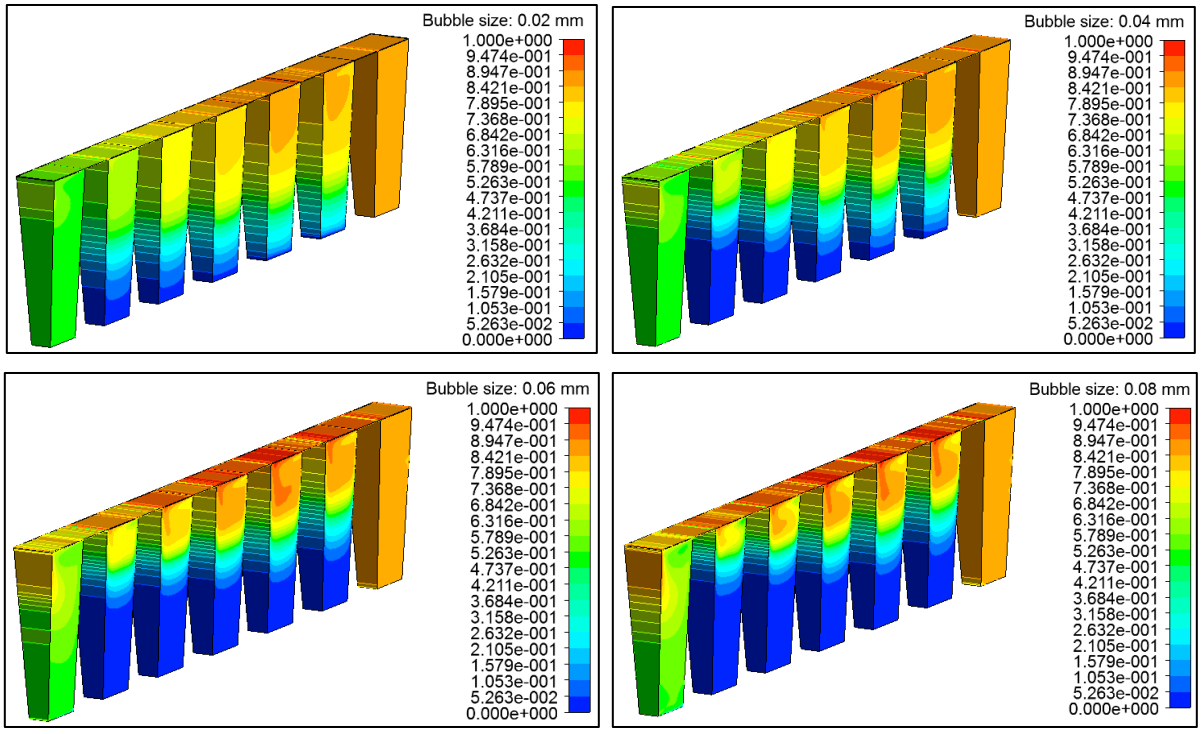

Figure 9.18: Effect of bubble size on the phase separation

Figure 9.18 shows the phase distribution of the water along the disc for 15 psi suction pressure 50 psi pressure rise and bubble size varying from 0.02 to 0.08. Due to leakage flow most of the compression occurs in the last cavity due to leakage flow of water from exhaust to the last chamber. However, bubble size has a significant impact on the phase separation, leakage flow rate, and the compression of the gas. Increase in bubble size leads to retardation of interphase exchange force exerted on dispersed phase which results in reduction of mass and momentum exchange between two phases. With lower bubble size there is effective compression of the gas as well as due to increased mass and momentum exchange there are increased bubbles in the clearances. Due to this effect the pressure drop is highest in the last chamber and higher gas infiltration in the

clearance close to suction leads to higher leakage flow rate. With increase in bubble size, separation becomes effective due to dominance of centrifugal force as compared to interphase force. With increased diameter, drag force increases, which lead to difficulty in the compression process. So overall result with increase in diameter is there is increased water content in the multiphase leakage flow which reduces the volumetric leakage flow rate, however difficulty in compression leads to linearized pressure profile across the liner. Figure 9.19 and Figure 9.20 shows the justification.

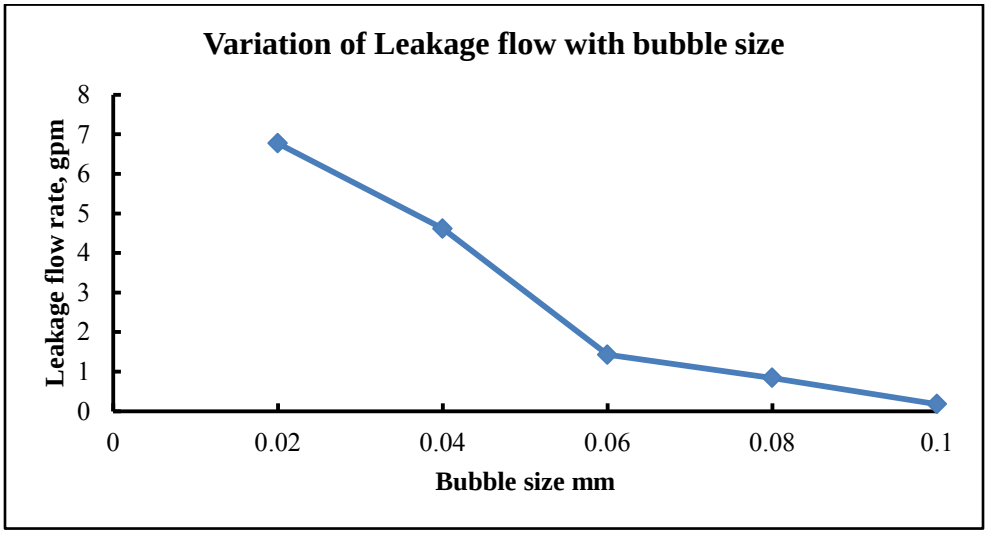

Figure 9.19: Leakage flow variation with different bubble sizes at IP=15 psi, DP=50 psi

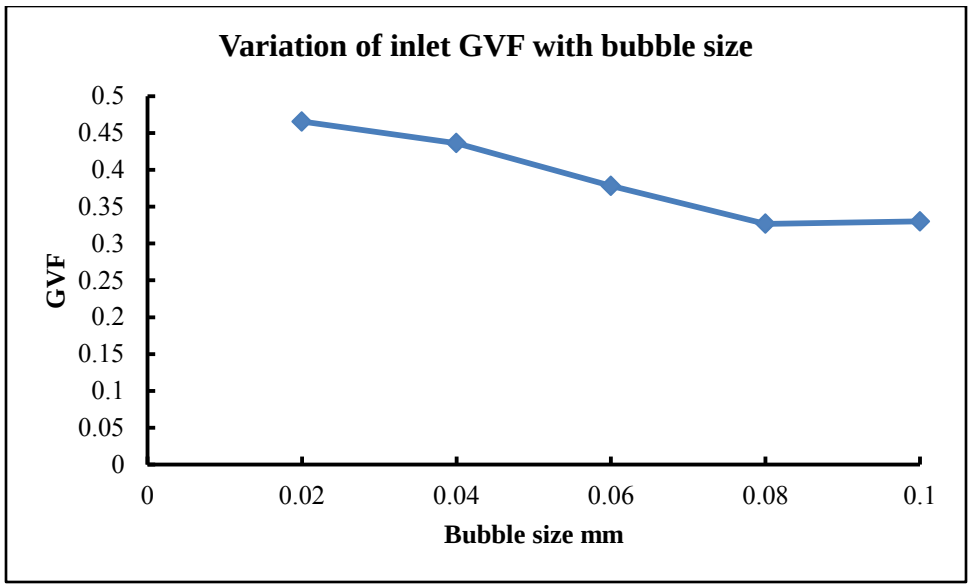

Figure 9.20: GVF variation with different bubble sizes at IP=15 psi, DP=50 psi

For the same boundary condition and GVF at the inlet, change in bubble size changes the phase distribution at the inlet. With increase in bubble size amount of water content in the leakage flow increases which reduces the GVF at the inlet and the total volumetric leakage flow rate.

One of the basic criterions to be validated for the CFD simulation of multiphase twin-screw pump apart from experimental results is the static pressure profile along the liner of the pump. Pressure drop across the land between two successive chambers is linear in case of single phase liquid flow due to the incompressibility of the liquid, However, the pressure profile for the two-phase flow varies from linear to the parabolic based on the GVF. Xu (2008) predicted close to linear pressure distribution for the GVF ranging from 0 to 50 %. 2D CFD predicts the relatively larger pressure drop across the last two chambers for the bubble size of 0.02 mm. Pressure drop across the clearance is

combined effect of drag force due to presence of air bubbles and the viscosity of the primary fluid, in this case water. Due to small dimension of the clearances the pressure drop due to viscous forces is dominant in this case. Due to smaller bubble size ability of water to compress the air is higher and hence the pressure drop across the last chamber is higher and pressure drop across fist chamber is lower (due to higher air content) in case of lower bubble size. With increase in bubble size there, there is reduction of interphase momentum exchange force and increase in separation. Due to this effect there is increase in water content in all the clearances. At the same time due to increase in bubble diameter there is difficulty in the compression. Hence, pressure drop across all the clearances tends to be equal. However, change in pressure drop is insignificant as compared to the separation of the phases with increase in bubble size (Figure 9.21). Proper selection of the bubble size should be based on combined CFD as well as experimental data.

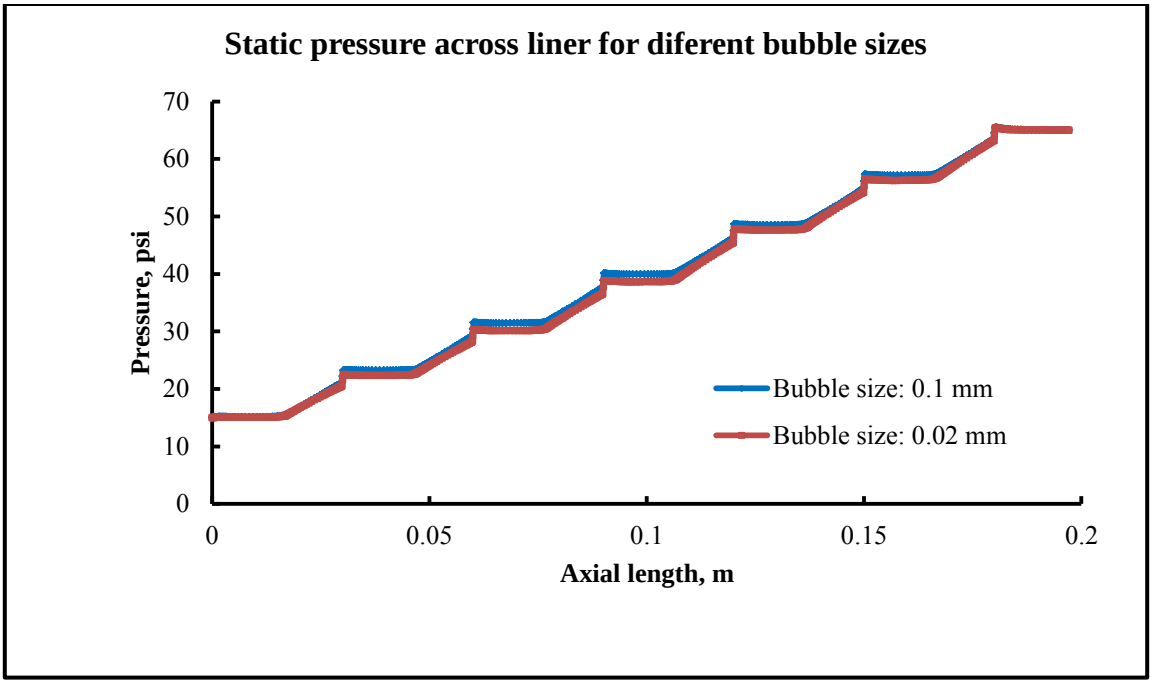

Figure 9.21: Static pressure distribution along the liner for different bubble size at IP=15 psi, DP=50 psi, GVF=50%.

Due to compression of the air there localized increase in the water temperature; however, the total temperature of the fluid at the outlet is unchanged due to high specific heat of the water. So compression follows isothermal process for 50% GVF. Temperature distribution is shown in Figure 9.22.

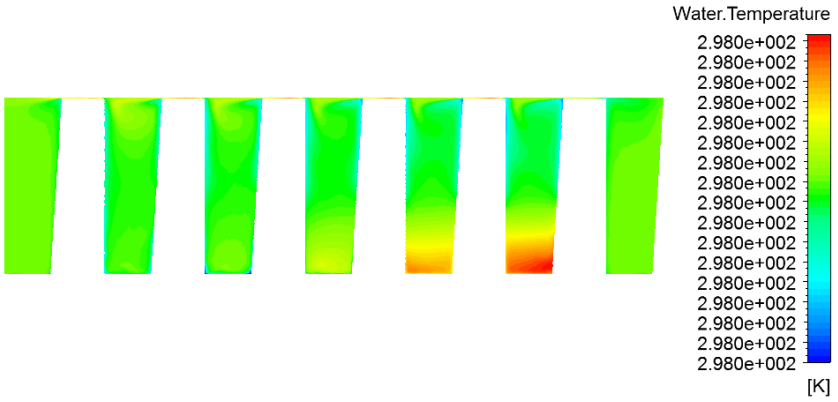

Figure 9.22: Temperature of the water at 15 psi inlet pressure and 50 psi pressure rise

9.2.2 3D CFD simulation of multiphase twin-screw pump for two phase flow

2D simulation assumes ideal circular path for the fluid and FLUENT allows such motion to model with rotating as well as translating frame of reference. This makes it easier to separate the two phases effectively, however, in case of 3D simulation; two phase mixture enclosed in the C-shaped chamber is driven by pressure differential across the clearances accompanied by effect of screw rotation on the flow separation. The intermeshing of the screws imposes the difficulty in the separation. Each "C" cavity is subjected to three walls with the same screw rotating in the same direction, stationary liner on the top, and the walls at the each leg of "C" from other screw rotating in opposite direction. This arrangement forces the fluid to move with relatively very small axial velocity. The component of axial velocity in the direction of rotation is opposite to the rotational velocity of the screw. So in the chamber, it is expected that the fluid near the screw wall is affected by the rotation while the fluid in the middle of the pocket

moves in the opposite direction. Figure 9.23 shows this condition. Fluid near the screw wall is moving in the direction of rotation while the fluid in the middle of cavity is moving in opposite direction. Fluid near the liner in the cavity is affected by the back flow from the clearances and the displacement effect from the screw.

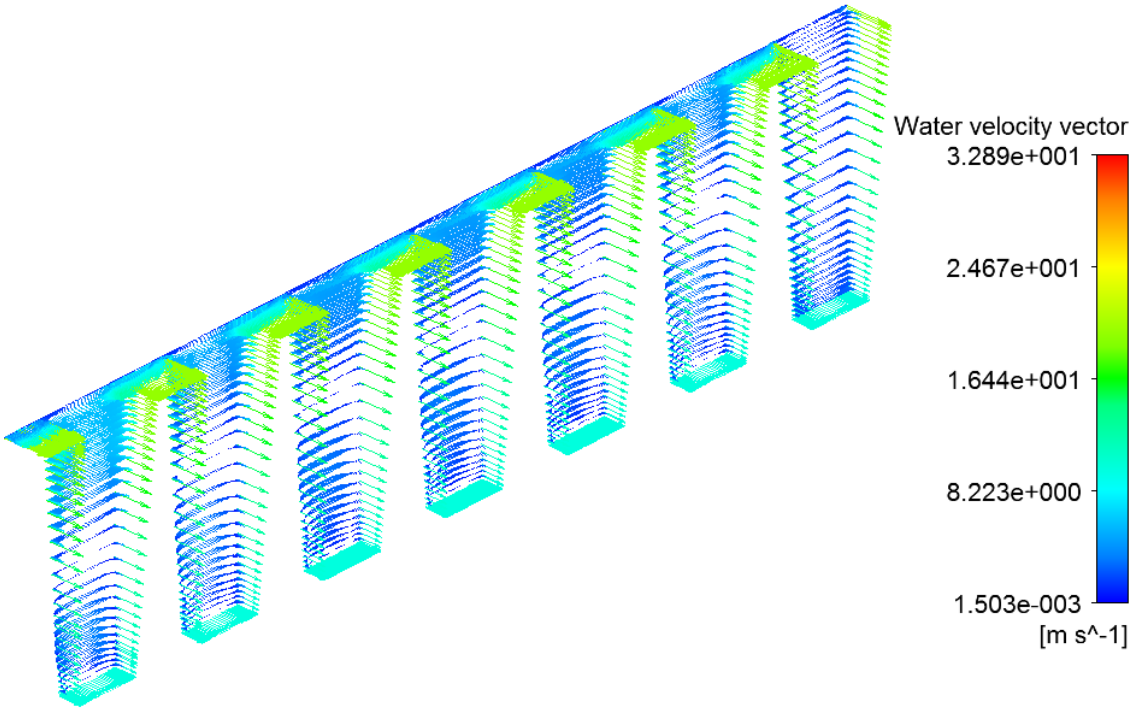

Figure 9.23: Water velocity vector for IP=50 psi, DP=50 psi, GVF=50%, 1800rpm

Figure 9.24 shows the transverse cross section of the flow path passing through three different cavities. The fluid flow is mainly driven by pressure difference rather than the speed of the screw. Flow near the wall in each cavity is subjected to rotation of both the screws and liner. So the rotation from both the screws encloses the fluid in the

cavity, however due to the presence of clearances fluid tries to escape from high pressure region to low pressure region. Figure 9.25 shows the contour and streamlines of water velocity in the flank clearances. Water flows to opposite cavities due to pressure difference.

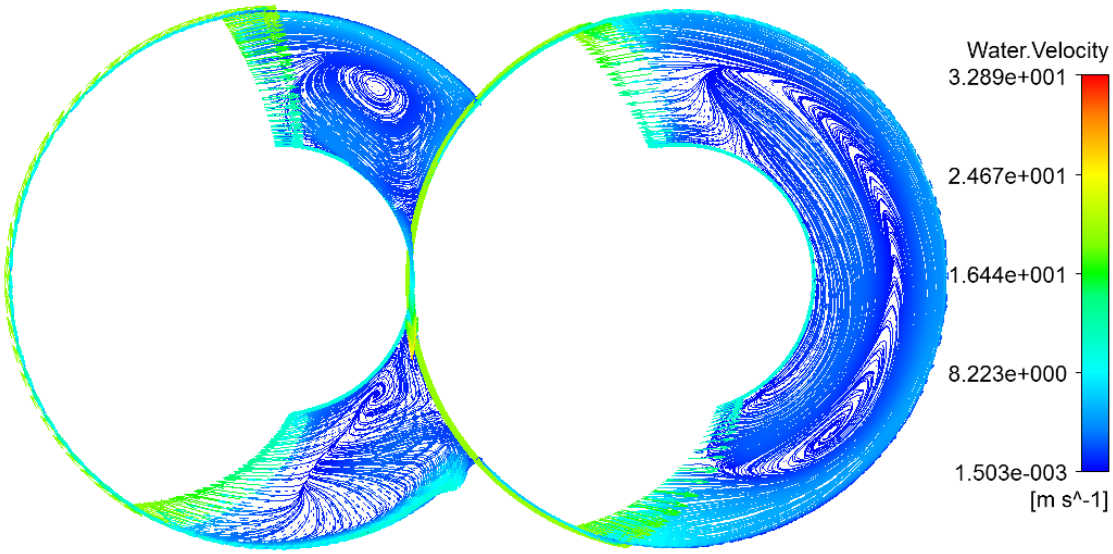

Figure 9.24: Cross section viewed from inlet showing velocity vectors and streamlines of water velocity.

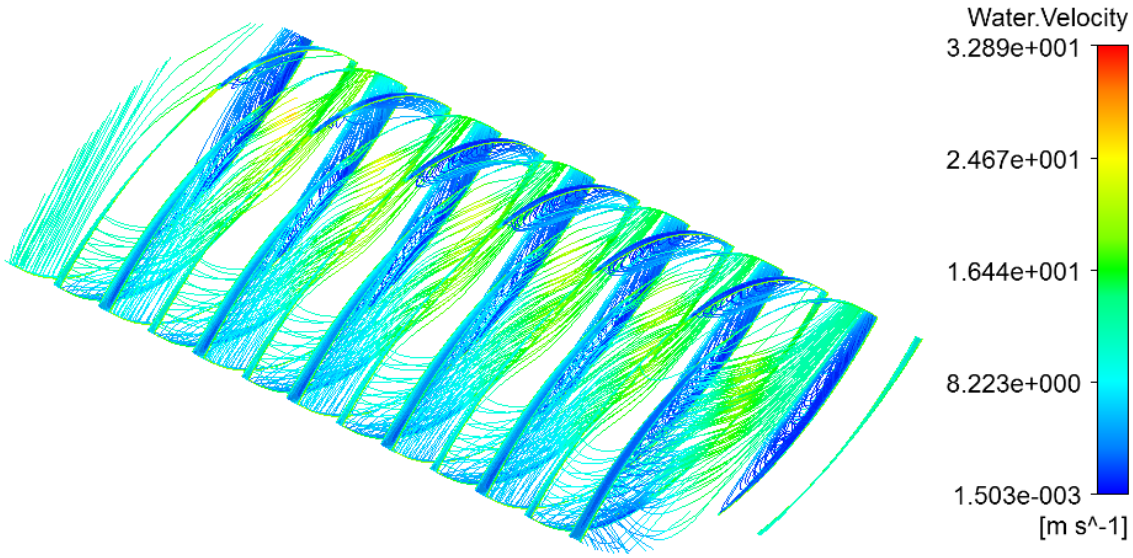

Figure 9.25: Velocity streamlines through flank clearances.

From the vector diagram it is seen that velocity of the air was consistently higher than water velocity along the domain due to momentum exchange between the two phases. Slip velocity is very small (2%-12%) near the wall region while it is highest in the domain away from the walls (up to 34%). Total velocity magnitude is very small in the cavity away from walls.

Separation process is affected by the opposite rotation of the screws and the drag force on the secondary fluid due to pressure difference across the different pockets. Although heavier fluid is pushed against the liner due to rotation of one screw, the momentum transferred due to rotation of the other screw is in the opposite direction and the overall result of this exchange causes the difficulty in the separation.

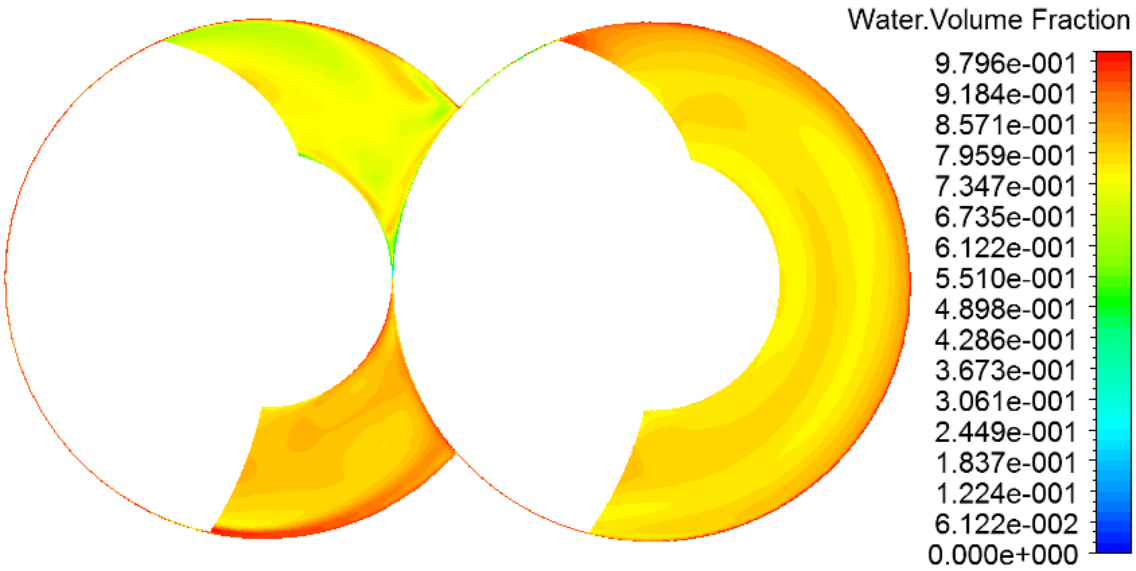

Figure 9.26: Cross section showing Distribution of water inside the cavity at IP=75, DP=150 psi, Bubble size 0.12 mm

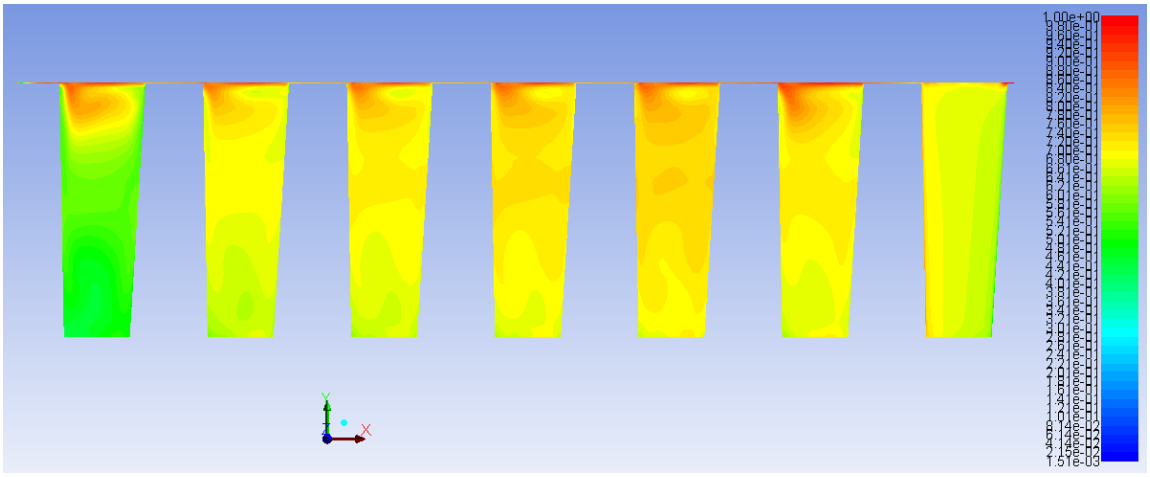

Figure 9.27: Axial cross section showing Distribution of water inside the cavity at IP=100, DP=50 psi, Bubble size 0.08 mm

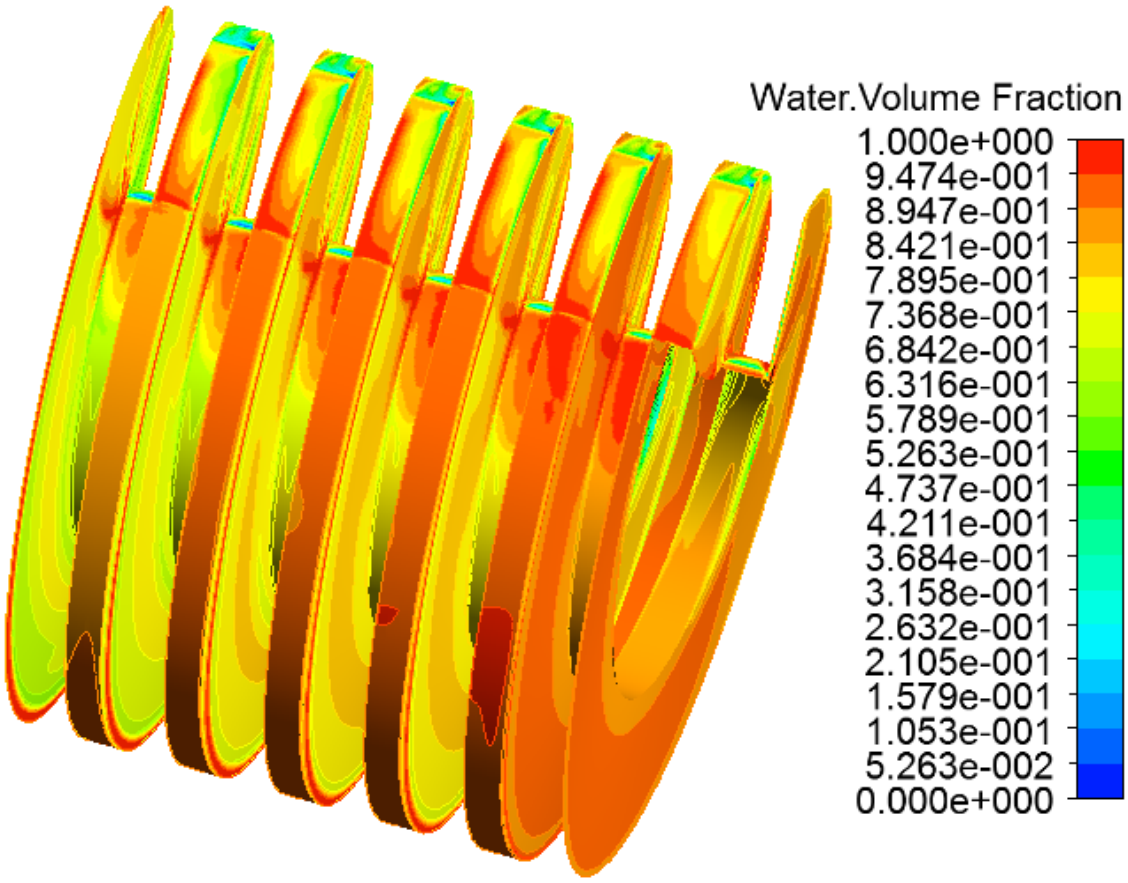

Figure 9.28: Water distribution along the root, flank and land of the screw at IP=75 psi, DP=150 psi, GVF=50%

Figure 9.26 shows the water distribution along the cross section of the fluid path. The simulation does not indicate the complete separation of the phases, however, rotation of the screw does have an effect on the mixture with water content is higher along the liner and air tends to agglomerate near the root. The same effect can be seen in Figure 9.27. First chamber in the Figure 9.27 is open to the inlet and hence the separation is quite effective as compared to the other closed cavities. Water is forced towards the suction side of the cavity due to the combined centrifugal and drag force and

occupies most of the circumferential clearances with small infiltration of air along with it. Second circumferential clearance from the exhaust side is mostly filled with water due to the backflow effect. Water distribution along the land of the screw indicates that circumferential clearances are mostly filled with water. Figure 9.28 shows the water distribution along the root, flank and land of the screw.

Air agglomeration near the root causes air to escape from one cavity to the other through root clearances. Due to the displacement effect the air entrained around the root is carried toward the intersection of circumferential clearance of both the screws and possibly, some part of it infiltrate inside the circumferential clearance. Presence of air in the root clearances acts as a cushion and avoids the root pressure to drop below saturation pressure hence avoiding the possibility of cavitation. Figure 9.29 shows the effect of presence of air on the pressure distribution along the screw. Hence it is advisable not to run the twin-screw pump at low suction pressure and single phase water flow.

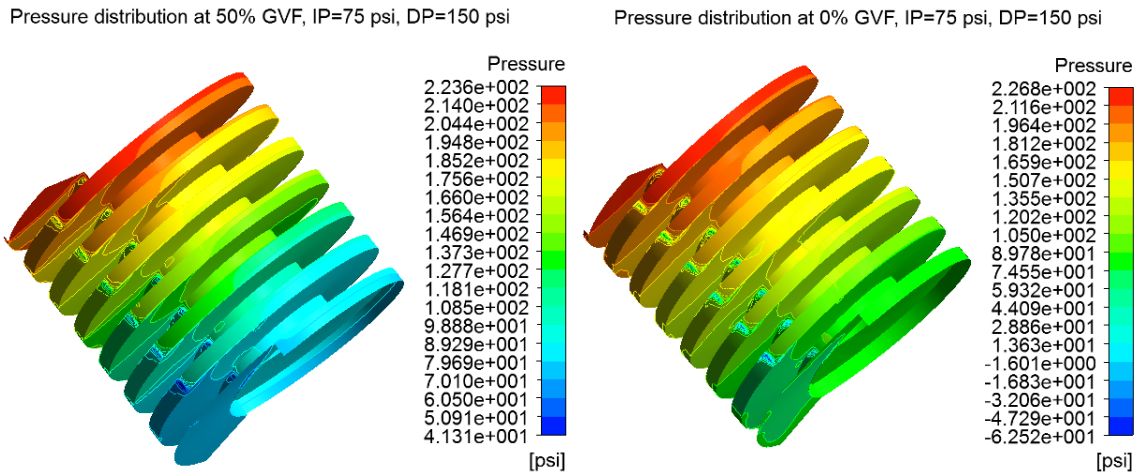

Figure 9.29: Effect of multiphase flow on the pressure in the root clearance

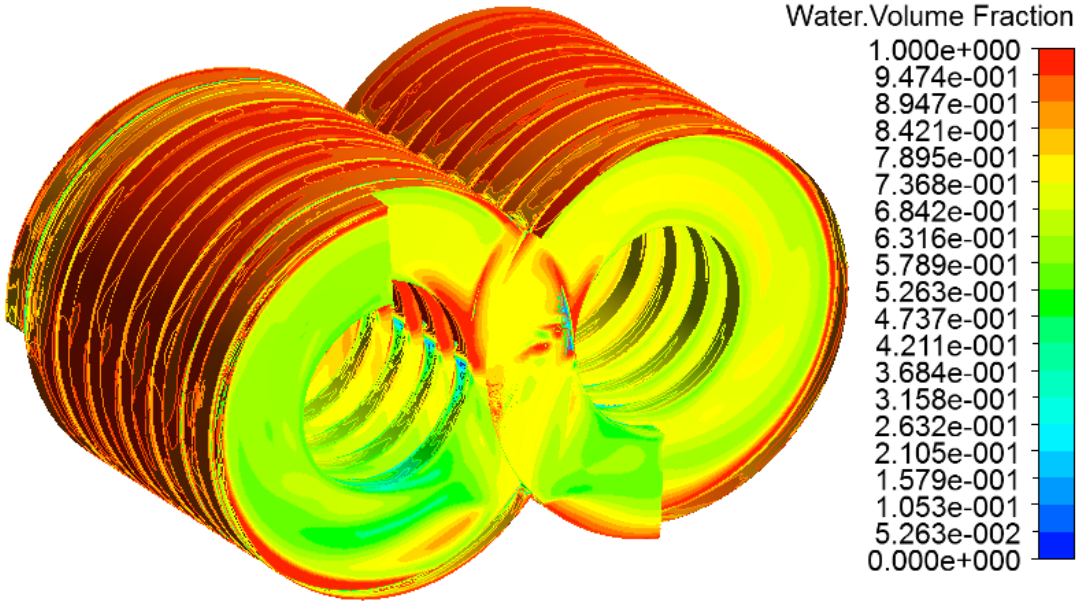

Figure 9.30: Water distribution along the liner and the screws at IP=75 psi, DP=150 psi, Bubble size=0.12 mm

Figure 9.30 shows the water distribution along the liner as well as the screws. Water is forced towards the liner. Circumferential clearances are mostly occupied with water with small amount of air escaping through it. Water accumulation is higher at the bottom of the liner due to the effect of gravity. Due to centrifugal force water is forced towards the leg of "C" chamber where it is restricted due to the presence of other screw.

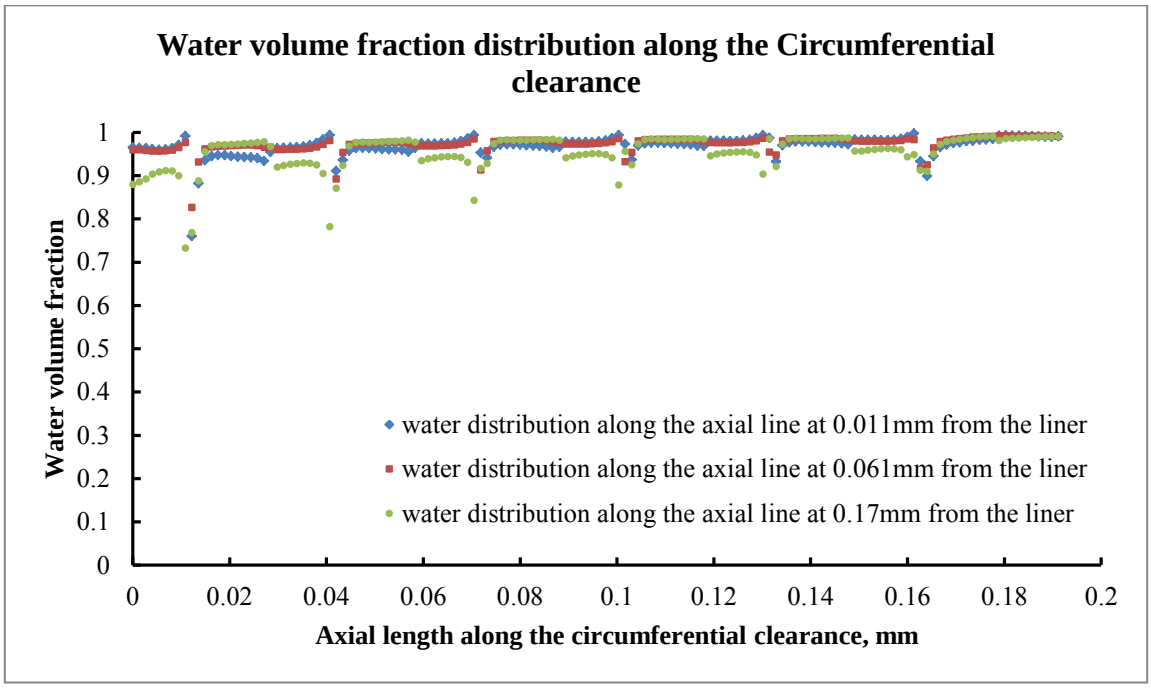

Figure 9.31: GVF distribution along the circumferential clearance and cavities at IP=75 psi, DP=150 psi, GVF=50%

Figure 9.31 shows the water volume distribution along the circumferential clearances and cavities for different radii along the axial direction. Three data lines at different radial distances from the liner and parallel to the axis are chosen to represent

the water content in the circumferential clearances and the cavities near the liner. Each data set represents the water distribution along the clearance as well as the cavities. Average distribution of the water volume fraction along different radii ranges from 0.9 to 0.98. Air infiltration increases along the clearances close to the suction chamber. Data set farthest from the liner shows highest air content in the cavity, however the water content in the clearances is consistently higher (around 98%) along all the data sets. There is sudden drop in water content at the outlet of each clearance due to backflow effect. This data represents the water content along the liner at bubble size of 0.12 mm.

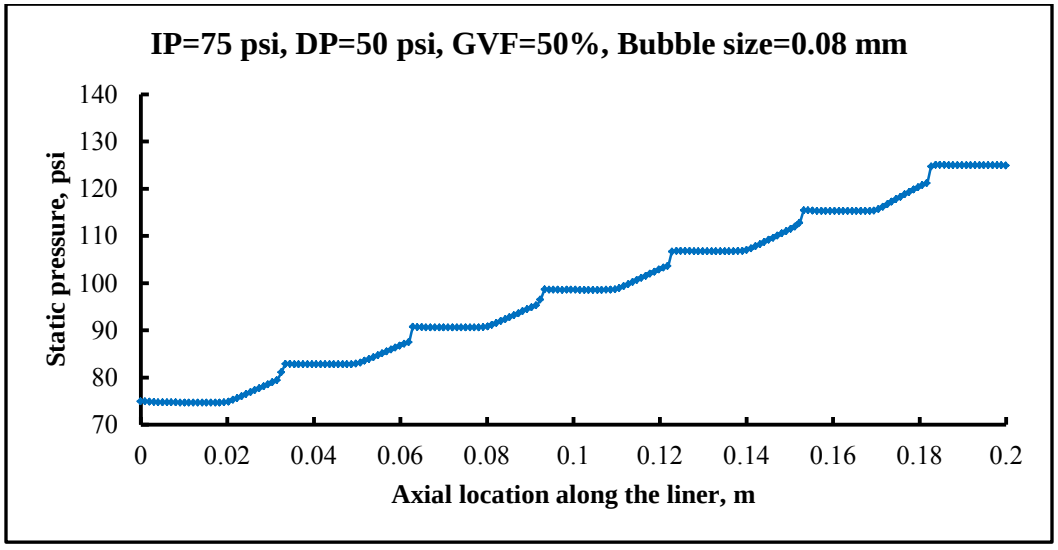

Figure 9.32: Static pressure distribution along the liner for IP=75 psi, DP=50 psi, GVF=50%, Bubble size=0.08 mm

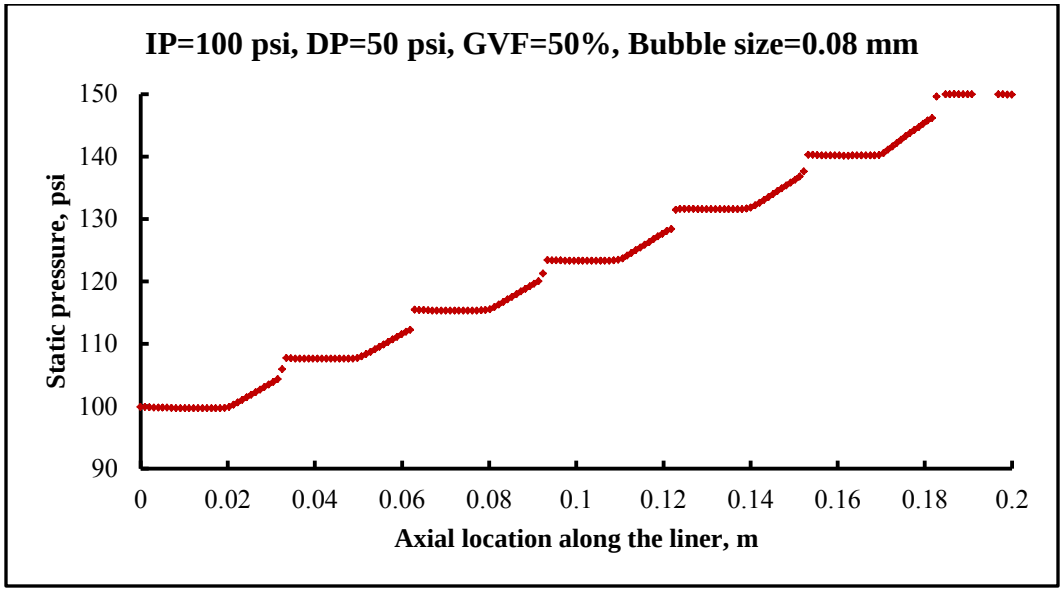

Figure 9.33: Static pressure distribution along the liner for IP=100 psi, DP=50 psi, GVF=50%, Bubble size=0.09 mm

Figure 9.32 and 9.33 shows the static pressure distribution along the liner for two different suction pressures at same bubble size. There is small difference in the curve for both the plots. Both the plot shows pressure drop across the last chamber is highest and gradually decreases towards the inlet. Pressure drop is smallest across inlet and the first chamber. For 75 psi suction pressure, pressure drop across the fist chamber is 8.05 psi while it is 8.12 psi for 100 psi suction pressure. This resulted is slightly higher leakage flow rate for 100 psi suction pressure.

Volumetric flow rate variation with different suction pressure is shown in the Figure 9.34. Increased pressure for the same bubble size increases the separation leading to lower leakage flow rate, however assigning same bubble size for different suction pressure is not realistic and hence in order to correctly represent the flow behavior it is

necessary to study the relationship between bubble size and the pressure acting on the two phase flow. For this study bubble size of 0.08 mm to 0.1 mm is used for different suction pressures. Bubble size of 0.1 was used for 15 psi suction pressure, 0.09 mm for 50 psi suction pressure and 0.08 mm for 75 psi and 100 psi suction pressure. Changing suction pressure has little effect on the flow regime. Pressure and flow separation across the chamber was dependent on bubble size rather than the suction pressure. Variation of flow rate was very small with change in suction pressure. Results agree well for given conditions.

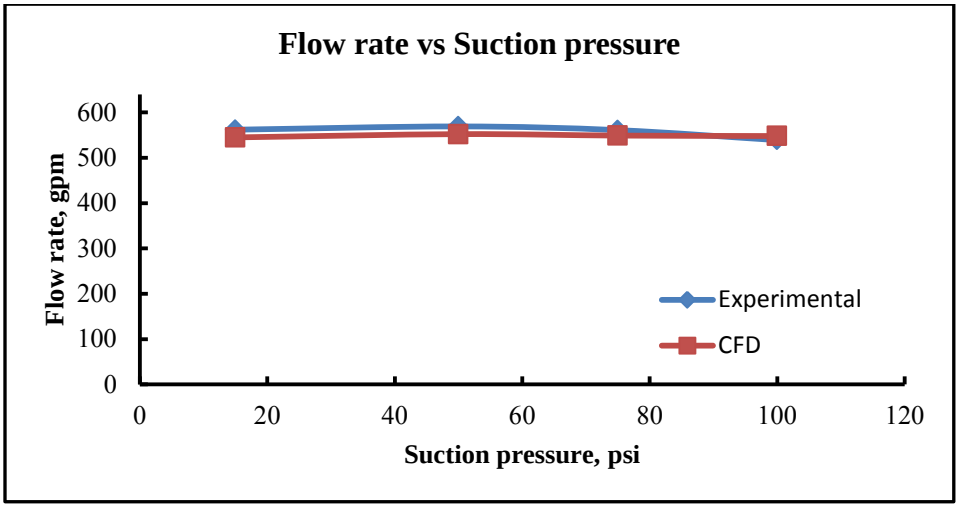

Figure 9.34: Total flow rate variation with 15 psi, 50 psi, 75 psi and 100 psi suction pressure at 50 psi pressure rise.

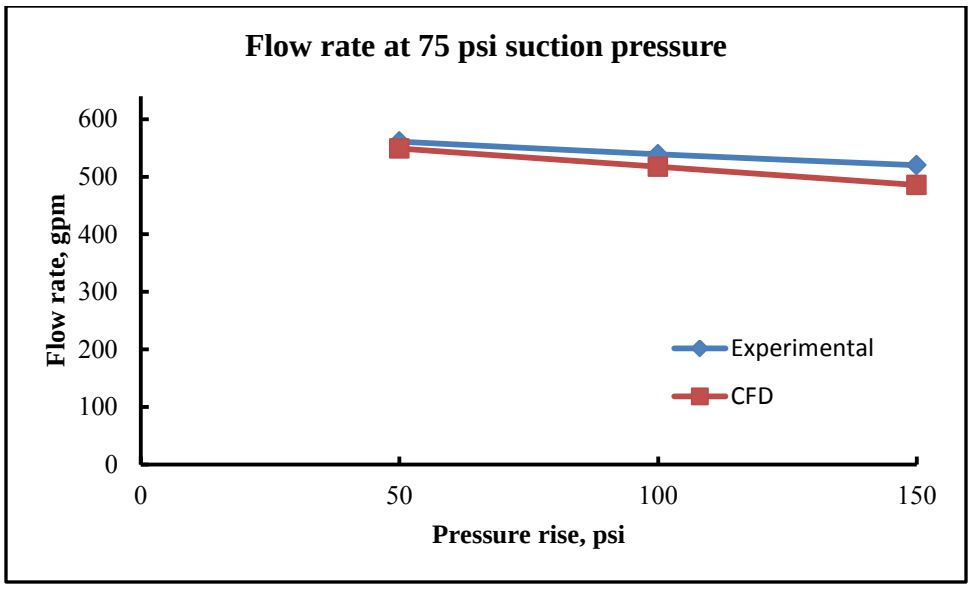

Figure 9.35: Total inlet multiphase flow rate comparison using 3D CFD and experimental data at IP=75 psi, bubble size=0.08mm

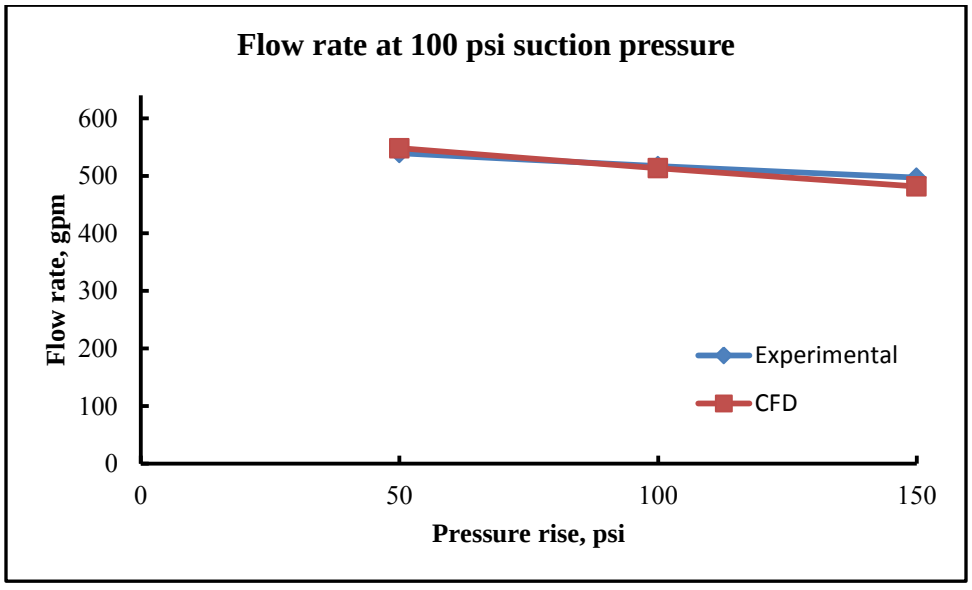

Figure 9.36: Total inlet multiphase flow rate comparison using 3D CFD and experimental data at IP=100 psi, bubble size=0.08 mm

Figure 9.35 and 9.36 compares CFD and experimental results at 75 psi and 100 psi suction pressure respectively for different pressure rise conditions. Same bubble size was used to model the flow behavior. Leakage flow rate is the function of pressure drop across the first chamber and the suction chamber and this pressure drop depends on GVF at the inlet and the suction pressure. However, in case of CFD, with the increase in suction pressure, there is very small change in the leakage flow predicted by CFD analysis, which indicated the pressure drop difference is very small for both the suction pressures. Experimental data shows a rise in the leakage flow with increase in suction pressure. Due to this, the CFD results under predicts the total flow at 75 psi suction pressure while leakage flow agrees quite well at 100 psi suction pressure for the same bubble size. From this it can also be predicted that with increase in suction pressure, density difference decreases and multiphase flow tends to be more homogeneous and pressure profile becomes linear along the liner. Existing CFD model uses mixture model for turbulent flow which is more suitable for fluids with smaller density difference. This type of model can be used to simulate the multiphase flow with higher suction pressures.

There are some issues which need to be highlighted in the future work. The current model assumes that the GVF right at the inlet and outlet of the screw is same as that of GVF at the inlet and outlet of chamber. However, in actual case there is loss of pressure head from inlet of the suction chamber to the inlet of screws due to rotation of screws which will change the GVF. GVF at the inlet of the screw can be considerably different than the GVF at the inlet of chamber due to leakage flow arising from the slit connecting inlet and outlet. Future extension of this work should consider modeling of

inlet and outlet chambers for better understanding of flow behavior at the inlet and outlet of the screw.

10 RESULTS-FLOW VISUALIZATION AND DYNAMIC PRESSURE MEASUREMENTS

10.1 Dynamic pressure measurements

The clear casing twin-screw pump manufactured by Bornemann was used for flow visualization and dynamic pressure measurement purpose. The pump suction was immersed in an oil tank which was 0.8 m below the pump. Discharge pressure was controlled manually using gate valve. The pump was instrumented with 6 dynamic pressure probes as shown in the Figure 10.1. Three probes are installed vertically and three probes are installed horizontally with axial distance between them equal to pitch of the screw. The distance between the horizontal and vertical probe is equal to width of the screw land.

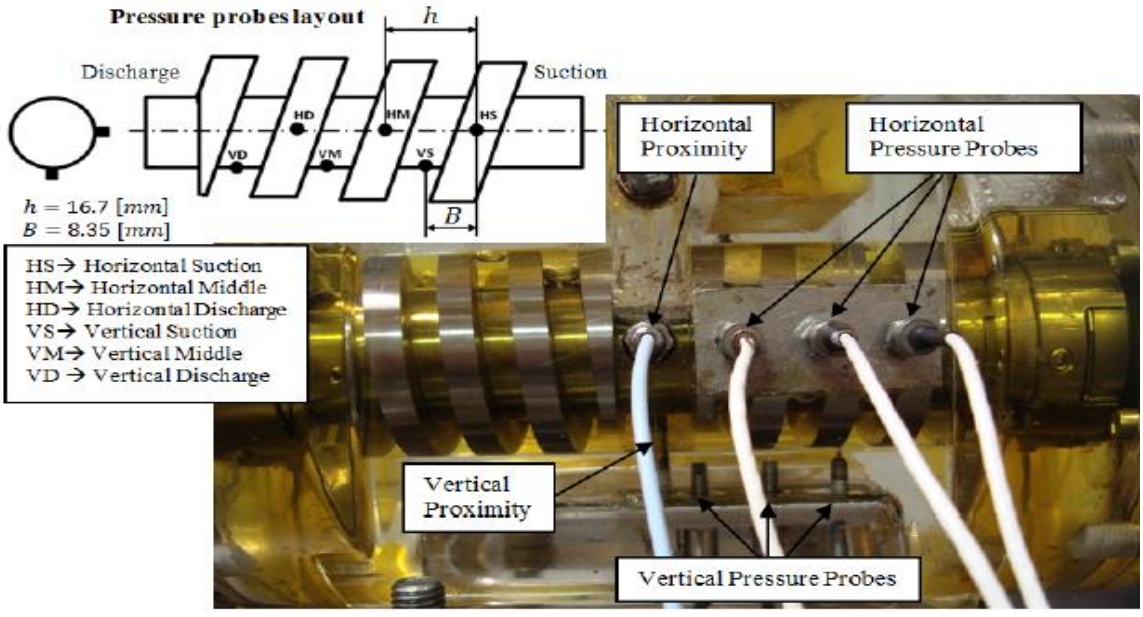

Figure 10.1: Layout of sensor arrangement

Dynamic pressure response in the horizontal and vertical plane is shown in Figure 10.2 and 10.3. For single phase flow the pressure rise across each clearance is equal confirming the linear pressure rise across the liner

Pressure probe installed in the suction chamber indicates negative pressure. Negative pressure in the suction is due to the 0.8 m elevation of the pump above the oil supply tank. The first horizontal probe reading oscillates around the suction pressure due to the suction effect right at the inlet of the screw. similarly there is pressure measured by middle probe exceeds the exhaust pressure for 20% of revolution due to exposure of the middle probe to the exhaust and sudden build of backflow pressure due to momentum of the fluid. From the curve, the dynamic events of pressure variations of the horizontal exhaust probe can be described. Pressure build up takes around 10% of revolution, for around 50 % of revolution sensor is exposed to discharge. Entrance loss makes significant contribution (around 50%) the total pressure drop followed by pressure drop due to viscous friction in the circumferential clearance.

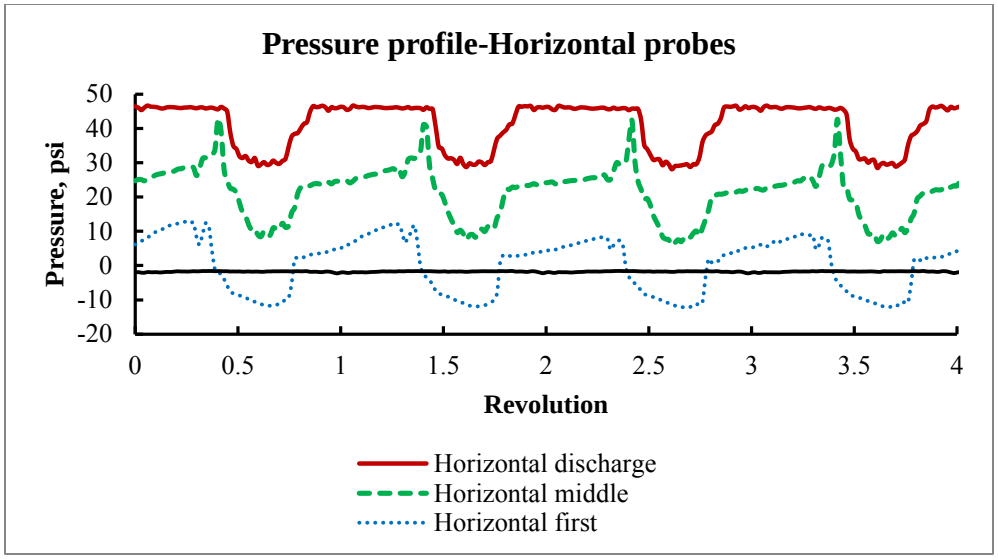

Figure 10.2: Dynamic pressure in the axial direction along the horizontal plane

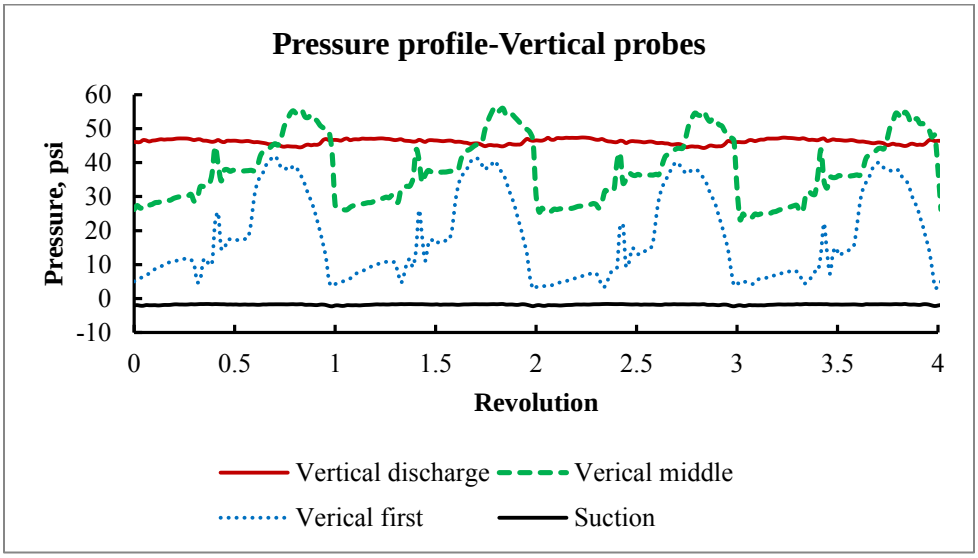

Figure 10.3: Dynamic pressure in the axial direction along the vertical plane

Constant suction and exhaust pressure justifies the boundary condition used in the CFD simulation. Signal also indicates that the pressure profile is stationary in type and can be modeled as a steady state problem.

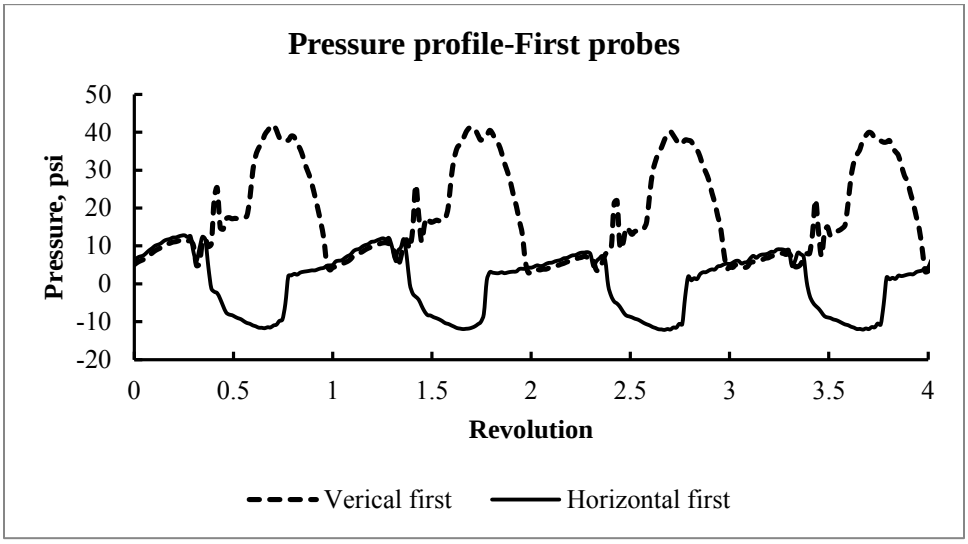

Figure 10.4: Pressure measurement by first probe in the horizontal and vertical plane

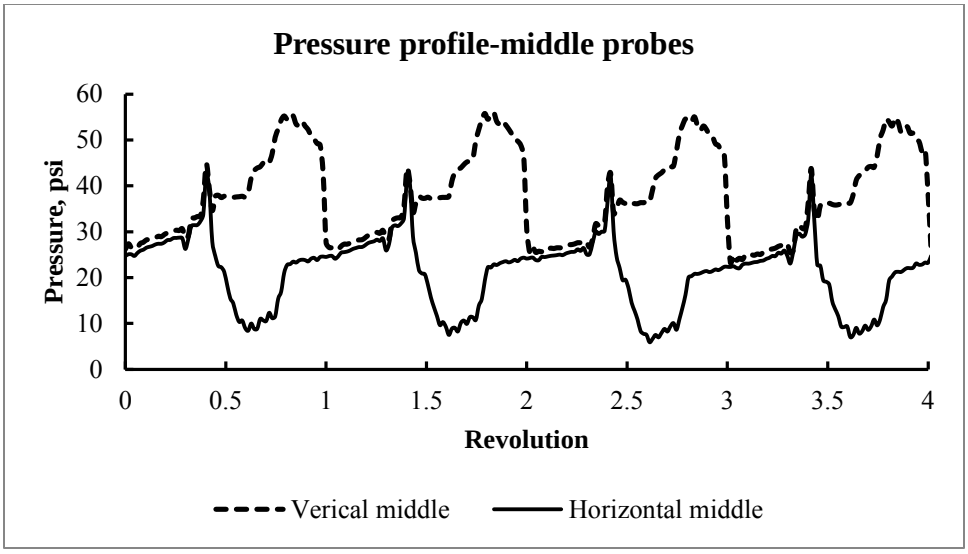

Figure 10.5: Pressure measurement by middle probe in the horizontal and vertical plane

Figure 10.4 and 10.5 shows the simultanious pressure measurement by first and middle pressure probes in the horizontal and vertcal plane. Pressure overlap with each other for around 40% of revolution due to exposure of both the sensor to the same cavity. This measurement validates the CFD data which shows constant pressure distribution in the cavity.

Figures 10.6 and 10.7 show the pressure profile for medium and high GVF. Pressure variation is higher in the case of multiphase flow than single phase flow. Sudden rise in the exhaust pressure indicates the parabolic pressure profile along the axis of the liner. Pressure rise in the last chamber is higher for the high GVF flow. Transient variation of the pressure in each cavity is similar to the single phase flow.

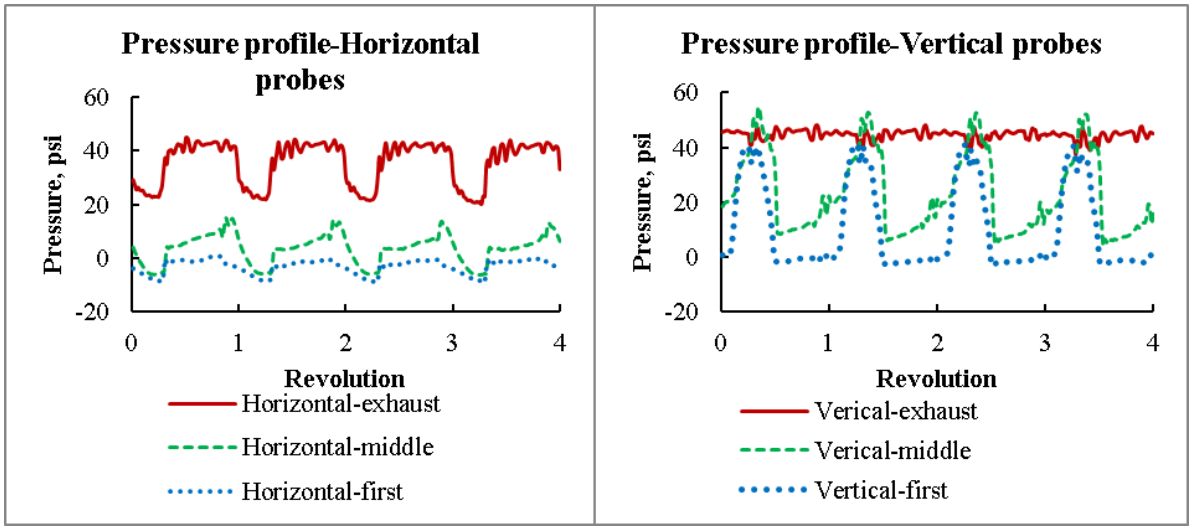

Figure 10.6: Horizontal and vertical pressure measurement at medium GVF

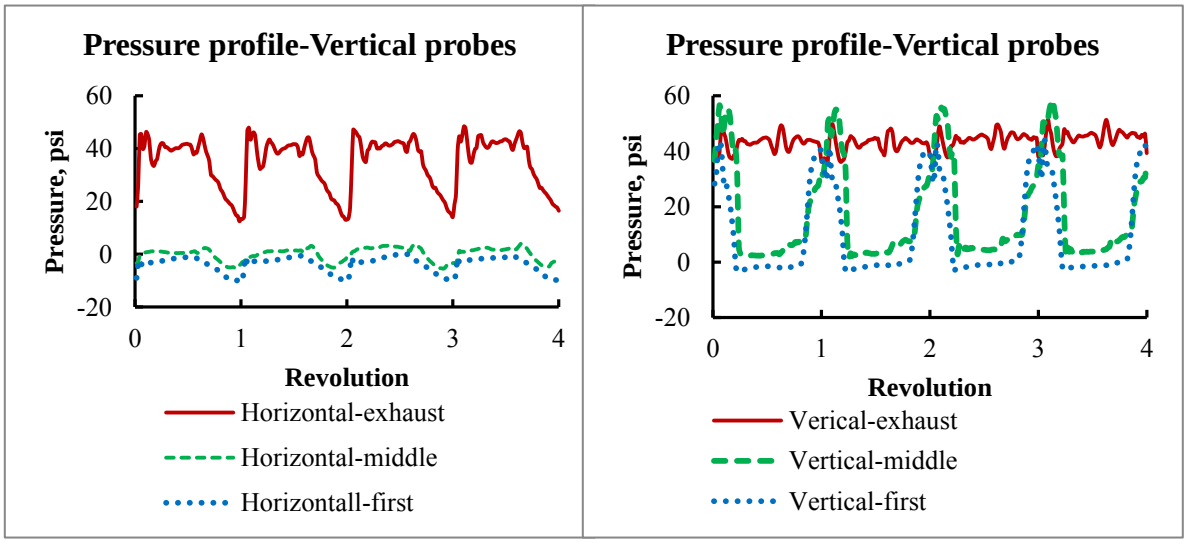

Figure 10.7: Horizontal and vertical pressure measurement at high GVF

10.2 Flow visualization study

This section deals with the flow visualization of the multiphase flow through twin-screw pump. Flow visualization study by Rabiger mainly focused on GVF more than 90%. The main objective of this study was to visualize the phase distribution inside the clearances for low GVF (10%-30%), medium GVF (40%-70%), and high GVF (70%-90%). All the tests were performed at 60 HZ speed, ~10 psia suction pressure and 50 psi pressure rise.

Oil and air is used as a two phase mixture. A Phantom v711 camera is used to capture the phase distribution inside the cavity and circumferential clearances.

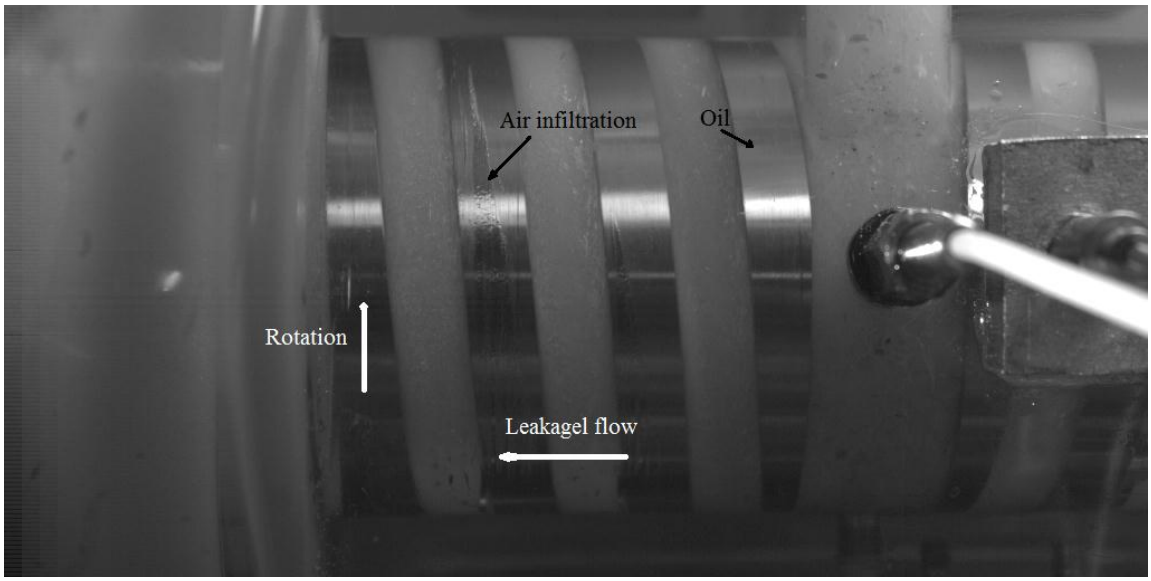

Figure 10.8: Phase distribution along the twin-screw pump at Low GVF

Figure 10.8 shows the phase distribution at low GVF. At low GVF air was well mixed with oil due to low drag. Flow behavior agrees well with the CFD. Flow near the screw is affected by near wall motion and it follows the screw direction, however fluid in the middle of cavity moves in opposite direction due to the opposite motion of fluid pocket. Leakage flow inside the last circumferential clearances (between exhaust and the last chamber) is mainly occupied by oil; however, there is air infiltration in the middle and the first circumferential clearance. This can be attributed to the uniform mixing of the oil and air and possible escape of air from the root of the other screw to land of the screw under study.

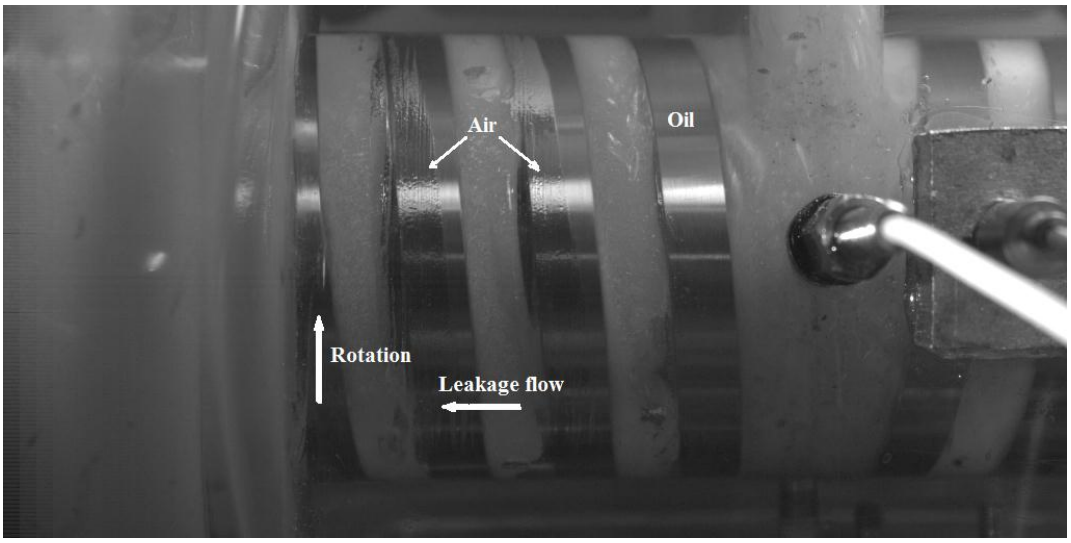

Figure 10.9: Phase distribution along the twin-screw pump at low/medium GVF

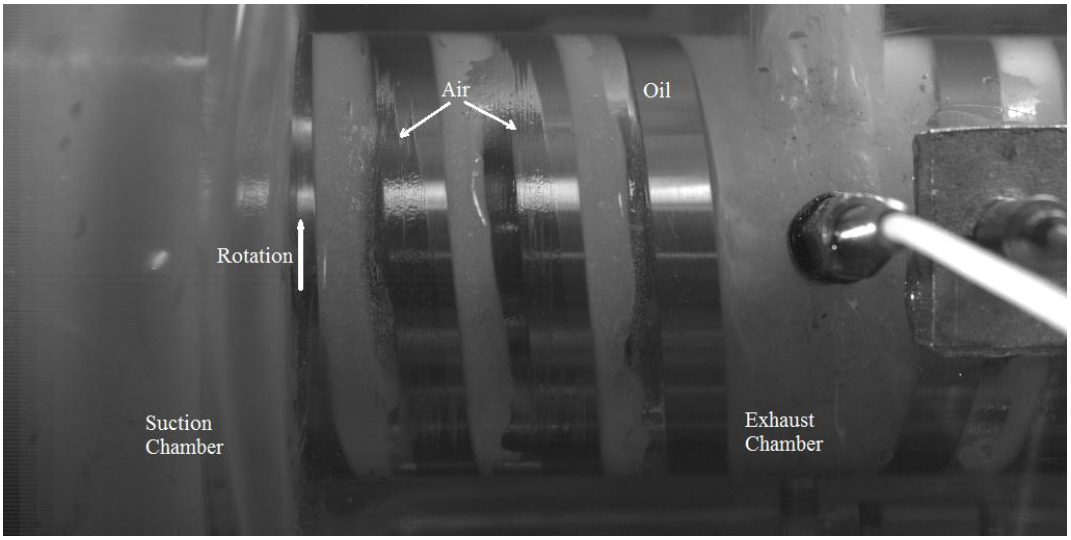

Figure 10.10: Phase distribution along the twin-screw pump at medium GVF, IP=10 psia, DP=50 psi

Figure 10.9 and Figure 10.10 shows the phase distribution in case of low to medium range of GVF at the inlet. With increase in GVF there is increased infiltration of air inside the circumferential clearances. Oil tends to be forced on the suction side of the cavity due to the forward motion of the screw and the centrifugal force while air occupies the discharge side of the cavity. The last chamber is mostly occupied with oil due to larger pressure drop across the last chamber and the exhaust while the first two clearances are characterized by separated two-phase flow. This observation shows that even at low GVF there is some infiltration of gas along with liquid. Observation may vary depending on the design of the screw pump and the different multiphase mixture.

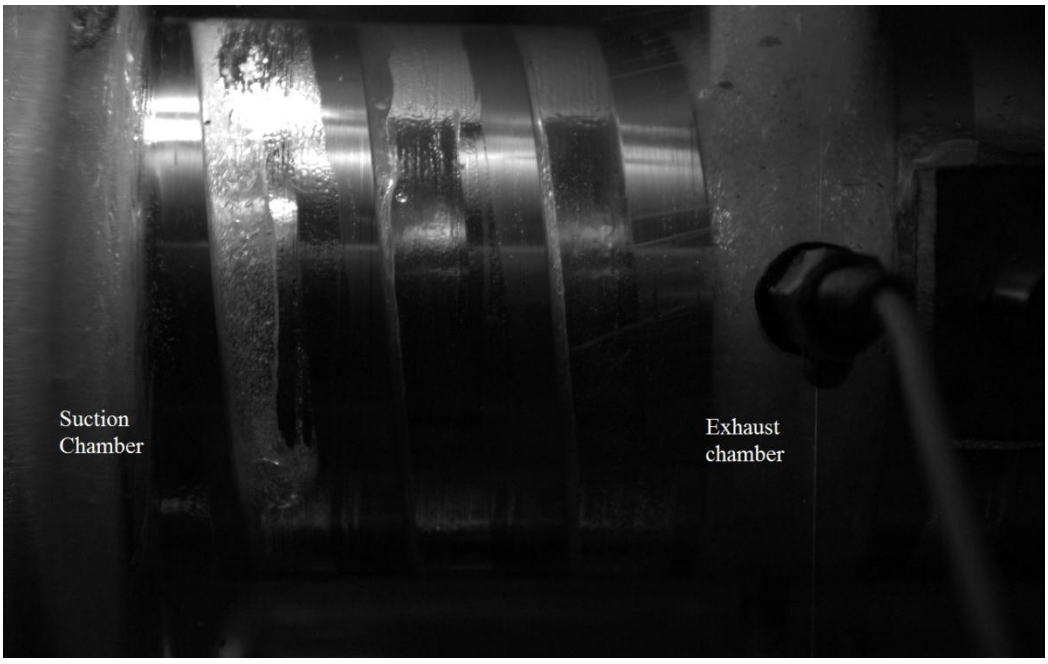

Figure 10.11: Phase distribution along the screw pump at high GVF, IP=10 psia, DP=50 psi

With high GVF (Figure 10.11), it has been seen that the most of the oil is leaked from first chamber to the suction chamber due to shifting of pressure build up from the last chamber to the first chamber. This observation indicates linearized pressure profile along the liner.

Figure 10.12 shows flow visualization at high GVF when the first cavity is exposed to the suction chamber. Due to absence of any constriction, oil is splashed toward the liner due to centrifugal action but at the same time due to forward movement of the screw and the pressure build up it is forced toward the circumferential clearance. Subsequent cavities are mostly occupied with air and clearances are characterized by presence of both the phases. Possible flow regime and the slip velocity between the two phases in the clearances still need to be understood. In this case, viscous drag from the

oil seems to play an important role in the clearances. Results might vary significantly with using water instead of oil.

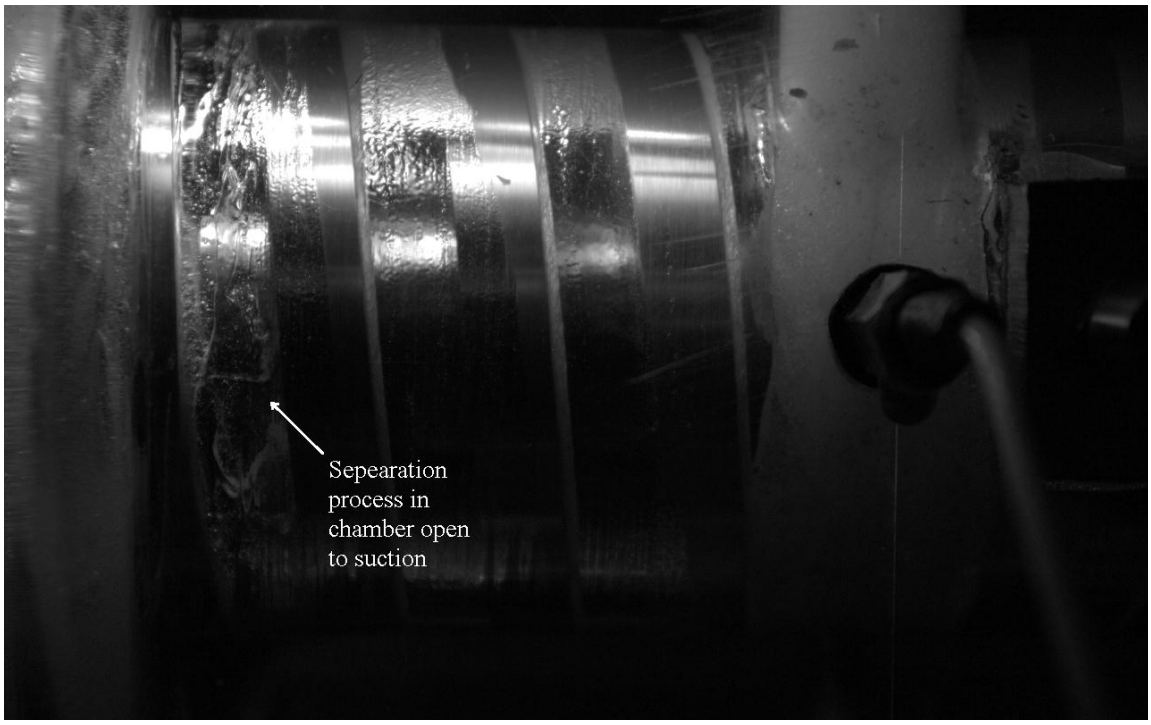

Figure 10.12: Phase distribution at high GVF

11 CONCLUSIONS

11.1 Experimental

The purpose of this study was to evaluate the performance of a twin-screw pump for the varying operating condition observed in actual field conditions. The objective was to assist Shell make informed choices about the selection of a pump. The parameters considered for evaluations are leakage flow, volumetric efficiency, effectiveness and mechanical efficiency of the pump. Experimental results provided detailed insight into the effect of compression of the gas with increase in GVF, changing the suction pressure and effect of changing the speed on pump behavior. The following section summarizes the main conclusions about steady state experimental analysis

Clearances between the rotors and housing insures the safety of the pump and act as an outlet while working with extreme condition but at the same time its capacity to deliver specified flow rate degrades and leakage flow goes up with increase in pressure rise. Twin-screw pumps are known to work well with high GVF, however, some quantity of liquid is always required to seal the gas from leaking through clearances. A study was conducted to determine the minimum seal flush flow estimates that at least 20 gpm of liquid recirculation (around 3% of total flow) is required to have optimum performance of the pump. So, if the wet gas GVF goes above 97%, some arrangement should be made to supply the liquid seal flush recirculation from an external supply. The quantity of liquid required for lower speed will be higher due to higher leakage flow rate.

Leakage flow analysis at 50 GVF shows leakage flow goes up with increase in suction pressure due to increased density of the gas; however increased density also increases the net mass transfer of the mixture. This is also true for higher GVF.

Condition of optimum sealing varies with suction pressure. Lower suction pressure needs higher liquid content to seal the gases, however, the total leakage flow is less compared to higher suction pressure due to low pressure drop between suction chamber and adjacent chamber.

Pump speed is an important parameter and used to adjust the suction pressure of depleting reservoir head, however, pump volumetric flow rate decreases with decreasing pump speed due to inefficient separation of the mixture.

Theoretical analysis of the pump effectiveness is simulated based on compression of the gas. Thermodynamic process varies from isothermal to isentropic. Pump effectiveness is mainly a function of suction pressure and GVF. Effectiveness of the pump to work as a compressor decreases as the GVF increases. While increase in suction pressure increases the pump effectiveness due to increased work done on the mixture. Polytropic index has secondary effect on the effectiveness with pump being more effective at isentropic process. Pump effectiveness is a theoretical term and independent of the pump speed.

Process efficiency represents the decreasing value of efficiency from an isentropic process to an isothermal process. Process efficiency increases with increase in suction pressure and decrease in GVF while it decreases with increase in pressure rise.

Power input increases with increase in pressure rise and it is independent of suction pressure. It is mildly affected by GVF. Mechanical efficiency of the pump is affected by suction pressure, pressure rise, GVF values and the speed. Mechanical efficiency peaks between 100 to 150 psi pressure rise for all the GVF and high speed. Efficiency was lowest for 15 psi suction pressure while this increase was very small for all the suction pressures onwards 50 psi.

Based on comparison with an isentropic compressor, it is seen that performance of the multiphase twin-screw pump is comparable with the conventional multiphase system for a wide range of GVF and not just the wet gas application. From the analysis it is seen that with increase in pressure, efficiency of the multiphase pump also goes up and even with high GVF it is still higher than the compressor. Further comparison should be done by experimentally testing both systems for specific volume flow rate, suction pressure, pressure rise and GVF.

Temperature of liquid recirculation has significant impact on the performance of twin screw pump when operating at high GVF and close loop system. From experiment it is seen that volumetric efficiency was degraded by 30% with rise in seal flush temperature from 90F to 180F. Cooling of sealflush fluid by using external heat exchanger improved the performance of the pump and cooled the total temperature at the inlet of the pump.

Effect of increase in the viscosity of liquid recirculation fluid on the pump performance was studied. In contrast to expectation, results show pump efficiency decreases with increase in viscosity of the pump.

From the summery above it can be concluded that the pump should be installed as close as possible to the source where the suction pressure is maximum and GVF is minimum.

In order to run the pump effectively and safely, it is recommended to use a cooling system for recirculating seal flush fluid for cases of the pump running with wet gas application. It may also be necessary to add liquid from an external source to maintain pump efficiency.

Characterization and selection of the twin-screw pump is more complex than for gas compressor or liquid pump.

Future work-Recommendations

- Pump performance at suction pressure higher than 100 psi
- Study of Colfax twin-screw pump with close loop fluid recirculation for better comparison with Leistritz pump.
- Using natural gas and oil as a multiphase mixture for better understanding of the pump in actual oilwell condition.
- Study of pump at high GVF using friction reducer.

11.2 CFD

Single phase CFD simulations are performed on multiphase twin-screw pump for different pressure rise conditions and 1800 rpm. It has been shown that the twin-screw pump can effectively be modeled using moving reference frame which is a simple but

accurate way of representing the twin-screw pump operation in a quasi-static way. The current simulations enforce the boundary condition at the inlet and outlet of clearances. Pressure and velocity profile obtained from the simulation gives valuable insight on how the twin-screw pump operation is affected by the intermeshing of the screws, pressure differential, and speed of the rotors. Leakage flow is mainly characterized by pressure differential in the case of single phase simulation. For the purpose of validation, leakage flow was obtained by calculating the average velocity of the flow in rectangular channel (which has the same dimensions as that of circumferential clearances) using the correlation for the friction factor and pressure rise for turbulent flow. Leakage flow obtained using CFD agrees well with the analytical solution.

Total Flow rate obtained using CFD agrees well within 5% of the experimental data for full speed. CFD simulations over predicts the total flow rate. This may be attributed to the variation in the boundary condition in the actual and CFD case and inability of k-epsilon model to correctly predict shear stresses especially at high pressure rise.

2D CFD simulation was performed on the disc rotating with uniform speed and translating at constant axial velocity. The purpose of this study was to understand the flow behavior when it is subjected to pure rotation. Results agree well with the assumptions made while designing the analytical tool to predict the flow rate. Bubble size has a significant impact on the leakage flow rate and the phase separation. No fix benchmark has been set related to the bubble size and the leakage flow rate.

3D CFD simulation was run for 50% GVF and different suction pressures and pressure rise conditions. Bubble size has a significant effect on the separation of the multiphase flow mixture. Better separation was realized by increasing the bubble size.

Flow separation is strongly affected by the forward movement of the screws coupled with pressure difference between different cavities. Intermeshing of the screws also causes difficulty in the separation. Leakage flow through the circumferential clearance is mainly the water with small infiltration of the air along with water. Air at the root is seen to be escaping through root clearance to the previous chamber. CFD data agrees well with the experimental data for increased suction pressure.

Future work-Recommendations

- Modeling of inlet and outlet plenum in order to accurately represent the boundary conditions.
- Validation of CFD data for 50% GVF using LDV measurement study.
- 3D CFD simulation of the pump at different GVF.
- Study the relationship between bubble size, GVF and suction pressure.
- Two phase CFD simulation at different speeds.

11.3 Dynamic pressure measurement and flow visualization

Dynamic pressure measurement shows linear pressures build up for single phase flow while parabolic pressure build up for multiphase flow.

Flow visualization in a twin-screw pump indicated some unexpected results. Flow visualization shows air infiltration even at low GVF at the suction. Low GVF

visualization indicated that two phases are well mixed inside the cavities while there is separation between the phases inside the clearances. Slip velocity is unknown at this stage. Two phases were well separated in the cavity as well as in the clearances at medium and high GVF due to the high viscosity of the oil.

Some aspects of flow visualization show good agreement with the CFD simulation.

Future work-recommendation

- Flow visualization study with air and water as a two-phase mixture.
- Increase the suction pressure by installing the boost pump at the inlet of the twin-screw pump.
- Measurement of GVF inside the clearances and the cavity and study the relationship.

REFERENCES

Beijnum, M. V. *CFD Simulation of Multiphase Twin Screw Pump.* MS Thesis, Eindhoven: Technische Universiteit Eindhoven, 2007.

Chan, Evan. *Wet-Gas Compression in Twin-Screw Multiphase Pumps.* MS Thesis, College Station: Texas A&M University, 2006.

Dal Porto, D.F., and Larson, L.A. "Multiphase-Pump FIeld Trials Demonstrate Practical Applications for the Technology." Denver, Colorado: SPE Production & Facilities, 1997.

Demirdzic, I., and Muzaferija, S. "Numerical Methods for Coupled FLuid Flow, Heat Transfer and Stress Analysis Using Unstructured Moving Meshes with Cells of Arbitrary Topology." *Comput. Methods Appl. Mech. Engrg.*, 1994: 235-255.

Dolan, P.J., Goodridge, R.A., and Leggate, J.S. "Development of a Twin-Screw Pump for Multiphase Duties." *SPE Production Engineering.* London: Society of Petrolium Engineers, 1988.

Dorenbos, C., Müeller-Link, D., and Jäeschke, A. "Sand Handling During Multiphase Operations with Twin-Screw Pumps." *SPE International Thermal Operations and Heavy Oil Symposium.* Porlamar: SPE, 2001. 1-9.

Egashira, K., Shoda, S., Tochikawa, T., and Furukawa, A. "Backflow in Twin-Screw-Type Multiphase Pump." SPE Production & Facilities, 1998. 64-69.

Feng, C., Yueyuan, P., Ziwen, X., and Pengcheng, S. "Thermodynamic Performance Simulation of a Twin-Screw Multiphase Pump." *Journal of Process Mechanical Engineering*, 2001: 157-162.

Fryc, O., and Vimmir, J. "Comparison of Various Turbulant Models Applied to Leakage Flow Through a Male Rotor-Housing Gap of Twin-Screw Compressor." *Applied Mechanics 8th International Scientific Conference.* 2006.

Hua, G., Falcone, G., Teodoriu, C., and Morrison, G. "Comparison of Multiphase Pumping Technology for Subsea and Downhole Applications." *SPE Annual Technical Conference and Exhibition.* Denver: Society of Petroleum Engineers, 2012. 36-46.

Karge, V. "Two-Spindle Screw Pumps for Handling Multiphase Mixtures." *Reprint of Pumps · Vacuum pumps · Compressors '88, Dr. Harnisch Verlagsgesellschaft mbH.* Frankfurt A. M.: Pump Group, Compressor, 1988. 14-20.

Kovacevic, A., Stosic, N., and Smith, I. K. "A Numerical Study of Fluid-Solid Interaction in Screw Compressors." *International Journal of Computer Application in Technology*, 2004: 148-158.

Kovacevic, A., Stosic, N., and Smith, I. K. "Three Dimensional Numerical Analysis of Screw Compressor Performance." *Journal of Computation Methods in Science and Engineering*, 2003: 259-284.

Kovacevic, A., Stosic, N., and Smith, I.K. "The CFD Analysis of a Screw Compressor Suction Flow." *2000 International Compressor Engineering Conference.* West Lafayette, Indiana: Purdue University, 25-28 July 2000.

Kovacevic, A., Stosic, N., Mujic, E., Smith, I. K., and Guerrato, D. "Extending the Role of Computational Fluid Dynamics in Screw Machines." *Proc. IMechE*, 2010: 83-97.

Martin, A.M. *Multiphase Twin Screw Pump Modeling for Oil and Gas Industry.* PhD Thesis, College Station: Texas A&M University, 2003.

Muller-Link, D., Brandt, J.-U., Reichwage, M., and Schroder, G. "Wet Gas Compression with Twin-Screw Multiphase Pumps." *Fluid Machinary for the Oil, Gas and Petrochemical Industry*, 2002: 117-125.

Neumann, W. "Efficient Multiphase Pump Station for Onshore Application and Prospects for Offshore Application." *International Pump Users Symposium*, 1991: 43-48.

Prang, A. J., and Cooper, P. "Enhanced Multiphase Flow Predictions in Twin-Screw Pump." *Proceedings of the 21st International Pump User Symposium.* Houston: Texas A&M University, 2004. 69-76.

Rabiger, K. *Fluid Dynamic and Thermodynamic Behaviour of Multiphase Screw Pumps Handling Gas-Liquid Mixtures with Very High Gas Volume Fractions.* Ph.D. Thesis, Faculty of Advanced Technology, University of Glamorgan, 2009.

Scott, S.L., Xu, J., and Lenz, C. "Subsea Multiphase Pressure Boosting and a New Approach for Speed Control Using a Hydrodynamic Variable-Speed Drive." *SPE annual Technical Conference.* San Antanio: SPE, 2006. SPE 103323.

Singh, A. *Modelling of Twin-Screw Multiphase Pump Performance During Periods of High Gas Volume Fraction.* MS Thesis, College Station: Texas A&M University, 2003.

Stosic, N., Smith, I. K., Kovacevic, A. "Optimization of Screw Compressor Design." *International Compressor Engineering Conference.* Purdue University, 2002.

Vetter, G., and Wincek, M. "Performance Prediction of Twin-Screw Pumps for Two-Phase Gas/Liquid Flow." *Pumping Machinery, ASME, Fluid Engineering Conference (FED).* Washington, D.C: ASME, 1993. 331-340.

Vetter, G., Wirth, W., Korner, H., and Pregler, S. "Multiphase Pumping with Twin-Screw pumps - Understand and Model Hydrodynamics and Hydroabrasive Wear." *7th International Pump User Symposium, Turbomachinery Laboratory.* Houston,: Texas A&M University, 2000. 153-169.

Vimmr, J., and Fryc, O. "Numerical Simulation of Leakage Flow Between Moving Rotor and Housing of Screw Compressor." *Modelowanie Inzynierskie.* Gliwice, 2006. 461-468.

Xu, Jian. *Modeling of Wet Gas Compression in Twin Screw Multiphase Pump.* PhD Thesis, College Station: Texas A&M University, 2008.